DÉVELOPPEMENT DE NANOPARTICULES MULTIFONCTIONNELLES À BASE DE POLYMÈRES STIMULI-RÉPONDANTS ET FORMÉES DE CHAÎNES INDIVIDUELLES

Par

Weizheng Fan

Thèse présentée au Département de chimie en vue

de l'obtention du grade de docteur ès science (Ph.D.)

FACULTÉ DES SCIENCES

UNIVERSITÉ DE SHERBROOKE

Sherbrooke, Québec, Canada, Juillet 2017

DEVELOPMENT OF MULTIFUNCTIONAL POLYMERIC SINGLE-CHAIN NANOPARTICLES BASED ON STIMULI-RESPONSIVE POLYMERS

by

Weizheng Fan

A Thesis

Presented to the Département of Chimie

in Partial Fulfillment of the Requirements for the Degree of

Doctor of Philosophy (Ph.D.)

FACULTÉ DES SCIENCES

UNIVERSITÉ DE SHERBROOKE

Sherbrooke, Québec, Canada, July 2017

Le 28 Juillet 2017

le jury a accepté la thèse de monsieur Weizheng Fan
dans sa version finale.

Membres du jury

Professeur Yue Zhao
Directeur de recherche
Département de chimie

Professeur Josée Brisson
Évaluateur externe
Département de chimie
Université Laval

Professeur Pierre D. Harvey
Évaluateur interne
Département de chimie

Professeur Yves Dory
Évaluateur interne
Département de chimie

Professeur Jean-Philippe Bellenger
Président-rapporteur
Département de chimie

SOMMAIRE

Comme je suis particulièrement intéressé par les nanosciences et les nombreuses applications des nanotechnologies, je me suis penché sur le développement de méthodes de fabrication de nanoparticules ultra-petites dont les fonctions peuvent être ajustées avec précision. Récemment, une nouvelle technologie appelée « technologie d'une seule chaîne », c'est-à-dire qui utilise une seule chaîne polymère, est devenue un sujet de recherche de plus en plus motivant pour la communauté scientifique. Cette technologie a l'avantage de dépendre d'une méthode facile de préparation de nanoparticules polymères d'une seule chaîne (SCNPs) et ayant des dimensions typiques de 1,5 à 20 nm. Leurs tailles ultra petites leur confèrent des propriétés spécifiques, ce qui permet de les utiliser comme capteurs, systèmes catalytiques, revêtements à faible viscosité, nanoréacteurs ou pour des applications biomédicales. Grâce aux contributions de nombreux scientifiques durant la dernière décennie, les méthodes de synthèse des SCNPs sont devenues très variées et représentent une technologie désormais mature. Néanmoins, de nombreux problèmes sont à résoudre dans ce domaine, ce qui permettra d'ajouter de nouvelles fonctions ou de les valoriser pour de nouvelles applications.

Les polymères sensibles à plusieurs stimuli sont une classe de matériaux intelligents dont les propriétés peuvent être modifiées par l'application d'un stimulus extérieur. Ils sont utilisés extensivement dans les domaines énergétique et biomédical. Comme leurs propriétés physiques et chimiques peuvent être modifiées aisément et efficacement par un contrôle de leur environnement externe, ces polymères sont des candidats pour fabriquer de nouvelles SCNPs.

Dans cette thèse, nous nous sommes intéressés au développement de SCNPs ayant de

multiples fonctionnalités car cela permet d'ouvrir la voie pour de nouvelles applications. Pour cela, de nombreux polymères sensibles à plusieurs stimuli ont été préparés comme précurseurs à des SCNPs. En concevant spécifiquement ces polymères, il fut possible d'ajouter leurs propriétés de réponse à des stimuli dans les systèmes SCNPs. Le cœur même de cette thèse consiste en trois projets qui utilisèrent trois classes de SCNPs provenant de polymères sensibles aux stimuli. Grâce à leur réponse à plusieurs stimuli, ces SCNPs remplirent de nombreuses fonctions et subirent des modifications soit de leur structure, soit de leur morphologie, soit de leurs propriétés. Et en plus de la variété de fonctions, chaque classe de SCNPs a le potentiel pour de nombreuses applications.

Dans la première étude présentée dans cette thèse (chapitre 1), nous avons préparé une classe de SCNPs photodégradables ayant une taille ajustable et inférieure à 10 nm. Il s'agit de polyesters rendus photosensibles par la présence de coumarines à l'intérieur de la chaîne principale (nommés CAPPG) grâce à la copolymérisation de coumarine diol, d'acide adipique et de propylène glycol (PPG). Cette incorporation de coumarines dans la chaîne principale permet au polymère d'être photosensible par deux façons. En effet, les coumarines peuvent se photo-dimériser, lorsqu'elles sont irradiées par des rayonnements UV (> 320 nm) en des cyclobutanes qui peuvent être ouverts à nouveau par d'autres rayonnements UV (254 nm) permettant la restauration des coumarines initiales. Cela a permis la création de SCNPs de tailles inférieures à 10 nm et incluant des propriétés de photodégradation. Cette propriété a été démontrée par une irradiation de 3 h avec des chaînes polymères de 13220 g/mol à 1385 g/mol dans les SCNPs. La taille de ces SNCPs (caractérisée par leur rayon hydrodynamique) peut être modifiée entre 3 nm et 5,3 nm en modifiant le taux de dimérisation des coumarines, ce qui est aisément obtenu en ajustant le temps d'irradiation UV. Les résultats ont démontré que cette méthode permet un contrôle aisé de la taille des SCNPs sans avoir recours à la

synthèse de nombreux polymères précurseurs. Finalement, comme le polyester était biodégradable et biocompatible, ces SCNPs peuvent être exploitées pour des applications biomédicales.

Dans la deuxième étude effectuée au cours de cette thèse (chapitre 2), nous avons préparé un nouveau type de SCNPs multifonctionnel à partir d'un polymère cristallin liquide. Il s'agit du polyméthacrylate de [2- (7-méthylcoumaryl) oxyéthyle - co - 6-[4-(4'-méthoxyphenylazo) phénoxy] hexyle] (PAzoMACMA). Les groupements latéraux du polymère contiennent, en majorité, des azobenzènes photoisomérisables et, en minorité, des coumarines photodimérisables. Les azobenzènes servent de mésogènes pour la formation de cristaux liquides alors que les coumarines ont été utilisées pour une réticulation photoinduite et intrachaîne. Malgré les dimensions inférieures à 15 nm, le confinement et la réticulation, les phases cristallines liquides (LC) persistèrent même dans les SCNPs. Ces SCNPs cristaux liquides (LC-SCNPs) présentèrent un certain nombre de propriétés intéressantes et particulières. Alors que leurs dispersions dans le THF n'étaient pas fluorescentes, celles dans le chloroforme l'étaient. En plus, ces nanoparticules s'agglomeraient quelque peu dans le chloroforme ce qui induisait des fluorescences différentes entre des SCNPs riches en isomères cis ou riches en isomères trans des azobenzènes. A cause de la photoisomérisation des azobenzènes, ces LC-SCNPs se déformaient sous irradiation comme le font les microparticules ou les colloïdes contenant des azobenzènes. Cependant, la déformation de ces nanoparticules dépend de la longueur d'onde de lumière polarisée. Alors que sous irradiation UV polarisée à 365 nm, l'élongation des SCNPs était perpendiculaire à la polarisation de la lumière incidente, sous irradiation visible polarisée entre 400 et 500 nm, l'étirement se faisait parallèlement à la polarisation. Finalement, un nanocomposite fut préparé par dispersion de LC-SCNPs dans une matrice de polyméthacrylate de méthyle

(PMMA). Si celui-ci était étiré mécaniquement, les azobenzènes s'orientaient dans la direction de la déformation induite. Ces propriétés intéressantes des LC-SCNPs que cette étude a permis de dévoiler, suggèrent de nouvelles applications potentielles.

Dans la troisième étude de cette thèse (chapitre 3), nous avons préparé une classe de SCNPs sensibles à la présence de CO_2 et leurs agrégats micellaires auto-assemblés. D'un côté, des SCNPs ont été préparées à partir d'un polyméthacrylate de {(N, N-diméthylaminoéthyle)-*co*-4-méthyl-[7-(méthacryloyl)-oxyéthyl-oxy] coumaryle} (PDMAEMA-*co*-CMA). Lorsqu'elles sont dispersées en solution aqueuse, les nanoparticules individuelles peuvent subir des cycles réversibles d'expansion et de rétrécissement sous une stimulation alternative de CO_2 et de N_2 qui vont protoner et déprotoner les amines tertiaires. D'un autre côté, des SCNPs de type 'Janus' (SCJNPs) ont été préparées à partir d'un copolymère dibloc amphiphile : PS-*b*-P(DMAEMA-*co*-CMA) (PS correspond au polystyrène qui est hydrophobe). Ce type de SCJNPs peut s'autoassembler sous forme de micelles en solution aqueuse. Sous stimulation CO_2 ou N_2, l'expansion ou le rétrécissement à l'intérieur des particules permet de grands changements de volume. En plus, ces particules ont été étudiées comme potentiels nanoréacteurs pour des nanoparticules d'or (AuNPs) que ce soit sous formes SCNPs ou micelles SCJNPs. La vitesse de formation des AuNPs augmente sous bullage de CO_2 et décroît sous N_2. Cela permet de rendre possible cette réaction contrôlable par ces deux gaz. Qui plus est, utiliser des micelles de SCJNPs dont le volume peut être modifié sur un large intervalle en changeant l'intensité de la stimulation de CO_2, permit d'obtenir des AuNPs de taille variable.

Mots clé : science des polymères, particules faites d'une seule chaîne, polymère sensibles à des stimuli, matériaux cristaux liquides, nanoréacteurs.

ABSTRACT

With interests on nanoscience and nanotechnology for many applications, there is a demand for development of fabrication technology of ultra-small nano-size objects that allow for precise size control and tailored functionality. Recently, a new technology called 'single-chain technology', which manipulates a single polymer chain, becomes a rapidly-growing research topic. This technology provides a facile method to prepare polymer single-chain nanoparticles (SCNPs) with a typical size of 1.5-20 nm. Due to the ultra-small size-enabled unique properties, SCNPs have wide range of applications, including sensor, catalytic system, low viscosity coating, nanoreactor and biomedical applications. Through the contributions by many scientists in the past decade, the synthetic methodologies to fabricate SCNPs have been reported using various chemistries and been getting mature. However, there are still several unsolved problems in the field of SCNPs including functions and application.

Stimuli-responsive polymers, as a class of smart materials whose properties can be changed by responding to external stimuli, have been widely used in energy and biomedical applications. Since their chemical and physical properties can be changed easily and efficiently *via* environmental control, stimuli-responsive polymers provide a potential pathway to preparing functional SCNPs.

In this thesis, we are focusing on developing functional SCNPs, especially systems with multi-functions, and expanding their applications. To achieve this target, various stimuli-responsive polymers were prepared as polymer precursors and their stimuli-responsive properties were introduced into the SCNP systems by rational design of their chemical structures. The core of this thesis is comprised of three projects which deal with three classes

of SCNPs from stimuli-responsive polymers. These stimuli-responsive SCNPs perform multi-functions and undergo certain change either in structure or morphology and properties. In addition, according to their variety of functions, each class of multi-functional SCNPs has diverse potential applications.

In the first study presented in the thesis (Chapter 1), we prepared a class of sub-10 nm photodegradable and size-tunable SCNPs based on photo-responsive main-chain coumarin-based polyesters Poly{[7-(hydroxypropoxy)-4-(hydroxymethyl)coumarin adipate]-*co*-(polypropylene glycol adipate)} (CAPPG) through copolymerization of coumarin diol, adipic acid and polypropylene glycol (PPG). By incorporating coumarin moieties into the chain backbone of a polyester, dual photo-responsive reaction, i.e. photo-dimerization (>320 nm) and photo-induced chain scission (254 nm), occur under two different wavelengths of UV irradiation, enabling the preparation of sub-10 nm SCNPs and their photo-degradation property. The photo-degradability of SCNPs is evidenced under 254 nm UV irradiation for 3 h, which molecular weight of SCNPs decreasing from 13220 g/mol to 1385 g/mol. Moreover, the size of SCNPs can be tunable from 5.3 nm to 3 nm (hydrodynamic diameter) by varying the dimerization degree of coumarin moieties, that is simply controlled by the UV irradiation time. These results demonstrate a facile method to control the size of SCNPs without the need for synthesizing different polymer precursors. Finally, due to the biocompatible and biodegradable nature of polyester as polymer precursor, the SCNPs with photo-degradability and size-tunability have the potential to be exploited for biomedical applications.

In the second study realized in this thesis (Chapter 2), we prepared a new type of multi-functional SCNPs from a side-chain liquid crystalline polymer (SCLCP), namely poly{6-[4-(4-methoxyphenylazo) phenoxy]hexylmethacrylate-*co*-4-methyl-[7-(methacr-yloyl) oxy-

ethyl-oxy]coumarin} (PAzoMACMA). The polymer's side groups comprise photo-isomerizable azobenzene in majority and photo-dimerizable coumarin in minority, with the former as mesogens and the latter for intra-chain photo-crosslinking. Despite the sub-15 nm size, confinement and crosslinking, the liquid crystalline (LC) phases of bulk PAzoMACMA persist in SCLCPs. Such LC-SCNPs exhibit a number of interesting and peculiar properties. While their dispersion in THF is non-fluorescent, when dispersed in chloroform, the nanoparticles appear to agglomerate to certain degree and display significant fluorescence that is different for SCNPs rich in the *trans* or *cis* isomer of azobenzene. The azobenzene LC-SCNPs also undergo photo-induced deformation, similar to azobenzene micro- or colloidal particles. However, the elongational deformation of the nanoparticles is dependent upon the linearly polarized excitation wavelength. While under polarized 365 nm UV irradiation the SCNP stretching direction is perpendicular to the light polarization, under polarized 400-500 nm visible light irradiation, the stretching takes place along the light polarization direction. Finally, an all-polymer nanocomposite was prepared by dispersing the LC-SCNPs in poly(methyl methacrylate) (PMMA), and mechanically stretching-induced orientation of azobenzene mesogens developed along the strain direction. The interesting properties of LC-SCNPs unveiled in this study suggest new possibilities for applications including bio-imaging and LC materials.

As the third study in this thesis (Chapter 3), we studied a class of CO_2-responsive SCNPs and their self-assembled micellar aggregates. On one hand, SCNPs are prepared from a random copolymer of poly{(N,N-dimethylaminoethyl methacrylate)-*co*-4-methyl-[7-(methacryloyl)oxyethyl-oxy]coumarin} (P(DMAEMA-*co*-CMA)). When dispersed in aqueous solution, individual nanoparticles can undergo reversible swelling/shrinking under alternating CO_2/N_2 stimulation as a result of the reversible protonation/deprotonation of

tertiary amine groups. On the other hand, tadpole-like single-chain 'Janus' nanoparticles (SCJNPs) are prepared using an amphiphilic diblock copolymer of PS-*b*-P(DMAEMA-*co*-CMA) (PS is hydrophobic polystyrene). This type of SCJNPs can self-assemble into core-shell micellar aggregates in aqueous solution. Under CO_2/N_2 stimulation, the collective swelling/shrinking of SCJNPs within the micelle results in large, reversible volume change. In addition, both P(DMAEMA-*co*-CMA) SCNPs and PS-*b*-P(DMAEMA-*co*-CMA) SCJNP micelles are explored as gas-tunable nanoreactors for gold nanoparticles (AuNPs). The rate of AuNP formation increases under CO_2 stimulation and decreases upon N_2 bubbling, which makes it possible to tune the reaction rate up and down (on/off switching) by using the two gases. Moreover, using the micelles of SCJNPs, whose volume can be controlled over a wide range by adjusting the CO_2 stimulation strength, variable-size AuNPs and their aggregates are obtained with continuous redshift of the surface plasmon resonance (SPR) into the long wavelength visible light region.

Keywords: Polymer science; Single-chain nanoparticles; Stimuli-responsive polymers; Liquid crystalline materials; Nano-reactor.

ACKNOWLEDGEMENT

After the accomplishment of this thesis, I would like to express my sincere gratitude to my supervisor Prof. Yue Zhao for his guidance, patience, encouragement and supports during my research. I appreciate him to provide me an opportunity to do research which I am interested in and support me to realize my ideas to some extent. I really learned a lot from Prof. Zhao, not only for the knowledge of science, but also the attitude for research. Also I would thank him to give me the financial support which make me finish my PhD program.

I would like to thank two members of my doctoral committee, who are also in the jury of my thesis, Prof. Jean-Philippe Bellenger and Prof. Pierre D. Harvey, as well as all the professors and staff working in the Department of Chemistry, Université de Sherbrooke for their kind help. I would like to thank Prof. Josée Brisson (Université Laval) and Prof. Yves Dory for serving in the jury of my thesis. I also would like to thank Prof. Jérôme Claverie and Dr. René Gagnon for the triple detection size exclusion chromatography tests conducted in a project.

I acknowledge the following people, my colleagues and dearest friends, who made my stay in Sherbrooke full of joys and memories: Mrs. Xia Tong, Dr. Olivier Boissière, Dr. Bing Yu, Dr. Feng Shi, Dr. Hongji Zhang, Dr. Shangyi Fu, Dr. Guo Li, Dr. Qiang Yan, Dr. Hu Zhang, Dr. Aurélie Lespes, Dr. Shengwei Guo, Dr. Xin Zhao, Dr. Juan Xuan, Dr. Rong Yang, Dr. Hojjat Seyedjamali, Mr Jun Xiang, Mrs. Hui Xiao, Mr. Damien Habault, Mr. Farhad Farnia, Mr. Xili Lu, Mr. Feijie Ge, Mr. Liangliang Dong, Mrs. Amélie Augé, Mr. Ricardo Da Silva Lemos, and Mrs. Laura Mourot.

I express my deepest gratitude to my entire family for their unselfish and everlasting love. I

wish to thank my parents that they have continuously supported me both morally and economically after my arrival in Canada, without which I would not have a chance to persevere to the end.

Finally, I would like to acknowledge the following organizations for their financial support: Natural Sciences and Engineering Research Council of Canada (NSERC), Le Fonds de recherche du Québec: Nature et technologies (FQRNT), Centre for Self-Assembled Chemical Structures (CSACS) and La Fondation de Université de Sherbrooke.

TABLE OF CONTENT

SOMMAIRE iv
ABSTRACT viii
ACKNOWLEDGEMENT xii
TABLE OF CONTENT xiv
LIST OF SCHEMES xix
LIST OF FIGURES xx
LIST OF TABLES xxviii
INTRODUCTION 1
I.1 Synthetic Methodology of Single-Chain Nanoparticles 4
I.1.1 Covalent crosslinking chemistry. 6
I.1.2 Dynamic covalent crosslinking chemistry 12
I.1.3 Non-covalent crosslinking chemistry 16
I.2 Characterization Techniques of Single-Chain Nanoparticles 21
I.2.1 Size-Exclusion Chromatography (SEC) 21
I.2.2 Viscometry 24
I.2.3 Nuclear Magnetic Resonance Spectroscopy (NMR) 25
I.2.4 Atomic Force Microscope (AFM) 26
I.2.5 Other characterization techniques 28
I.3 Development of Functional Single-Chain Nanoparticles 29
I.3.1 Functional SCNPs based on rational design of polymer structure 29
I.3.2 Functional SCNPs based on stimuli-responsive polymers 32
I.4 Potential Applications of Single-Chain Nanoparticles 35
I.5 Remaining Challenges of Single-Chain Nanoparticles 36

I.6 Brief Background of Stimuli-Responsive Polymers 37
I.6.1 Stimuli-responsive polymers sensitive to various stimuli 38
I.6.1.1 Light as stimulus 38
I.6.1.2 Temperature as stimulus 39
I.6.1.3 pH as stimulus 40
I.6.1.4 CO_2 as stimulus 40
I.6.2 Stimuli-responsive molecular structures used in this thesis 40
I.6.2.1 Coumarin 40
I.6.2.2 Azobenzene 42
I.6.2.3 2-(Dimethylamino)ethyl methacrylate (DMAEMA) 42
I.7 Objective of the Thesis 43
CHAPTER 1 PHOTODEGRADABLE AND SIZE-TUNABLE SINGLE-CHAIN NANOPARTICLES PREPARED FROM A SINGLE MAIN-CHAIN COUMARIN-CONTAINING POLYMER PRECURSOR 46
1.1 Introduction 46
1.2 Experimental Section 48
1.2.1 Materials 48
1.2.2 Synthesis of the coumarin monomer 49
1.2.2.1 Synthesis of 7-hydroxy-4-(chloromethyl) coumarin 49
1.2.2.2 Synthesis of 7-hydroxy-4-4(hydroxymethyl) coumarin 49
1.2.2.3 Synthesis of 7-(hydroxypropoxy)-4-(hydroxymethyl) coumarin 49
1.2.3 Synthesis of the coumarin-containing polymer precursor CAPPG 50
1.2.4 Preparation of single-chain nanoparticles of CAPPG 50
1.2.5 SEC measurements of CAPPG polymer precursor, SCNPs and SCNPs after

photo-degradation 53
1.2.6 Instruments and measurements 54
1.3 Results and Discussion 55
1.4 Conclusion 61
1.5 Statement of Contribution 63
CHAPTER 2 PHOTO-RESPONSIVE LIQUID CRYSTALLINE POLYMER SINGLE-CHAIN NANOPARTICLES 64
2.1 Introduction 64
2.2 Experimental Section 67
2.2.1 Materials 67
2.2.2 Synthesis of polymer precursor PAzoMACMA 68
2.2.3 Preparation of PAzoMACMA single-chain nanoparticles 68
2.2.4 Characterization of single-chain nanoparticles 69
2.2.5 Photo-induced deformation of single-chain nanoparticles 70
2.2.6 Nanocomposite preparation and characterization 70
2.2.7 Instruments and measurements 71
2.3 Results and Discussion 72
2.3.1 Design of polymer precursor 72
2.3.2 Single-chain nanoparticle preparation and characterization 73
2.3.3 Liquid crystal order in PAzoMACMA SCNPs 77
2.3.4 Optical behaviours of LC-SCNPs 79
2.3.5 Photo-induced deformation of LC-SCNPs 81
2.3.6 Stretching-induced orientation in a nanocomposite with LC-SCNPs 84
2.4 Conclusion 86

2.5 Statement of Contribution 87

CHAPTER 3 CO_2-RESPONSIVE POLYMER SINGLE-CHAIN NANOPARTICLES FOR GAS-SENSITIVE SELF-ASSEMBLY AND NANOREACTORS 88

3.1 Introduction 88

3.2 Experimental Section 92

3.2.1 Materials 92

3.2.2 Synthesis of P(DMAEMA-*co*-CMA) 93

3.2.3 Synthesis of PS-*b*-P(DMAEMA-*co*-CMA) 93

3.2.3.1 Synthesis of PS macro-initiator 94

3.2.3.2 Synthesis of PS-*b*-P(DMAEMA-*co*-CMA). 95

3.2.4 Preparation of single-chain nanoparticles of P(DMAEMA-*co*-CMA). 95

3.2.5 Preparation of tadpole-like single-chain 'Janus' nanoparticles and self-assembly. 96

3.2.6 Synthesis of gold nanoparticles using CO_2-responsive nano-reactors of SCNPs or SCJNP micelles 97

3.2.7 Instrumentation and characterization methods. 98

3.3 Results and Discussion 100

3.3.1 Preparation and characterization of P(DMAEMA-*co*-CMA) SCNPs 100

3.3.2 Preparation and characterization of PS-*b*-P(DMAEMA-*co*-CMA) SCJNPs 101

3.3.3 CO_2-responsive single-chain nanoparticles of P(DMAEMA-*co*-CMA). 104

3.3.4 CO_2-responsive micellar aggregates of single-chain 'Janus' nanoparticles of PS-*b*-P(DMAEMA-*co*-CMA). 106

3.3.5 Gas-tunable formation rate of AuNPs using SCNPs as nanoreactors. 108

3.3.6 Gas-tunable size of AuNPs using micelles of SCJNPs as nanoreactors..... 111
3.4 Conclusion 116
3.5 Statement of Contribution..... 117
CHAPTER 4 GENERAL DISCUSSION AND PERSPECTIVE..... 118
4.1 General Discussion 118
4.2 Perspective 121
4.2.1 Compartmentalized 'Janus' single-chain nanoparticles with multi-functions... 122
4.2.2 Stimuli-responsive single-chain nanoparticles in drug delivery system..... 123
CONCLUSION 125
BIBLIOGRAPHY 127

LIST OF SCHEMES

Scheme 1. Photochemical reactions of coumarin compound. 41

Scheme 2. Photoisomerization of azobenzene. 42

Scheme 3. Protonation/deprotonation of PDMAEMA by pH or gas stimulation. 43

Scheme 4. Synthesis procedure for the CAPPG polymer precursor 51

Scheme 5. Photo-crosslinking and photo-degradation of SCNP of the main chain coumarin-containing polymer. Under the 254 nm UV irradiation, cleavage of the coumarin-4-yl methyl ester, resulting in chain scission, can occur with coumarin in the monomeric form (as drawn in the scheme) or in the dimer form (not shown). 59

Scheme 6. Synthesis procedure of PAzoMACMA polymer precursor 69

Scheme 7. Chemical structure of P(MEO_2MA-*co*-MAA)-*b*-PEO-b P(MEO_2MA-*co*-MAA) 92

Scheme 8. Schematic illustration of SCNPs for drug delivery applications. 124

LIST OF FIGURES

Figure 1. Conceptual illustration of single-chain folding of linear polymer. 2

Figure 2. Schematic representation of the four strategies utilized for the synthesis of SCNPs: (A) Homo-functional chain collapse; (B) Hetero-bifunctional chain collapse; (C) Cross-linker-mediated chain collapse; (D) One-block collapse of diblock or triblock copolymers. 5

Figure 3. Synthetic route and graphical representation of (a) the oxidative polymerization of pendant ProDOT groups of poly(ProDOT-Sty) yielding conjugated polymeric nanoparticles and (b) their subsequent reduction to poly(vinylbenzyl alcohol) and poly(ProDOT-OH). 9

Figure 4. Conjugation of polymer chains to form intramolecularly crosslinked SCNPs, and their subsequent reversible transformation into an intermolecularly crosslinked hydrogel. 14

Figure 5. (a) Schematic illustration of preparation of polymer SCNPs through intra-chain photo-crosslinking. (b) Chemical structures of coumarin-containing random copolymers of P(DMAEMA-*co*-CMA) and the reversible photo-crosslinking reaction activated by UV light at two different wavelengths. 15

Figure 6. UV irradiation induced collapse of a single polymer chain into a nanoparticle for an example that the functional group with hydrogen bonding units are protected in some way to prevent forming aggregation. 18

Figure 7. SEC traces of polymer precursor and single-chain nanoparticles with different irradiation time describing the characterization of SCNP formation *via* SEC. 22

Figure 8. MALS and RI detection traces for SEC of SCNPs highlighting the ability of MALS to detect large, multi-chain aggregates. 23

Figure 9. Relative viscosity of linear polymer and SCNPs at various concentrations.....25

Figure 10. AFM images of well-separated single-chain nanoparticles prepared on mica (a,b) and graphite (c, d) under dilute concentration. 27

Figure 11. AFM images of SCNPs display the relationship between molecular weight and single-chain nanoparticles size. 27

Figure 12. (a) Synthetic scheme for the proof of principle reaction of the profluorescent SCNP with Maleimide-functional microspheres. (b) Image of solution of SCNP in THF irradiated with a hand-held UV-lamp (366 nm). (c, d) Fluorescence microscopy image and three-dimensional reconstruction of a confocal image stack of SCNP-functionalized microspheres. 30

Figure 13. Processes for preparation of polymeric mono-functional nanoparticles. 31

Figure 14. Schematic depiction of the self-assembly of monotailed SCNPs into aggregates with different morphologies.....32

Figure 15. Schematic representation of the formation of SCNPs *via* intramolecular host-guest interaction and the voltage responsiveness of SCNPs.....34

Figure 16. (a) Transmittance change as a function of temperature for SCNPs solution with different photo-dimerization degree (b) Photographs of SCNP solution at 40ºC with different dimerization degree which demonstrate the photo-tunable LCST properties of SCNPs. 34

Figure 17. Classification of stimuli-responsive polymers. 38

Figure 18. Schematic illustration for the preparation of variable-size SCNPs using a single polymer precursor based on intra-chain photo-dimerization of coumarin moieties and the photodegradable feature of the SCNPs. 48

Figure 19. ^{1}H-NMR spectrum of 7-hydroxy-4-(chloromethyl) coumarin (a) (DMSO-d6). 51

Figure 20. ^{1}H-NMR spectrum of 7-hydroxy-4-4(hydroxymethyl) coumarin (b) (DMSO-d6). 52

Figure 21. ^{1}H-NMR spectrum of 7-(hydroxypropoxy)-4-(hydroxymethyl) coumarin (c) (in DMSO-d6). 52

Figure 22. ^{1}H-NMR spectrum of the CAPPG polymer precursor (in $CDCl_3$). 53

Figure 23. (a) Absorption spectra of CAPPG in $CHCl_3$ (0.2 mg/mL) recorded after different times of >320 nm UV irradiation showing intra-chain photodimerization (crosslinking). Inset is the plot of the photodimerization degree of coumarin *vs.* UV irradiation time. (b) SEC traces of the CAPPG precursor, SCNPs of varying photocrosslinking density obtained by exposing the same dilute CAPPG solution (0.2 mg/mL) to >320 nm UV light for different times, and SCNPs of the highest crosslinking density after subsequent 254 nm UV irradiation for 3 h. (c) AFM and (d) TEM image of the SCNPs with the highest crosslinking density, cast from a dilute polymer solution in $CHCl_3$ (0.02 mg/mL). 57

Figure 24. SEC traces over the full retention time scale for the CAPPG precursor, its SCNPs prepared upon 30 and 120 min >320 nm UV irradiation, respectively, and the photodegraded SCNP obtained after 254 nm UV irradiation. 58

Figure 25. AFM images of SCNPs (after 120 min UV irradiation) dispersed in water.....58

Figure 26. ^{1}H-NMR spectra of the CAPPG precursor and the SCNP after photo-degradation. The spectral changes upon 254 nm UV irradiation provide evidence for the photo-induced scission of chain backbone leading to the photo-degradation of SCNP: peak a in the polymer precursor being replaced by peak a' for the SCNP after photo-degradation.....60

Figure 27. (a) Number-weighted size distribution of the precursor and SCNPs prepared with different >320 nm UV irradiation times. (b) Average hydrodynamic diameter, D_H, *vs.* UV irradiation time (from 8 measurements).....61

Figure 28. AFM images of SCNPs formed after different UV irradiation time (a:30 min, b:60 min, c:120 min).....62

Figure 29. Schematic illustration for the preparation of liquid crystalline single-chain nanoparticles (LC-SCNPs) based on intra-chain photodimerization of coumarin moieties in the chemical structure of the used side-chain liquid crystalline polymer bearing azobenzene mesogens 67

Figure 30. ^{1}H-NMR spectrum of PAzoMACMA in $CDCl_3$.....73

Figure 31. (a) UV-vis spectra of PAzoMACMA before and after 320-480 nm irradiation for different times (5 cm distance) (b) UV-vis spectra recorded after the solution in (a) was subjected to a second UV irradiation (365 nm) for 15 min. (c) SEC results from LS detection (90°) of linear polymer and SCNPs (d) TEM images of SCNPs. 75

Figure 32. SEC traces of PAzoMACMA polymer precursor and SCNPs, a) Refractive Index (RI) detection traces. b) Light scattering (LS) detection traces (15°). c) Viscometric (VS) detection traces. 76

Figure 33. DLS results of linear polymer precursor of PAzoMACMA in THF and SCNPs in both THF and $CHCl_3$ 76

Figure 34. (a) DSC heating curves of polymer precursor and SCNPs. (b-d) Polarizing optical microscopy observation of SCNPs aggregates at room temperature (b), 185 ºC (c) and after annealing at 110 ºC (d). 78

Figure 35. (a) UV-vis absorption spectra of SCNPs in THF (0.2 mg/mL) for initial solution and, subsequently, after 365 nm UV irradiation for 5 min, after 400-500 nm visible light irradiation for 5 min and after 365 nm UV irradiation for 5 min again). (b) UV-vis absorption spectra of SCNPs in chloroform (0.2 mg/mL) in the rich-in-*cis* state after 365 nm UV irradiation for 15 min and in the subsequent rich-in-*trans* state after thermal relaxation at 70 ºC for 1 h. (c) Fluorescence emission spectra of SCNPs in chloroform in both rich-in-*cis* and rich-in-*trans* state and, in each case, under excitation at 365 nm and 460 nm, respectively. 82

Figure 36. AFM images of LC-SCNPs: a) initial, b) after linearly polarized UV irradiation (365 nm), and c) after linearly polarized visible light irradiation (400-500 nm). The arrow indicates the light polarization direction and the insert shows an enlarged image of a single deformed nanoparticle.....83

Figure 37. AFM images of deformed SCNPs under linearly polarized UV (365 nm) (a) and visible light (400-500 nm) irradiation (b). The arrow indicates the light polarization direction. 84

Figure 38. (a) Photograph of a PMMA/LC-SCNP nanocomposite film. (b) Polarized UV-vis spectra of the PMMA/LC-SCNP film stretched at 113 ºC to 400 % strain followed by cooling to room temperature, being recorded with the spectrophotometer's beam polarized parallel and perpendicular, respectively, to the film stretching direction. 85

Figure 39. Schematic illustration for: (a) preparation of P(DMAEMA-*co*-CMA) single-chain nanoparticles (SCNPs) through intra-chain photo-crosslinking (*via* photo-dimerization of coumarin groups) and the gas-switchable size change of SCNPs in aqueous solution; and (b) preparation of amphiphilic, tadpole-like PS-*b*-P(DMAEMA-*co*-CMA) single-chain 'Janus' nanoparticles (SCJNPs) and their gas-responsive self-assembled micellar aggregates. 91

Figure 40. ^{1}H-NMR spectra of P(DMAEMA-*co*-CMA) polymer precursor in $CDCl_3$.....94

Figure 41. ^{1}H-NMR spectra of PS-b-P(DMAEMA-*co*-CMA) polymer precursor in $CDCl_3$ 96

Figure 42. (a) Absorption spectra of P(DMAEMA-*co*-CMA) in THF (0.5 mg/mL) recorded before and after 320-480 nm light irradiation for different times, showing photodimerization of coumarin moieties. Inset is the plot of photodimerization degree *vs.* irradiation time. (b) SEC traces of P(DMAEMA-*co*-CMA) in THF (0.5 mg/mL) before and after 30 min irradiation, indicating the transition from coil to a more compact particle structure (SCNP) upon photodimerization of coumarin. (c) AFM and (d) TEM image of SCNPs obtained by casting a dilute polymer solution in THF (0.02 mg/mL). 102

Figure 43. (a) Absorption spectra of PS-*b*-(DMAEMA-*co*-CMA) in THF recorded before and after 320-480 nm light irradiation for different times, showing intra-chain photodimerization of coumarin moieties. Inset is the plot of photodimerization degree *vs.* irradiation time. (b) SEC traces of PS-*b*-P(DMAEMA-*co*-CMA) in THF (0.5 mg/mL) before and after 20 min irradiation, indicating the transition from coil to a more compact particle structure (SCJNP) upon photo-dimerization of coumarin. 103

Figure 44. TEM image of the PS-*b*-P(DMAEMA-*co*-CMA) SCJNPs cast from a dilute polymer solution in THF.....103

Figure 45. (a) Number-weighted size distribution for P(DMAEMA-*co*-CMA) SCNPs before CO_2 bubbling, after bubbling CO_2 for 10 min and after subsequent N_2 bubbling for 10 min. (b) Reversible change in average hydrodynamic diameter, D_H, of P(DMAEMA-*co*-CMA) SCNPs upon repeated cycles of alternating CO_2/N_2 bubbling. (c) Transmittance *vs.* temperature for aqueous solutions of P(DMAEMA-*co*-CMA) polymer precursor and SCNPs (3 mg/mL), with both solutions subjected to 30 s CO_2 and 2 min N_2 bubbling.....105

Figure 46. (a) Number-weighted size distribution for PS-*b*-P(DMAEMA-*co*-CMA) SCJNP micellar aggregates before CO_2 bubbling, after bubbling CO for 10 min and after subsequent N_2 bubbling for 10 min. (b) Reversible change in average hydrodynamic diameters, D_H, for PS-*b*-P(DMAEMA-*co*-CMA) SCJNP micellar aggregates upon repeated alternating CO_2/N_2 bubbling. TEM images of the micellar aggregates (c) before CO_2 bubbling, (d) after CO_2 bubbling for 10 min and (e) after subsequent N_2 bubbling for 10 min.....107

Figure 47. (a) Photos of three reaction solutions for AuNP formation at different times with SCNP1 (solution 1, with no CO_2), SCNP2 (solution 2, 30 s CO_2 bubbling) and SCNP3 (solution 3, 2 min CO_2 bubbling). (b)-(d) Absorption spectra of SCNP1, SCNP2 and SCNP3 solutions over reaction time, respectively. (e) Absorbance of AuNPs at 530 nm *vs.* reaction time for the three solutions. Insert is a zooming for the first 5 h of reaction. 110

Figure 48. Absorbance of AuNPs at 530 nm *vs.* reaction time for a solution bubbled with CO_2 for 30 s at first and then subjected to alternating CO_2/N_2 bubbling (each for 30 s)

and, for comparison, the same solution only bubbled with CO_2 for 30 s at the beginning of reaction. 111

Figure 49. Preparation of AuNPs using micelles of PS-*b*-P(DMAEMA-*co*-CMA) SCJNPs subjected to different CO_2 bubbling through the solution. (a)-(c) Absorption spectra of SA1 (no CO_2), SA2 (30 s CO_2 bubbling) and SA3 (2 min CO_2 bubbling) solutions over reaction time, respectively. (d) Absorbance of AuNPs at 530 nm *vs.* reaction time for the three solutions. Insert is a zooming for the first 3 h of reaction. (e) Absorption spectra of AuNPs solutions of SCNP3, SA1, SA2 and SA3, respectively, after 48 h of reaction. 113

Figure 50. TEM images of AuNPs prepared using (a) SCNP3, (b) SA1, (c) SA2 and (d) SA3 (see Table 5 for different samples). 114

Figure 51. Photos for aqueous solutions of P(MEO_2MA-*co*-MAA)-*b*-PEO-*b*-P(MEO_2MA-*co*-MAA) (10 wt%) containing AuNPs (0.12 wt%) prepared using SCNP3 (a, b) and SA3 (c, d) respectively, showing the gelation only occurred in the latter solution after exposure to 635 nm red light at room temperature for 10 min. 115

Figure 52. Photographs of thermal-induced of sol-gel transition of pure P(MEO_2MA-*co*-MAA)-*b*-PEO-*b*-P(MEO_2MA-*co*-MAA)..... 115

Figure 53. Preparation procedure of Janus SCNPs 123

LIST OF TABLES

Table 1. Covalent crosslinking chemistry for generating SCNPs 10

Table 2. Dynamic covalent crosslinking chemistry for generating SCNPs 16

Table 3. Non-covalent crosslinking chemistry for generating SCNPs 19

Table 4. Triple detection SEC data of PAzoMACMA precursors and SCNPs 77

Table 5. Conditions for the synthesis of AuNPs in water using nanoreactors of either P(DMAEMA-*co*-CMA) SCNPs or micelles of PS-*b*-P(DMAEMA-*co*-CMA) SCJNPs. 98

INTRODUCTION

Polymeric nanoparticles have attracted much attention in the field of nanoscience and nanotechnology due to the ease of fabrication and wide range of potential applications in many areas such as energy, biosensor, drug delivery system, specialty coating and high performance materials. (1, 2) However, the general particle sizes of 20-100 nm are not the best suitable for some applications with specific requirements. For example, in nanomedicine, it has been reported that drug delivery systems of less than 30 nm can avoid accumulation in the liver and spleen, as well as rapid renal exclusion. (3) Although the preparation of polymer nanoparticles above 20 nm is usually successful, it is still a challenge to develop fabrication techniques for sub-20 nm nano-objects with precise size control and tailored arrangement of functional groups. (4) There are various techniques reported in the literature to control the structure of synthetic polymers on the nanometer scale including the synthesis of sequence controlled polymers (5, 6), dendrimers (7), star polymers (8) and step-growth polymers with evenly spaced functional groups. (9) However, none of these can yield completely defined 3-D microstructures of polymers without any defects.

To solve these problems, scientists are looking for new technology inspired by nature. The capability of folding into functional nanostructures by precisely defined linear polymers is ubiquitous in nature. As a typical example, proteins have been found to function under unique conformations which require for the precise monomer sequence (primary structure), the formation of α-helices or β-sheets (secondary structure), determining the global morphology of the protein (tertiary structure) and promoting the formation of well-defined multi-aggregates (quaternary structure). (10, 11)

Therefore, in order to prepare well-defined sub-20 nm polymeric nanomaterials with biomolecule mimic functions, a new technology called 'single-chain technology', which produces nanoparticles by the manipulation of single polymer chains, has gained growing interests recently. (12) By means of these technologies, precisely defined linear polymer chains can be self-folded and formed so-called 'single-chain nanoparticles' (SCNPs) with well-defined three-dimension architecture *via* intramolecular crosslinking and collapse. (Figure 1) The general size of SCNPs are in the range of 1.5-20 nm. Although, the principle of SCNP formation is simple, it is quite complicated in practice including synthetic procedure and characterization. (13)

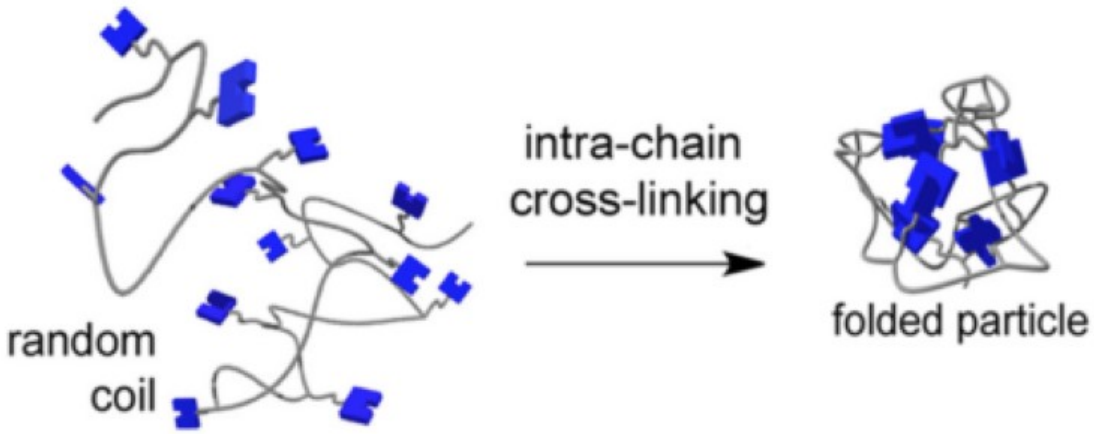

Figure 1. Conceptual illustration of single-chain folding of linear polymer. Reprinted with permission from [14].

The concept of SCNPs constructed *via* intra-chain crosslinking or collapse of single linear polymer precursors was introduced in 2002 by Mecerreyes, Miller and coworkers. (15) This pioneering work established a new pathway for polymeric nanoparticles fabrication, i.e.

manipulation of single polymer chain to form ultra-small functional nano-objects. In this 15 years, a number of reports provide a series of researches focusing on SCNPs including fabrication methodology, characterization technology and so on. However, several unsolved problems still exist and further research of SCNPs including functionalization and application are limited. (16)

Stimuli-responsive polymers, called 'smart polymers', are a kind of high performance materials that can change chemical and physical properties according to the surrounding environment. (17) Such materials can be sensitive to several types of stimuli, such as temperature, humidity, pH, gas, light with various wavelengths or intensities, and electric or magnetic field, and can respond in various ways, like altering colour or transparency, adjusting mechanical strength, becoming conductive or permeable to water or changing shape. Using stimuli-responsive polymers provides an interesting method to fabricate SCNPs due to the ease of controllability and efficiency. Moreover, stimuli-response can also provide possibilities for new functional SCNPs and new applications.

In this thesis, we are focusing on developing new functional SCNPs based on a variety of stimuli-responsive polymers. The stimuli include different wavelengths of UV/visible light, CO_2 and temperature. Furthermore, several applications of these functional SCNPs will also be reported. This introduction chapter will highlight the current research results of SCNPs and provide a brief background knowledge of the variety of stimuli-responsive polymers: (i) Fabrication methodology of SCNPs; (ii) Characterization techniques of SCNPs; (iii) Functional SCNPs; (iv) Potential applications of SCNPs; (v) Remaining challenges of SCNPs; (vi) Brief background of stimuli-responsive polymers and (vii) Objectives of the thesis.

I.1 Synthetic Methodology of Single-Chain Nanoparticles

The possibility to prepare nanoparticles *via* self-folding a linear polymer chain provides a simple method to fabricate ultra-small polymeric nanoparticles with size from 1.5 nm to 20 nm in diameter. The general strategy for the synthesis of SCNPs includes the collapse of a single polymer chain and the stabilization of the resulting nanoparticle by intra-chain crosslink. In most cases, the linear polymer precursors are first dissolved in a good solvent to leave the polymer chain molecularly dissolved and freely mobile. In addition, the SCNPs should be formed by self-folding the polymer precursors in very dilute solution (< 1 mg/mL) to get rid of inter-chain crosslinking. (4, 18-20)

According to the approaches to realizing self-folding of linear polymer chains, the preparation of SCNPs can be classified into four main strategies which are illustrated in Figure 2. (4) In the homo-functional chain collapse, the linear polymer precursors with reactive self-complementary 'R' groups can react intra-molecularly in the process of self-folding. The ratio of 'R' groups can be varied from 10-100 % and covalent or non-covalent crosslinking can be used. The hetero-bifunctional chain collapse strategy is using two complementary functional moieties ('R' and 'X') in one random copolymer to realize intramolecular crosslinking.

The crosslinker mediated chain collapse strategy makes use of an additional crosslinker for fabricating the SCNPs. The polymer chain with only one type of functional groups 'R', can be collapsed by reacting with the crosslinker with two 'X' end-groups. Except for dilute concentration condition, slowly adding one of the components to the other is also necessary to avoid intermolecular crosslinking. The one-block collapse strategy provides the possibility

to prepare a class of 'tad-pole' like single-chain nanoparticles. As shown in Figure 2d, the functional groups are just in one of the blocks of the polymer precursor and the intra-chain crosslinking can be performed in any of the previous three strategies. When the intramolecular crosslinking occurs, this block forms a compact globule and the rest of polymer chain still maintains as a coil. These tad-pole like SCNPs provide a possibility for further self-assembly.

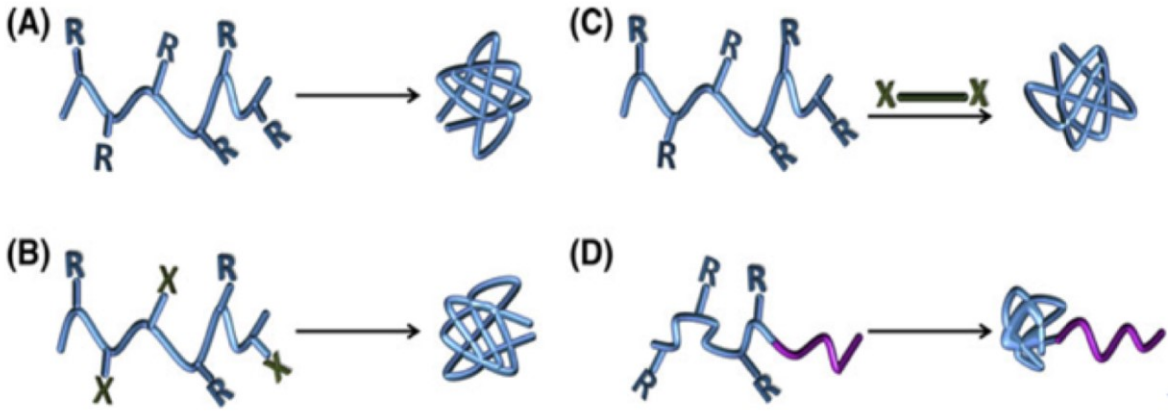

Figure 2. Schematic representation of the four strategies utilized for the synthesis of SCNPs: (A) Homo-functional chain collapse; (B) Hetero-bifunctional chain collapse; (C) Crosslinker-mediated chain collapse; (D) One-block collapse of diblock or triblock copolymers. Adapted with permission from [4].

Through these four strategies as described above, a number of synthetic methodologies have been reported to prepare SCNPs based on the use of various chemistry methods in recent years. Herein, we divide the discussion of intra-chain crosslinking chemistry into three major categories: covalent crosslinking chemistry, dynamic covalent crosslinking chemistry and non-covalent crosslinking chemistry.

I.1.1 Covalent crosslinking chemistry.

The intra-chain crosslinking *via* covalent crosslinking chemistry is a general method to fabricate SCNPs, because it provides irreversible and stable nanoparticles. However, SCNPs prepared *via* covalent crosslinking are unsuitable for some biomimetic applications, because the irreversibility of covalent crosslinking will lose the dynamic nature of SCNPs. (21) Table 1 summarizes the examples of SCNPs formed by covalent crosslinking chemistry including the illustration of chemical transformation and the chemical structure.

The intramolecular crosslinking of covalent bond was early studied by using functionalized polystyrene derivatives. Antonietti *et al.* studied the dynamic behavior of polystyrene micro-gels by using Friedel-Crafts alkylation chemistry as a crosslinking method and observed the existence of intramolecular crosslinking. (22) Davankov *et al.* utilized a similar method to obtain the intramolecularly hyper-crosslinked 'nanosponge'. (23) Free radical coupling was also used to prepare SCNPs in earlier studies, since there is no need to use any additional crosslinkers. Miller and coworkers reported the collapse of various polymers with acryloyl or methacryloyl groups *via* radical mediated intra-chain crosslinking. (15) Another example of free radical polymerization was reported by Jiang and Thayumanuvan to prepare amine-functionalized polystyrene nanoparticles. (24)

High temperature provides a good driving force for intramolecular dimerization reaction to prepare SCNPs. Hawker and coworkers synthesized architecture defined SCNPs *via* intramolecular dimerization of the benzocyclobutene (BCB) group at both high temperature (200 ºC) and low temperature (100 ºC) due to the '4+4' cycloaddition reaction. (25, 26) The size of this kind of SCNPs was observed with an average diameter in the range of 10-20 nm.

They also studied the morphology and physical properties of the nanoparticles formed by benzocyclobutene crosslinking chemistry. (27-29) The thermal cycloaddition was also used to prepare SCNPs by dimerization of benzosulfone. (30, 31) Pu and coworkers prepared SCNPs by thermal extrusion of nitrogen from sulfonyl azide groups at 190 ºC. However, the formed intra-chain crosslinks are not well-defined, because of the highly reactive nature of sulfonyl nitrenes. (32)

Moreover, the 'click' chemistry with high efficiency, high functional group tolerance and mild reaction conditions, provides an attractive means for synthesizing SCNPs. Luzuriaga *et al.* reported an efficient and convenient method to synthesize bioconjugable SCNPs *via* the copper(I)-catalyzed click chemistry. (33) The main advantages of using metal-mediated click chemistry are highly efficient and mild condition (the crosslinking can be conducted at room temperature). Another example of click-type chemistry used in SCNP formation is the copper-catalyzed alkyne homo-coupling Glaser-Hay coupling. Sanchez-Sanchez *et al.* prepared SCNPs based on poly(methyl methacrylate-*co*-propargyl acrylate) (poly(MMA-*co*-PgA)) by using this C-C click chemistry. (34) Other click chemistry methods including thiol-ene addition have also been used as crosslinking methods for SCNP formation. (35-38)

The fabrication methods of SCNPs *via* a variety of polymerization was also reported, such as the oxidative polymerization induced intramolecular crosslinking. (39) Dirlam *et al.* synthesized polystyrenic linear precursors based on a novel propylene dioxythiophene (ProDOT) functional styrenic monomer. The well-defined polymer precursors were subsequently oxidatively polymerized to promote tandem intramolecular crosslinking of ProDOT side chains and installation of electroactive moieties. (Figure 3) In addition, Pomposo and coworkers endowed SCNPs with enzyme-mimetic activity through cationic

polymerization of epoxide. (40) Ring-opening polymerization (ROP) is another crosslinking strategy for intra-chain crosslinking. Qiao and coworkers presented a kind of biocompatible SCNPs *via* organo-catalyzed ROP. (41) The intramolecularly crosslinking *via* ROP is reacted by benzyl alcohol (initiator) and methanesulfonic acid (organo-catalyst). A Similar ring-opening polymerization of benzoxazine was reported by Wang *et al.*in 2011. (42)

A number of photo-induced coupling reactions have been examined for SCNP formation due to their clean, high yielding and relatively fast. Altintas *et al.* applied photo-induced Diels-Alder reaction for the intramolecular crosslinking to prepare SCNPs. (43) Barner-Kowollik and coworkers exploited the use of photo-triggered nitrile imine-mediated tetrazole-ene cycloaddition (NITEC) for the generation of profluorescent SCNPs. (44) Berda *et al.* recently studied the potential of anthracene '2+2' light-induced cycloaddition as a suitable chemistry for SCNP fabrication. (45) Similar chemistry of cinnamoyl groups for SCNP formations was also reported. (46, 47)

In addition to those described above, there are other chemical reactions that can be used for covalent connection to fabricate SCNPs, including olefin metathesis (48), isocyanate-amine coupling (49), Bergman cyclization (50, 51), Menschutkin reaction (52), etc., which are just introduced briefly here.

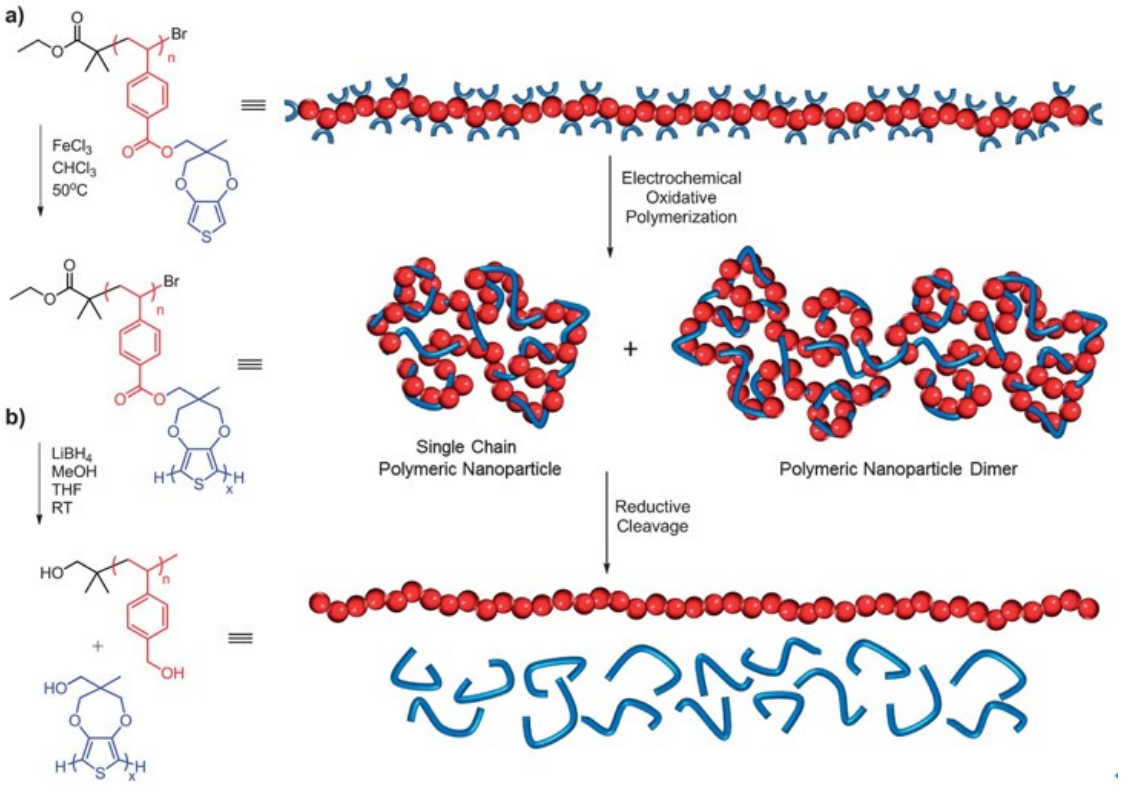

Figure 3. Synthetic route and graphical representation of (a) the oxidative polymerization of pendant ProDOT groups of poly(ProDOT-Sty) yielding conjugated polymeric nanoparticles and (b) their subsequent reduction to poly(vinylbenzyl alcohol) and poly(ProDOT-OH). Reprinted with permission from [39].

Table 1. Covalent crosslinking chemistry for generating SCNPs

Before crosslinking	Structure of crosslink	Type of chemistry
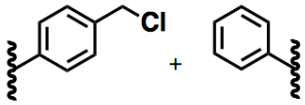	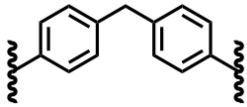	Friedel-Crafts alkylation (22, 23)
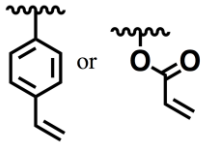	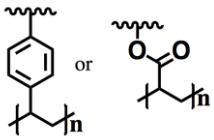	Free radical coupling (15, 24)
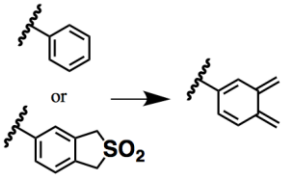	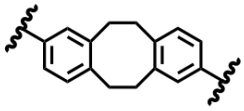	Thermal [4+4] cycloaddition (25-31)
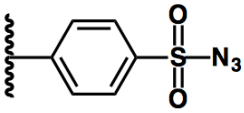	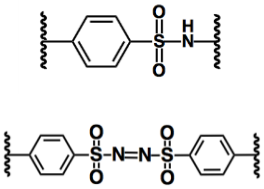	Sulfonyl nitrene coupling (32)
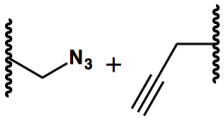	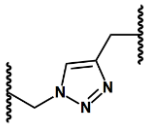	Azide-alkyne 'click' chemistry (33)
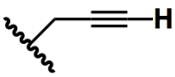	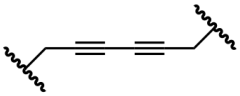	Glaser-Hay coupling (34, 36)
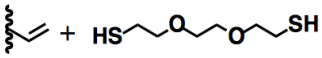	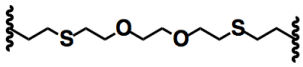	Thiol-ene 'click' chemistry (38)

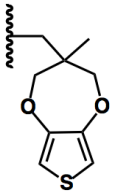	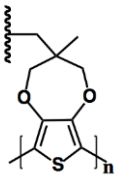	Oxidative polymerization of thiophene (39)
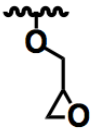	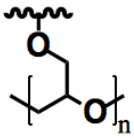	Cationic polymerization of epoxide (40)
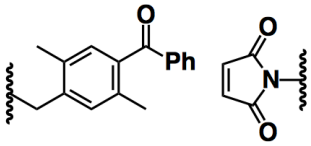	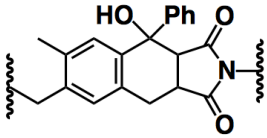	Photo-induced D-A reaction (43)
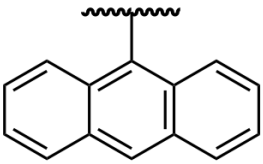	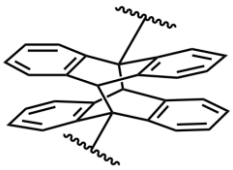	Photodimerization of anthracene (45)
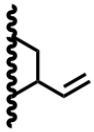	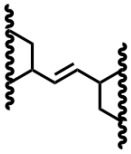	Olefin metathesis (48)
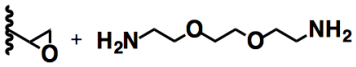	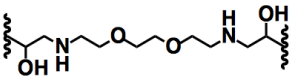	Epoxide-amine (49)
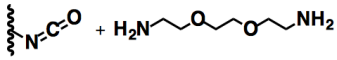	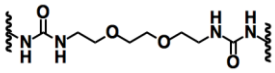	Isocyanate-amine (49)
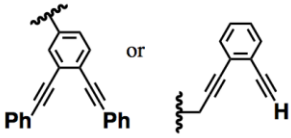	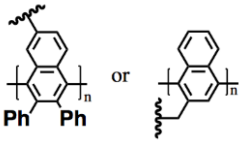	Bergman cyclization (50, 51)
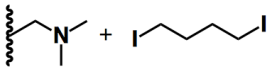	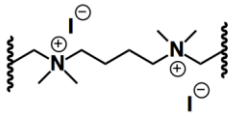	Menschutkin reaction (52)

I.1.2 Dynamic covalent crosslinking chemistry

Dynamic covalent crosslinking is an interesting method to fabricate SCNPs. In principle, the dynamic covalent bonds can perform reversibly in nature and can be kinetically fixed or cleaved under a variety of stimuli. (53-55) Table 2 summarizes the examples of dynamic covalent crosslinking chemistry for SCNPs preparation.

Disulfide chemistry is one of the general reactions in dynamic covalent chemistry. Moreover, disulfide chemistry is the method for making covalent bridges in protein and is sensitive to redox chemistry. The intra-chain crosslinking of disulfide chemistry was first reported by Ravi and coworkers to prepare water soluble polyacrylamide nanogels, with size ranging from 20 to 200 nm. (56) Berda and coworkers demonstrated an interesting approach to reversible single-chain collapse based on disulfide linkages. (57) The reduction of the disulfide groups allows the particle to unfold into a coil and the re-oxidation of the resultant thiols leads the coil to refold into a particle.

Enamine chemistry is another class of dynamic covalent chemistry for preparation of reversible SCNPs. Enamine bonds can be formed by condensation reaction of ketones with amines and can be easily reversible under acidic condition. Pomposo and coworkers exploited the use of enamine 'click' chemistry for metal-free poly(methyl methacrylate) (PMMA) nanoparticles at room temperature. They further synthesized pH-responsive SCNPs by using the same chemistry. (58, 59)

In addition, hydrazide chemistry as the crosslinking method is also a suitable chemistry for intra-chain collapse. Fulton and coworkers demonstrated that the linear polymer chain of poly(vinylbenzaldehyde) (PVBA) could be intramolecularly crosslinked through the

formation of dynamic covalent acylhydrazone bonds with a bis-hydrazide crosslinker. (60) Furthermore, the hydrazide crosslinking chemistry was used to prepare thermo-responsive dynamic covalent nanoparticles that can reversibly transform into hydrogels. (61) In their work, the SCNPs was prepared based on oligo(ethylene glycol)methoxy methacrylate (OEGMA) copolymers that feature reactive aromatic aldehyde functions, which serve as handles for the formation of acyl hydrazine crosslinks. The obtained SCNPs exhibited the thermo-responsive property of the parent polymer chain and formed a hydrogel network when the temperature is above the LCST of polymer precursor. (Figure 4)

In our group, we focus on SCNP formation *via* photo-induced reversible cycloaddition. Coumarin-containing polymers can be reversibly crosslinked upon UV irradiation with different wavelengths, which provide an ideal approach to prepare SCNPs. He *et al.* firstly reported SCNPs preparation based on P(DMAEMA-*co*-CMA) (Poly{(N,N-dimethylaminoethyl methacrylate)-*co*-4-methyl-[7-(methacryloyl)oxy-ethyl-oxy] coumarin}). (62) The SCNPs can be formed *via* photo-dimerization reaction of coumarin under >310 nm UV irradiation. In addition, upon irradiation under 254 nm UV light, partial reverse photo-decrosslinking was observed. (Figure 5). The coumarin based polymers were further reported to be used in preparation of SCNPs with LCST and the LCST of the obtained SCNPs was increased with the degree of intramolecular crosslinking. (63)

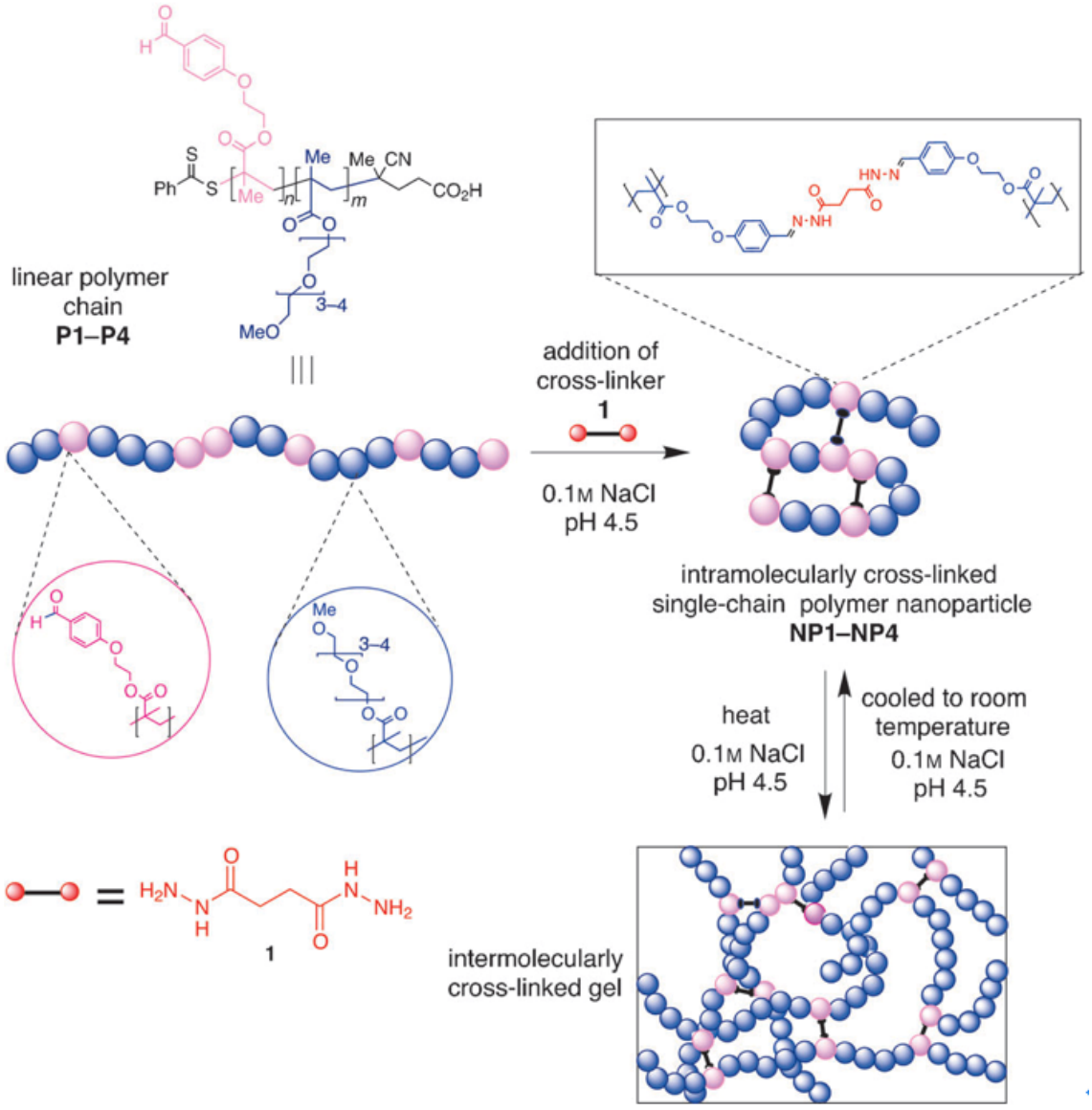

Figure 4. Conjugation of polymer chains to form intramolecularly crosslinked SCNPs, and their subsequent reversible transformation into an intermolecularly crosslinked hydrogel. Adapted with permission from [61].

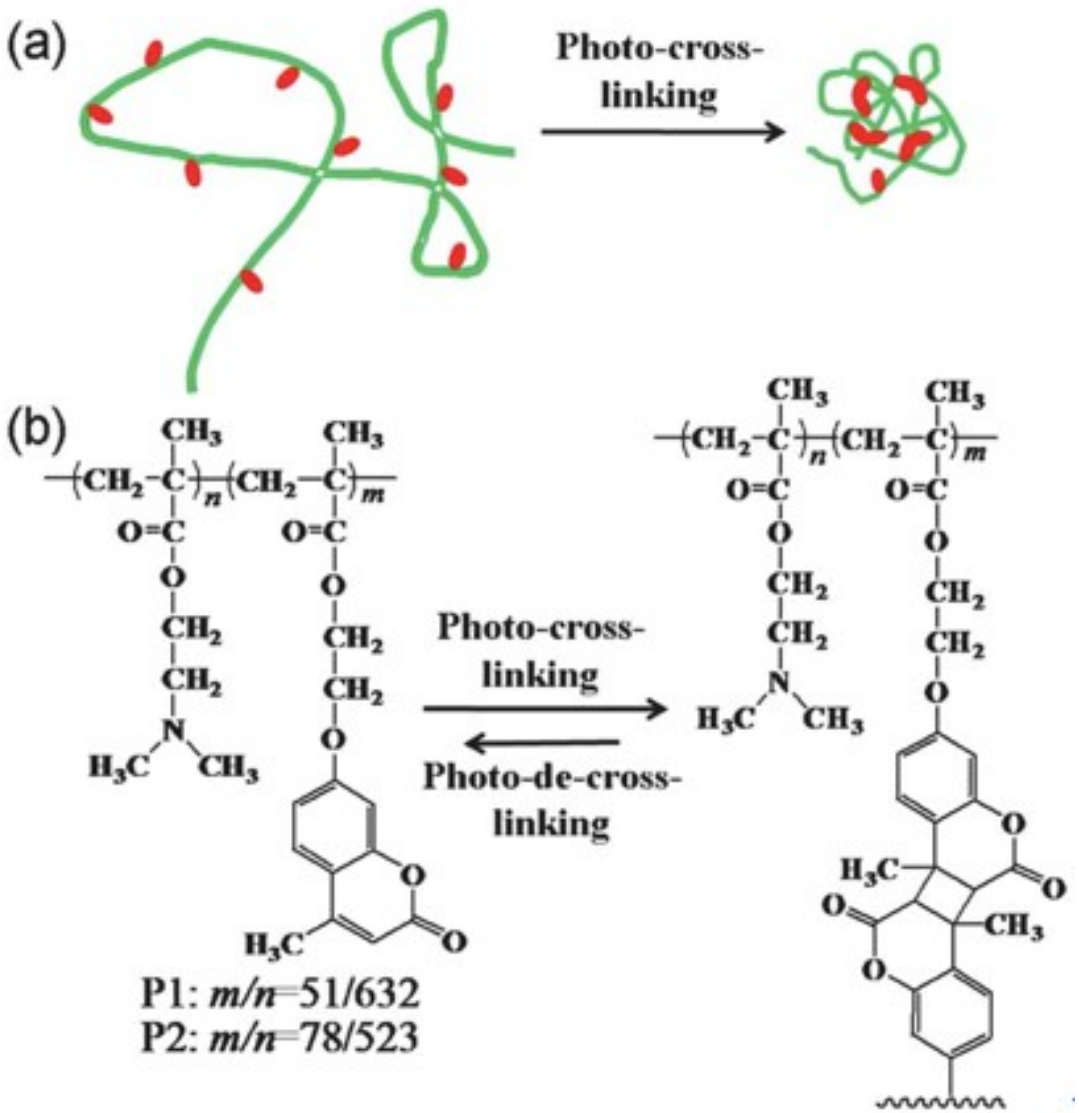

Figure 5. (a) Schematic illustration of preparation of polymer SCNPs through intra-chain photo-crosslinking. (b) Chemical structures of coumarin-containing random copolymers of P(DMAEMA-*co*-CMA) and the reversible photo-crosslinking reaction activated by UV light at two different wavelengths. Adapted with permission from [62].

Table 2. Dynamic covalent crosslinking chemistry for generating SCNPs

Before crosslinking	Structure of crosslink	Type of chemistry
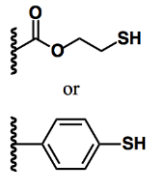	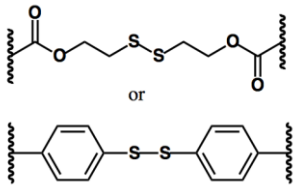	Disulfide formation (56, 57)
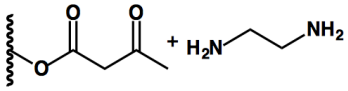	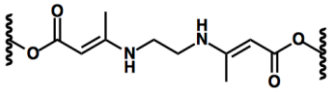	Enamine formation (58, 59)
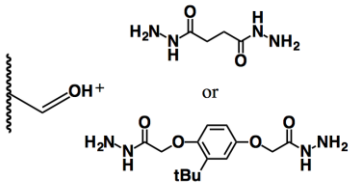	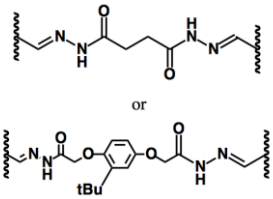	Hydrazone formation (60, 61)
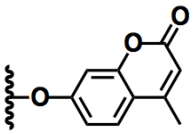	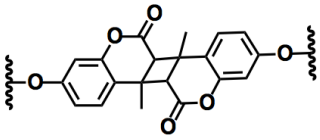	Photodimerization of coumarin (62, 63)

I.1.3 Non-covalent crosslinking chemistry

Non-covalent crosslinking chemistry plays an important role in the formation of SCNPs, that can be used to prepare thermodynamically stable SCNPs. Due to the relatively low energy barriers of non-covalent interactions, it may be possible to achieve reversible collapse of a single-chain polymer by changing external conditions for specific applications, such as, drug delivery, smart adaptable systems and self-healing. (21) Table 3 summarizes the examples of non-covalent crosslinking chemistry for SCNPs preparation.

Hydrogen bonding as a common non-covalent interaction has been examined in SCNP synthesis by many groups. In general, the hydrogen bonding units are protected in some way to prevent the polymers from forming aggregates during their synthesis. (Figure 6) (64-67) The use of hydrogen bond to form SCNPs was firstly reported by Hawker and coworkers. They synthesized a series of SCNPs based on dimerization of benzamide which is driven by non-covalent crosslinking of dendritic self-complementary hydrogen-bonding units (SHB). (64) Meijier and coworkers demonstrated SCNPs formation based on dimerization of uriedopyrimidinone (UPy) in several publications. (65-67) They refer to these SCNPs as in 'metastable' condition, because the film of SCNPs remains soluble in $CHCl_3$ and becomes insoluble as the result of the formation of an insoluble supramolecularly crosslinked network. In addition, the preparation of PS chain bearing α,ω complementary hydrogen-bonding motifs was reported by Altintas *et al.* The hydrogen bonding recognition units, based on both three-point thymine (Thy)-diaminopyridine (DAP) and six-point cyanuric acid (CA)-Hamilton wedge (HW) interactions, induced a single chain self-folding process. (68-70)

Metal complexation is another major non-covalent crosslinking for SCNP formation. Barner-Kowollik group synthesized a class of SCNPs *via* organometallic bonds. The SCNPs were formed by using telechelic triphenylphosphine macromolecular ligands capable of binding to a Pd metal center. (71, 72) Lemcoff and coworkers recently reported a series of SCNPs through complexation of rhodium(I). They also demonstrated the kinetic process of rhodium complexation formation *via* both experimental and theoretical study. (73-75) In addition, Jeong *et al.* synthesized SCNPs through the intra-chain formation of copper phthalocyanine from polystyrene-*co*-poly[4-((4-vinylbenzyl)oxy)phthalonitrile] under diluted conditions. (76)

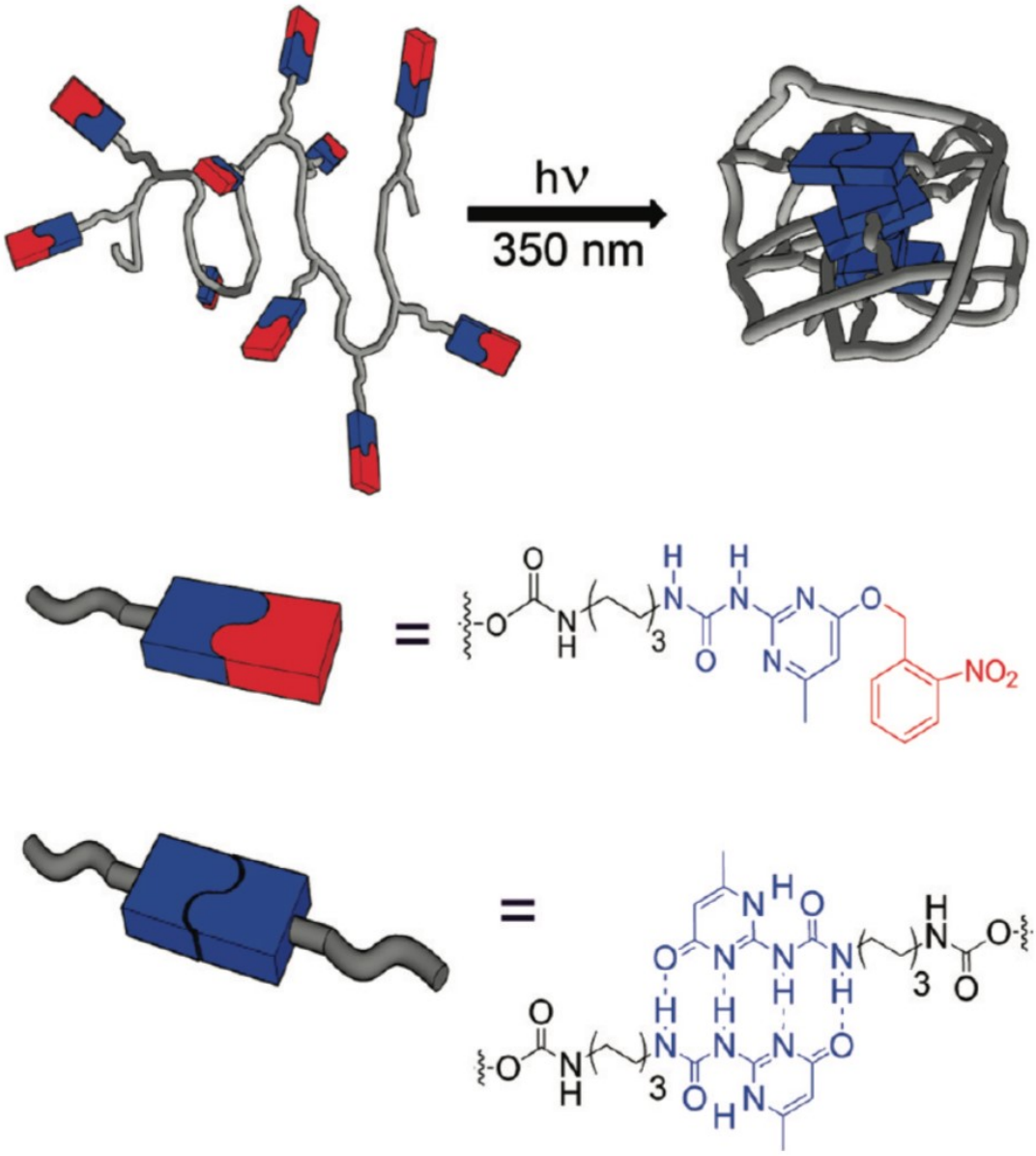

Figure 6. UV irradiation induced collapse of a single polymer chain into a nanoparticle for an example that the functional group with hydrogen bonding units are protected in some way to prevent forming aggregation. Reprinted with permission from [66].

Recently, Scherman *et al.* reported a class of SCNPs based on host-guest interaction of cucuribit[n]urils. (77) In their work, methylviologem and naphthyl funcationalized polymers were complexed with cucurbit[n]urils to form ternary host-guest complexes. However, due to the huge aromatic molecules, the SCNPs formation was only observed in extremely dilute solution: 0.1 mg/mL, that is only one-tenth of typical concentration of SCNPs. Above 0.1 mg/mL, significant aggregation was observed. In addition to the mentioned studies, other non-covalent interactions were also reported to be useful in forming single-chain nanoparticles such as hydrophobic interaction (78) and π-stacking (79).

Table 3. Non-covalent crosslinking chemistry for generating SCNPs

Before crosslinking	Structure of crosslink	Type of chemistry
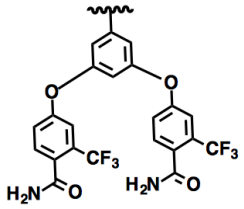	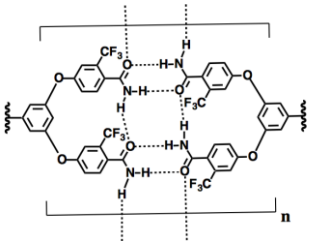	Benzamide dimerization (64)
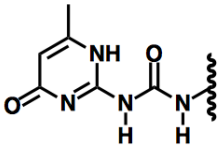	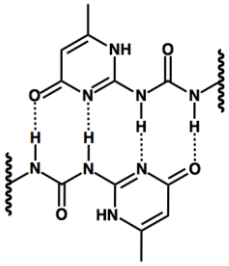	UPy dimerization (65-67)

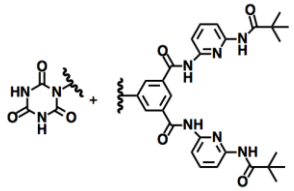	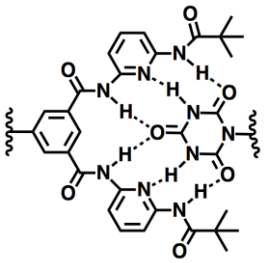	Hamilton's wedge-cyanuric acid association (64-66)
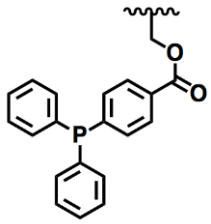	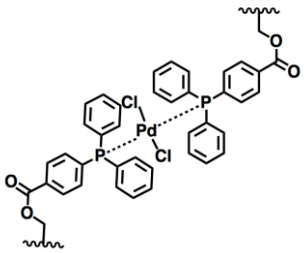	Palladium coordination (71, 72)
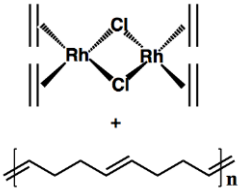	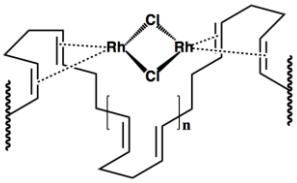	Rhodium coordination (73-75)
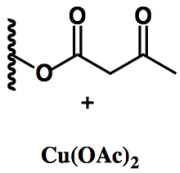	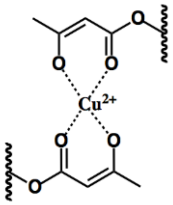	Copper coordination (76)
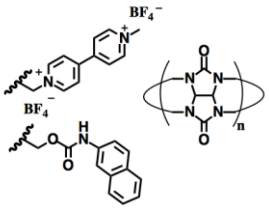	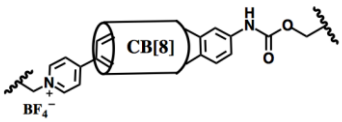	Host-guest interaction (77)
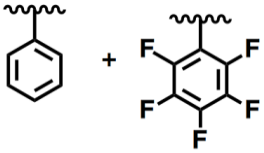	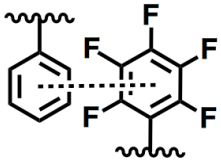	π-stacking (79)

I.2 Characterization Techniques of Single-Chain Nanoparticles

There are many techniques that can be used to characterize SCNPs. The main purposes of characterization of SCNPs is to detect the process of intra-chain crosslinking and to investigate the size and morphology of SCNPs. Due to the definition of SCNPs, it is necessary to prove the nanoparticles are formed by a single polymer chain without any intermolecular crosslinking or aggregation. Therefore, it is necessary to choose techniques which are sensitive in low concentration to detect the aggregates formed by intermolecular crosslinking and to prove single polymer chain forming nanoparticles. (13)

I.2.1 Size-Exclusion Chromatography (SEC)

Size-exclusion chromatography (SEC) with conventional calibration is one of the standard techniques used to characterize SCNPs formation. It consists in comparing the retention times of the linear polymer precursors and SCNPs, since intramolecular crosslinking, which brings the polymer chain to a more compact structure, typically shifts the elution peak to longer retention times. (14) This result indicates a decrease in hydrodynamic volume for SCNPs based on the working principle of SEC. (80-82) On the other hand, no extra peak appears in short retention time can prove that there is no intermolecular crosslinking occurred. Importantly, to prove the SCNP formation by SEC, one should ensure that this is truly an effect of conformational changes and not due to different interaction between the SEC columns, or any other factors. For examples, Figure 7 shows the SEC trace of polymer precursor and SCNPs folded by intra-chain dimerization of pendant anthracene units. (45) The peaks of SCNPs shift to longer retention time as irradiation time increases which indicates a reduction in hydrodynamic volume and proves single chain forming nanoparticles.

However, there are still some weakness for conventional SEC, especially with regards to actual changes in molecular weight (or lack thereof) before and after intra-chain crosslinking. (14) Because the conventional SEC is only used to measure the relative molecular weight and retention time, it is impossible to characterize the absolute molecular weight of SCNPs. On the other hand, although the shifting of retention time indicates the decrease of hydrodynamic volume, it is impossible to quantify these changes with conventional SEC measurements alone.

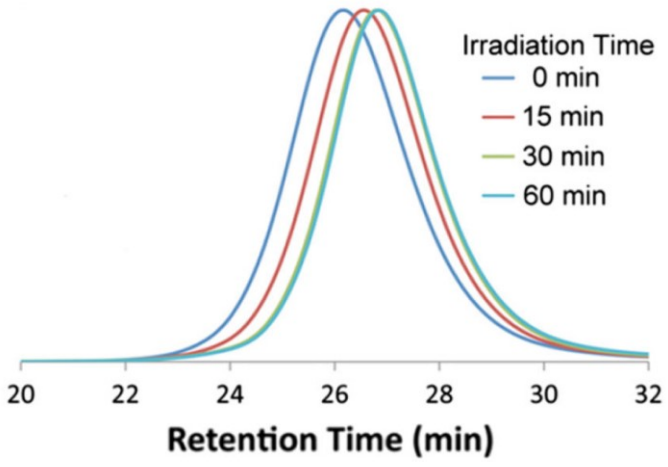

Figure 7. SEC traces of polymer precursor and single-chain nanoparticles with different irradiation time describing the characterization of SCNP formation *via* SEC. Reprinted with permission from [14].

Recently, Berda's group reported a new system of SEC with triple detections to characterize the formation of SCNPs. In addition to the conventional SEC with UV or RI detector, the new system contains multi-angle light scattering (MALS) detection and viscometer detection. (14) The use of MALS detection with SEC allows the determination of absolute molecular

weight which is independent of retention time. By using SEC with MALS detection, the absolute molecular weight (weight-average molecular weight) of polymer precursor can be easily measured which is the same as SCNPs. (83) The inline differential viscometer detection can characterize the molecular deformation including hydrodynamic volume, for each thin chromatographic slice as the sample elutes from the SEC column. (45) With this system, changes in hydrodynamic volume of linear polymer precursors and SCNPs can be measured quantitatively. Furthermore, in Berda's experience, MALS is capable of detecting multi-chain aggregates in minimum concentrations while traditional SEC with UV or RI detectors is not. (45, 57) As shown in Figure 8, multi-chain aggregates were detectable *via* MALS while virtually unseen in RI traces. (45)

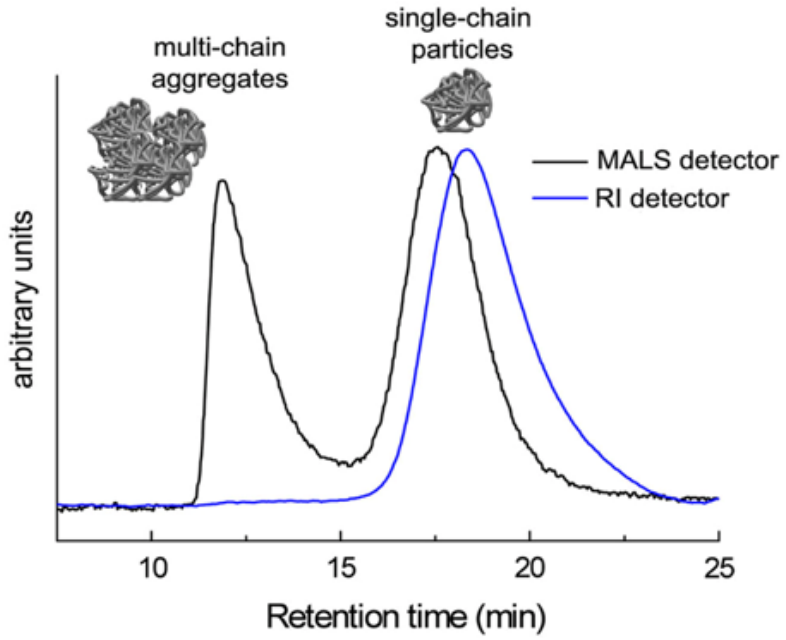

Figure 8. MALS and RI detection traces for SEC of SCNPs highlighting the ability of MALS to detect large, multi-chain aggregates. Adapted with permission from [14].

I.2.2 Viscometry

Solution viscometry is a valuable technique in the characterization of SCNPs. Firstly, the viscometry can be used to measure the molecular weight and size of SCNPs in solvent. The relationship between intrinsic viscosity and molecular weight of polymer is known by the Mark-Houwink equation. (Eq. I.1). The hydrodynamic volume (V_H) and hydrodynamic radius (R_H) can be further calculated by viscometry *via* Einstein-Simha Relation. (Eq. I.2&I.3)

Mark-Houwink Equation: $[\eta] = KM^a$ [I.1]

Einstein-Simha Equation: $V_H = M[\eta]/(2.5N_A)$ [I.2]

Einstein-Simha Equation: $R_H = (3V_H/4\pi)^{1/3}$ [I.3]

Where [η] is intrinsic viscosity, K and a are constants characteristic of the polymer and solvent, M is molar mass, and N_A Avagadro constant.

Secondly, viscometry can also be used to characterize the SCNPs formation. From previous research in our group, the relative viscosities of linear polymer P(DMAEMA-*co*-CMA) and SCNPs were measured in THF at room temperature respectively (Figure 9). (62) The relative viscosity of the linear polymer increased rapidly with increasing polymer concentration due to strong intermolecular interaction. By contrast, the increase in relative viscosity of SCNPs becomes negligible when increasing the concentration of SCNPs. This behavior indicates less intermolecular interaction of collapsed SCNPs and induces less increase of the solution viscosity because of a lower degree of entanglement of SCNPs. Hawker and coworkers have also found a similar phenomenon during SCNPs formation. (49)

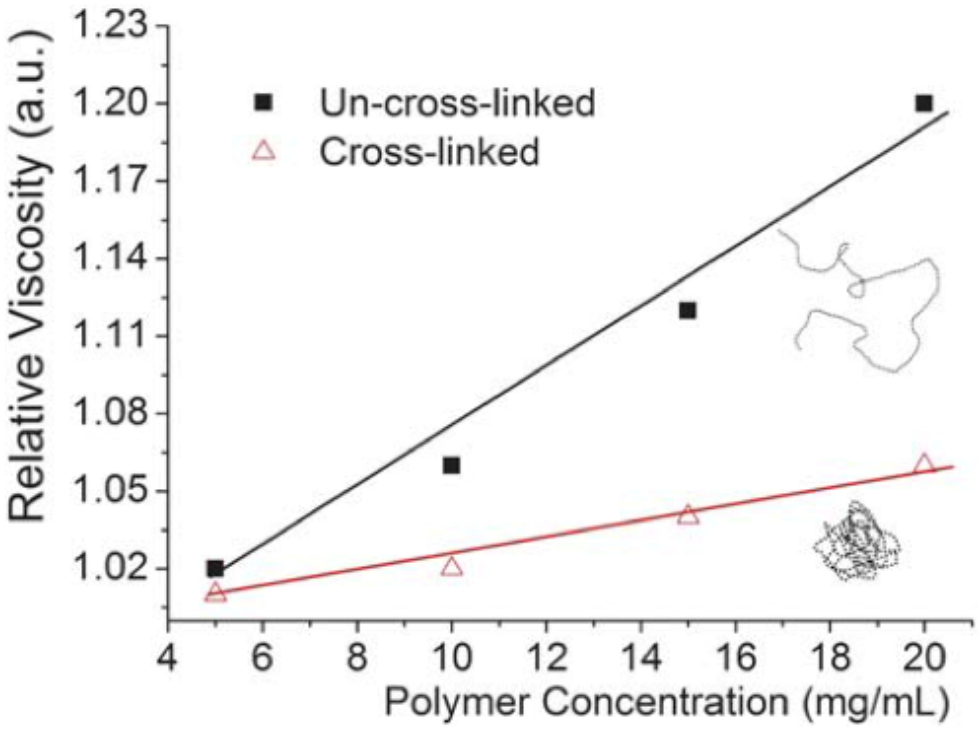

Figure 9. Relative viscosity of linear polymer and SCNPs at various concentrations. Reprinted with permission from [62].

I.2.3 Nuclear Magnetic Resonance Spectroscopy (NMR)

NMR spectroscopy can usually be useful to prove coil-to-particle transition of SCNPs by monitoring the appearance or disappearance of signals from crosslinkers. Moreover, Loinaz and coworkers confirmed the SCNP formation of Poly(N-isopropylacrylamide) by 2D-DOSY experiments. (84) From 2D-DOSY measurement, the increase of the diffusion coefficient which is inversely proportional to the hydrodynamic volume, provides the evidence of SCNP formation. In our group, the coil-to-globule transition induced by intra-chain photo-crosslinking of coumarin was investigated by using ^{1}H-NMR spin-spin relaxation time (T_2) which is sensitive to molecular motion. (62)

I.2.4 Atomic Force Microscope (AFM)

One of the most important aspects of the characterization of SCNPs is to measure their size and morphology. Primarily atomic force microscopy (AFM) provides insight into the size and shape of SCNPs. To obtain well-separated SCNPs, the samples should be prepared in very dilute solution (at least 10 times dilution of SCNP preparation concentration) for AFM measurements.

Meijer and coworkers did several research works on characterization of SCNPs by AFM. They deduced the possible morphology of SCNPs formed from different polymer chain through AFM measurements. (65, 66) The well-separated SCNPs can be observed by AFM under very low concentration and the size distribution of SCNPs was similar to the SEC results. (Figure 10) At high concentration, the SCNPs can aggregate and the degree of aggregation is dependent on variety of factors, such as solvent, concentration and rate of evaporation. Slow evaporation resulted in an increase in aggregation. They concluded that the major factors affecting the morphologies observed by AFM are nanoparticle mobility before solvent evaporation and the rate of solvent evaporation. Moreover, in another study of Meijer *et al.*, they show a direct relationship between molecular weight of the polymer precursor and size of the SCNPs by AFM. An increase in molecular weight of the polymer precursors results in an increase in size of SCNPs (Figure 11). (85) However, although AFM can be used to characterize the size and shape of the SCNPs directly, several factors are still not clear, such as the effect in absence of solvent and the interaction between nanoparticles and substrates. On the other hand, it is difficult to find the exact position of well-separated SCNPs on the mica due to the limitation of scanning areas and slow scanning rate. The tip of AFM may also change the morphology of SCNPs during the measurement. (13)

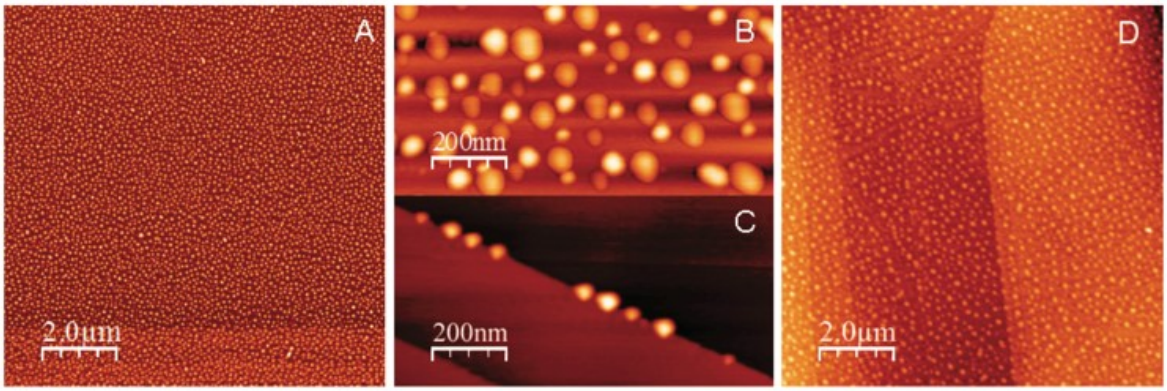

Figure 10. AFM images of well-separated single-chain nanoparticles prepared on mica (a,b) and graphite (c, d) under dilute concentration. Reprinted with permission from [65].

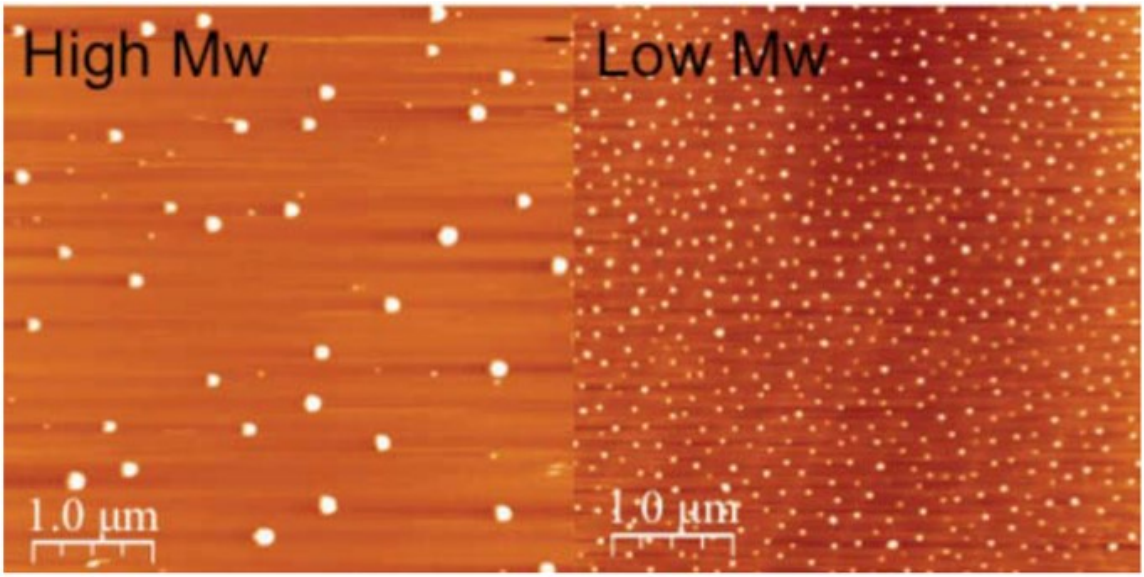

Figure 11. AFM images of SCNPs display the relationship between molecular weight and single-chain nanoparticles size. Reprinted with permission from [85].

I.2.5 Other characterization techniques

In addition to these characterization methods described above, several techniques have also been reported in characterizing SCNPs. Dynamic light scattering (DLS) is a very useful method to measure the size of SCNPs and their aggregates. Unlike AFM, DLS can be used to measure the hydrodynamic volume of SCNPs and their size distribution, and to characterize the effect of solvent on SCNPs. However, high dilution of SCNPs solution will affect the accuracy of DLS, which is confirmed by several groups. (38, 86, 87)

Transmission Electron Microscope (TEM) is another useful method to characterize the size and morphology of SCNPs. TEM is an efficient characterization method compared with AFM, although it can only provide 2D images of SCNPs. On the other hand, it is reported that TEM results have better diameter correlation with DLS data than AFM, most likely due to the error resulting from the broadness of the AFM tip. Zhao and coworkers measured the size of multiple SCNPs by AFM, TEM and DLS. (52) They found that the AFM results showed larger diameter while TEM results are closer to the hydrodynamic volume measured by DLS. Similar conclusion was also reported by Pomposo. In their study, TEM can provide a more accurate size of SCNPs as they behave in solution. (40)

Recently, Barner-Kowollik's group introduced high-resolution electrospray ionization mass spectrometry (ESI-MS) as a powerful tool to assess the folding of a collapse linear polymer into a SCNP. (88) The ESI-MS can characterize the mass changes of SCNPs and polymer precursor which provide detailed mechanistic information regarding the folding mechanism.

I.3 Development of Functional Single-Chain Nanoparticles

In addition to the research on synthesis and characterization methods of SCNPs, developing functional SCNPs is equally important for SCNPs studies. However, the difficulty of maintaining the function in SCNPs system and characterizing their properties become the main barrier limiting the development of functional SCNPs. Currently, few reports report functional SCNPs prepared by specific designing of polymer precursors and introducing stimuli-responsive polymers. Although some groups have already reported some examples for functionalization of SCNPs, the studies of these two aspects are still not complete.

I.3.1 Functional SCNPs based on rational design of polymer structure

Most examples of functional SCNPs are achieved by introducing the functional groups into the polymer precursors. Therefore, the rational design of the polymer structure is necessary to prepare functional SCNPs.

Barner-Kowollik and coworkers designed functional fluorescent SCNPs by subsequent one-pot postpolymerization modification with a protected maleimide and tetrazole moiety. The residual surface expressed tetrazole moieties can be reacted with maleimide functional polymeric microsphere to further functionalize and prepare fluorescent SCNPs. (44) They show that these SCNPs feature a broad fluorescence band (500-700 nm) in biocompatible excitation ranges (>400 nm), making them ideal candidates for intracellular transport imaging applications (Figure 12). They also reported fluorescent SCNPs based on tetrazole chemistry directly in pure water recently. (89)

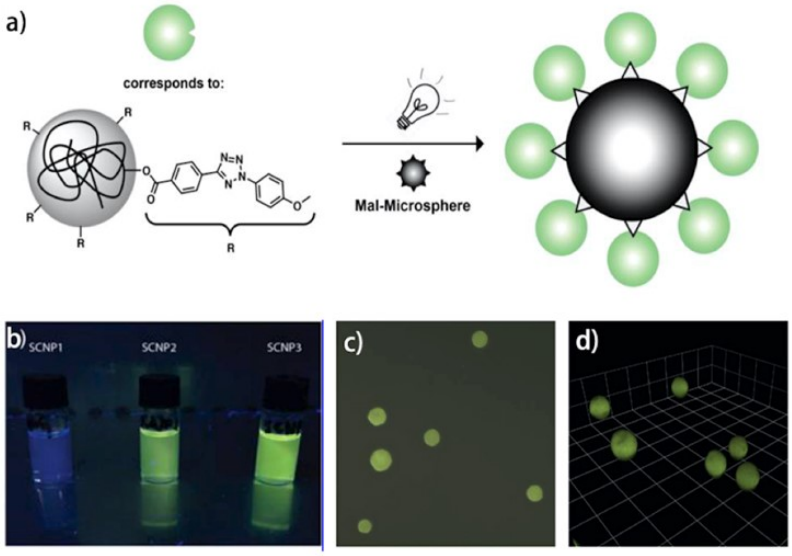

Figure 12. (a) Synthetic scheme of the profluorescent SCNP with Maleimide-functional microspheres. (b) Image of SCNP dispersed in THF under 366nm UV irradiation. (c, d) Fluorescence microscopy and 3-D reconstruction of a confocal image stack of SCNP. Reproduced and rearranged with permission from [44].

For biomedical applications, Qiao's group reported a kind of biocompatible SCNPs based on poly(oligo(ethylene glycol) acrylate precursors containing pendent lactone moieties. Furthermore, cytotoxicity studies revealed that this kind of SCNPs, which were covalently crosslinked by biodegradable polyester linkages, were nontoxic toward human embryonic kidney (HEK293T) cells. (41) In a recently report, Loinaz's group described a straightforward way to biocompatible and easy to handle dextran-based SCNPs and provided the possibility to conjugate biomolecules to the nanoparticle by incorporating chemical reactive groups. (90)

Functional SCNPs can also be realized to be size- and shape-controllable. Xie *et al.* prepared SCNP with exactly one functional group exposed on their surface. The mono-functional

SCNPs were prepared by sparse grafting on the surface on sacrificial silica spheres. When the SCNP were removed from the silica particles, dumbbell-like SCNP dimers were prepared *via* a one-to-one coupling reaction between the SCNPs (Figure 13). (47) Zhao's groups synthesized mono-tailed SCNPs from amphiphilic polymer precursor. Depending on the block length and the size of SCNPs, the mono-tailed SCNPs can be self-assemble into micellar or vesicular structures (Figure 14). (52, 91)

These examples of functional SCNPs were prepared based on well-designed chemical structure of polymer precursors and under specific condition. Therefore, it is necessary to develop a simple idea to design and prepare functional SCNPs.

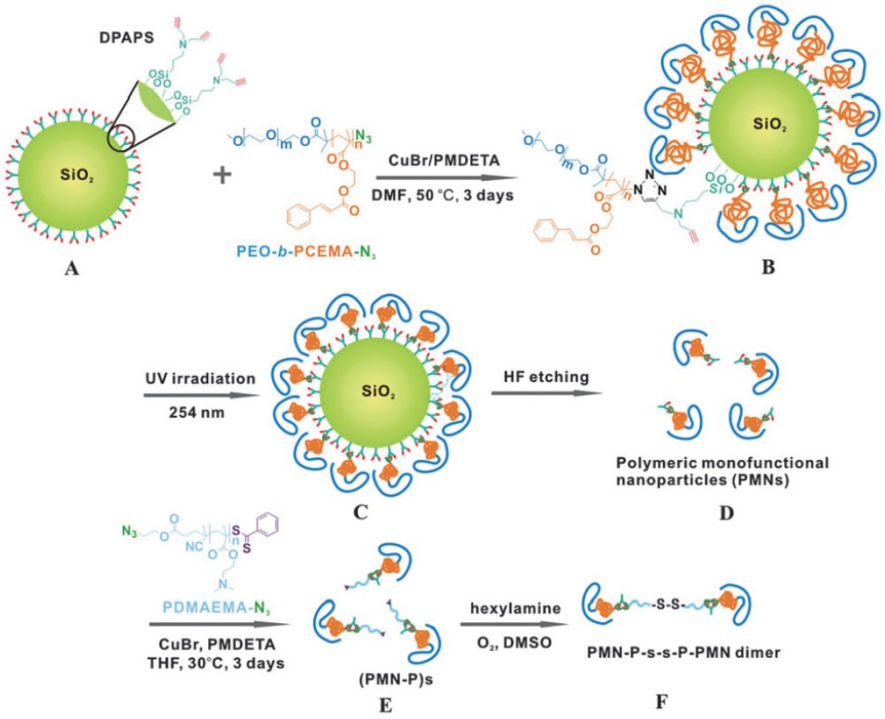

Figure 13. Processes for preparation of polymeric mono-functional nanoparticles. Reprinted with permission from [47].

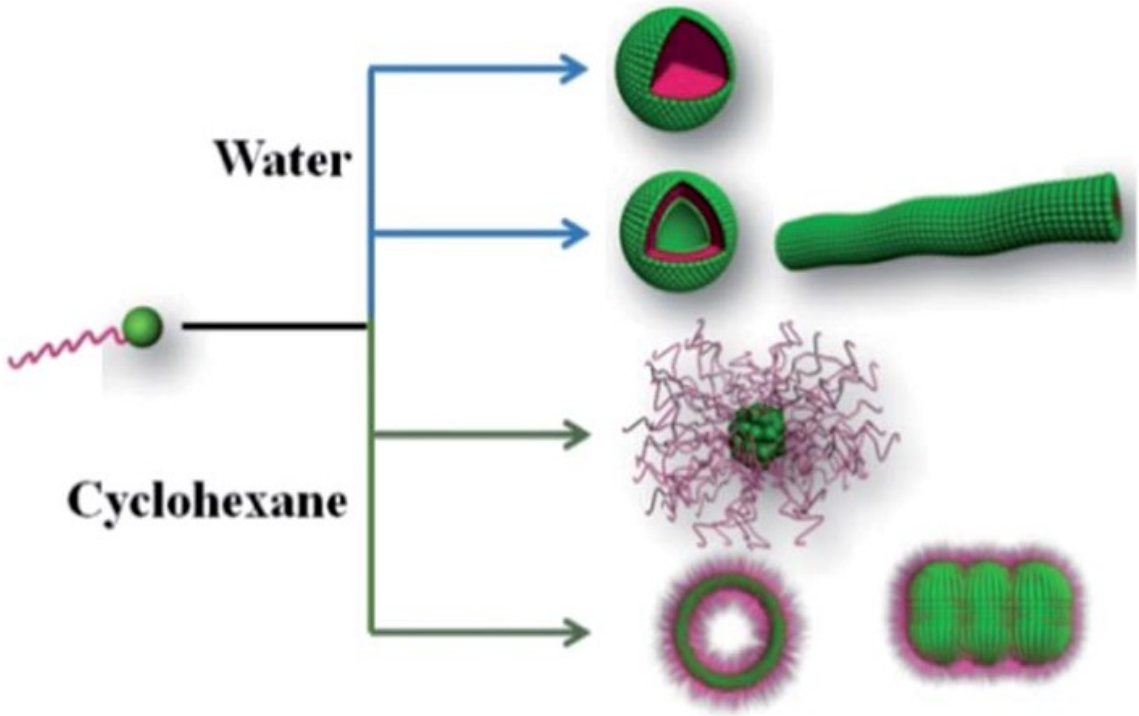

Figure 14. Schematic depiction of the self-assembly of monotailed SCNPs into aggregates with different morphologies. Reprinted with permission from [91].

I.3.2 Functional SCNPs based on stimuli-responsive polymers

The introducing of stimuli-responsiveness to SCNPs provides a facile method to develop SCNPs not only for fabrication, but also for functionalization. Due to their convenience and efficiency, these kinds of SCNPs can respond to external stimuli (such as pH, (59, 65) light, (92) redox, (57) temperature, (61, 84, 93) ultrasonic (94) and etc.) to realize the self-folding procedure and change the morphology and properties of the SCNPs and their aggregates.

Some groups have already reported studies on functional SCNPs from a variety of stimuli-responsive polymers. Loinaz's group prepared SCNPs from poly(N-isopropylacrylamide)

(pNIPAM), a typical thermo-responsive polymer with lower critical solution temperature (LCST). (84) The resulting SCNPs also showed thermo-responsiveness and their LCST and cloud point (CP) were very close. Moreover, sharp transition curves were observed for linear polymer precursors. Furthermore, the thermo-responsive properties of SCNPs were studies in all the pH range, which indicated that transmittance *vs.* temperature curves were buffer and salt concentration dependent. Thayumanavan and coworkers reported a kind of redox-responsive SCNPs with host-guest features. They highlight that the SCNPs exhibit host-guest properties to stably encapsulate hydrophobic guest molecules and can be released in response to a trigger by unraveling the nanoparticles. (95) Pu and Che introduced voltage-responsive polymers to SCNP system. The SCNPs based on poly(N-(2-hydroxyethyl)acrylamide) with pendant β-cyclodextrin performed reversible transformation of coil-to-particle *via* external voltage stimuli (Figure 15). (96) Recently, Ding *et al.* prepared photo-responsive SCNPs from reactive star azo-polymers. Under UV and visible light irradiation, the SCNPs exhibit size-tunable properties due to photo-isomerization reaction of azobenzene moieties. (97) Ultrasound and pH were also used as stimulus for responsive SCNPs. (59, 94)

Our group is one of the earliest groups to develop stimuli-responsive SCNPs. In a previous study, we developed thermo-responsive SCNPs based on poly(N,N-dimethylaminoethyl methacrylate) (PDMAEMA). (63) In addition, the cloud point (or LCST) was optically tunable depending on different intramolecular dimerization degree (by adjusting UV irradiation time) due to a topological effect. However, preparing functional SCNPs from stimuli-responsive polymers is still challenging and not widely studied due to the difficulty of maintaining the stimuli-responsiveness in the SCNP system and characterization of their properties. (Figure 16)

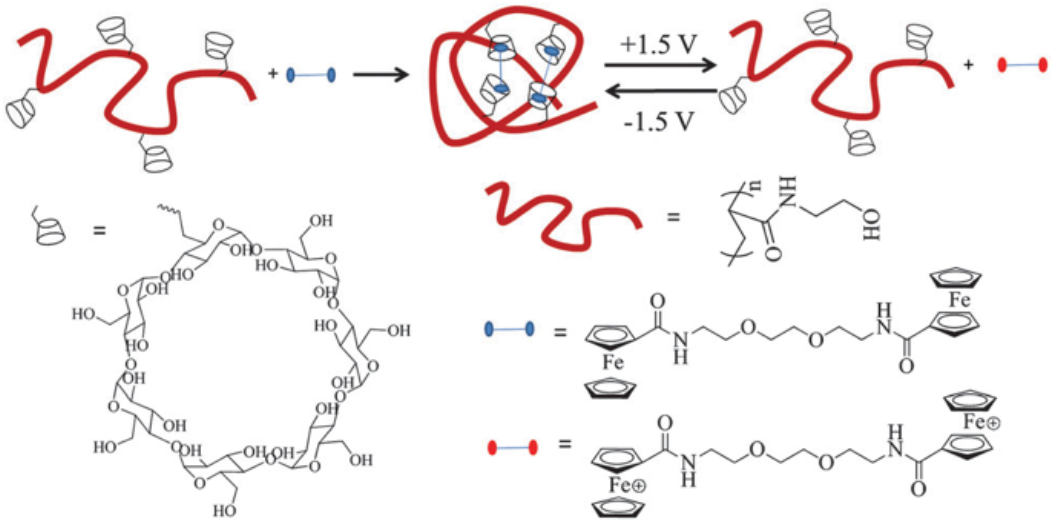

Figure 15. Schematic representation of the formation of SCNPs *via* host-guest interaction and the voltage responsiveness of SCNPs. Adapted with permission from [96].

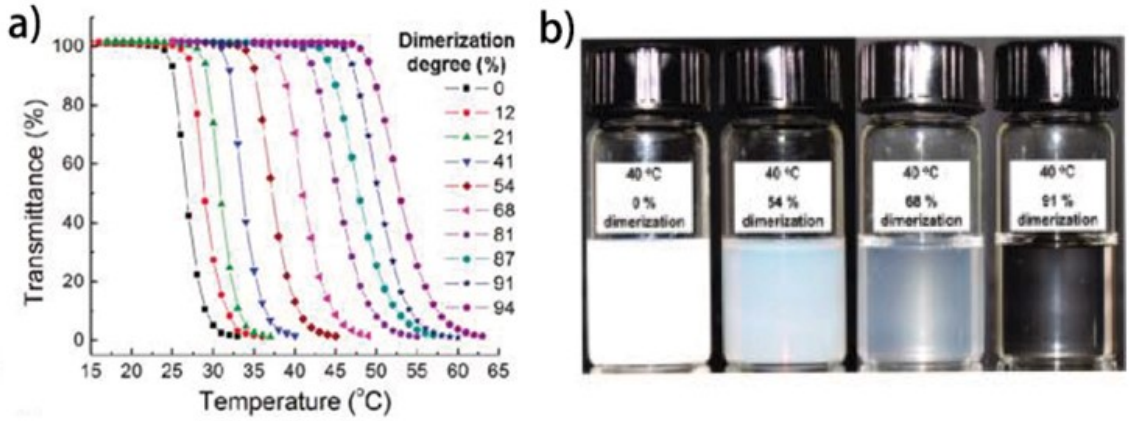

Figure 16. (a) Transmittance change as a function of temperature for SCNPs solution with different photo-dimerization degree (b) Photographs of SCNP solution at 40°C with different dimerization degree which demonstrate the photo-tunable LCST properties of SCNPs. Reproduced and rearranged with permission from [63].

I.4 Potential Applications of Single-Chain Nanoparticles

Although the research of SCNPs has been primarily fundamental, these materials were also found to possess some practical uses. The advantages of SCNPs technology include the ultra-small size of the nanoparticles and the ease in which they can be tailored to specific uses. (13) Recently, a series of applied research involving SCNPs were reported including catalysis, sensors, nano-reactors and biomedical applications.

Gillissen *et al.* reported SCNPs from self-folded 3, 3-bis(acylamino)-2, 2-bipyridine substituted benzene-1, 3, 5-tricarboxamide (BiPy-BTA) grafted polynorbornene polymers that act as compartmentalized sensors for metal ions. (79) These SCNPs are effective sensors for metal ions due to their affinity to the 2, 2-bipyridine units. Pomposo and coworkers synthesized a class of catalytically active SCNPs based on metallo-folded polymer chains containing complexed Cu(II) ions. (98) The SCNPs were then used as a catalyst for alkyne homo-coupling. In addition, Bai *et al.* reported SCNPs from Cu(II)-mediated intramolecular crosslinking of aspartate-containing polyolefins. (99) The SCNPs can be used as highly efficient supramolecular catalysts for alkyne-azide 'click chemistry' reactions, yielding the desired 1, 4-adducts at low parts per million catalyst levels. From the previous work in our lab, the SCNPs based on P(DMAEMA-*co*-CMA) were used as nano-reactors to synthesize gold-nanoparticles (AuNPs) *in situ*. (62) The experiment was conducted in both THF and water, and AuNPs formation was faster when increasing the degree of intra-chain crosslinking.

In the field of biomedical applications, Loinaz's group prepared a kind of biocompatible SCNPs based on poly(methacrylic acid) and functionalized with the somatostatin analogue

PTR86 as the targeting moiety. The SCNPs were proved for targeting and imaging pancreatic tumors *in vivo*. (100) In a recent work, Nguyen and coworkers designed a random polymers containing oligoethylene glycol (OEG), amine and hydrophobic groups to prepare SCNPs which can kill planktonic and biofilm bacteria. The hydrophobic groups can influence membrane cell wall disruption to affect antimicrobial activity and the OEG side chain serves to prevent undesirable protein complexation. The SCNPs exhibit excellent antimicrobial activity against Gtam-negative bacteria at micromolar concentration and remarkably kill over 99.99 % of both planktonic cells and biofilm within an hour. (101) In addition, SCNPs can also be used as gene delivery vectors which reported by Gao and coworkers. (102)

I.5 Remaining Challenges of Single-Chain Nanoparticles

Although several groups studying SCNPs have already reported a number of works for developing SCNPs ranging from fabrication, characterization, functionalization to applications, there are still some unresolved issues and challenges for SCNP research. Recently, Berda's group listed the main challenges and innovation needs for advancement in the field of SCNPs. (16) There are mainly three aspects: improvement of preparation and characterization methods, precise biomimicry of biomolecules based on SCNPs, development of functionalizations and applications.

For fabrication of SCNPs, a limitation in most SCNP syntheses is the requirement of dilute polymer solution to avoid the occurrence of intermolecular interactions. However, the high dilute conditions reduce the practicality of large scale industrial production of SCNPs. Therefore, it is necessary to find practical scalable methods to prepare SCNPs. Moreover, although a series of characterization techniques have been reported, the characterization of

the internal folding structure of SCNPs has not yet been fully demonstrated.

Secondly, one of the purposes of SCNPs is to mimic the biomolecules such as protein. Proteins can undergo guided precise folding in solution to complex structures stabilized by noncovalent or covalent interactions. Unique functions of these natural materials are a derivative of their shape, which is imparted by the precise folding process. (10, 103) Therefore, the precise folding of SCNPs is necessary for proteins biomimicry. Even if there are some examples reporting step-wise folding of SCNP formation by different crosslinking units, it is still difficult to control the chain folding during the process of SCNPs formation. (104-107) Because of that, complex synthetic design of polymer precursor and using simulation may provide possibilities to achieve the controllable folding. What's more, self-assembly of SCNPs can further mimic tertiary structure of biomolecules.

Finally, further developing new functions of SCNPs and expanding their applications are very important to make the SCNPs practically used. Currently, the examples of functional SCNPs are quite simple, that is, most of functional SCNPs have only a single function. Therefore, there is a need to explore the possibility of introducing stimuli-responsive polymers to prepare multi-functional SCNPs, because it may provide more possibilities of potential application of SCNPs.

I.6 Brief Background of Stimuli-Responsive Polymers

Stimuli-responsive polymers are a kind of high performance materials that can change their chemical and/or physical properties in response to changing environmental conditions. (108, 109) These polymers can respond to stimuli in many ways including light transmitting ability, conductivity, shape, solubility, wettability and so on. The degree of response of these

polymers can be easily controlled by the intensity of applied stimuli. Many researchers have already developed a large number of stimuli-responsive polymers for a variety of stimuli such as, temperature, (110, 111) pH, (112) electric/magnetic field, (113, 114) exposure to light, (115-117) gas, (118-122) ultrasound (123, 124) and etc. (Figure 17) These smart polymers can be highly suitable for numerous household and industrial applications. (109) In what follows, we provide some background information about the common stimuli and the specific stimuli-responsive functional groups used in this thesis.

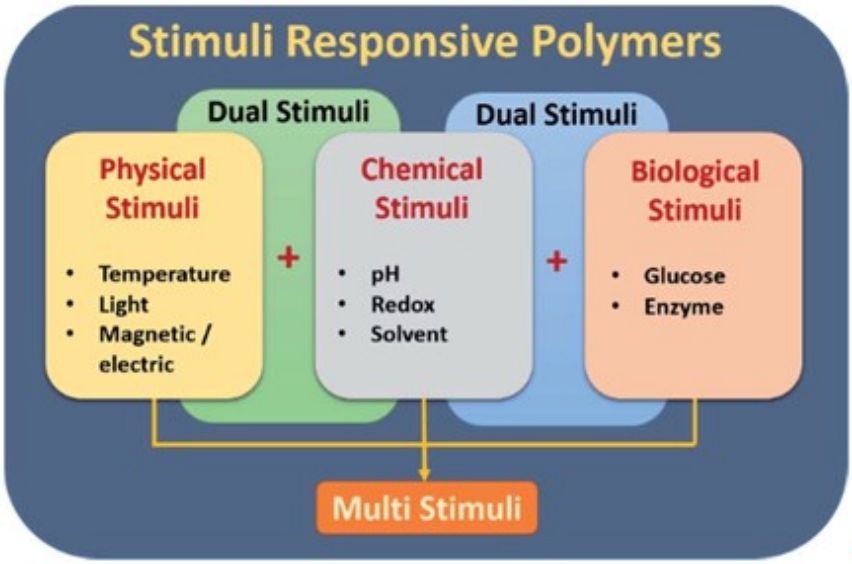

Figure 17. Classification of stimuli-responsive polymers. Adapted with permission from [108].

I.6.1 Stimuli-responsive polymers sensitive to various stimuli

<u>I.6.1.1 Light as stimulus</u>

Light is one of the most desirable external stimuli for smart polymers due to its high accuracy

and easy control. The energy of external stimuli can be controlled by irradiation time and intensity of light. Light-responsive polymers have been widely developed from deep ultra-violet to infra-red which allows diversity in application. Many reports show that photo-activation can be used to control various polymer properties such as release or capture of additives, light activated bending, modulation of refractive index, or phase behavior. Highly investigated photo-responsive molecules include azobenzene (*trans-cis* isomerization) (125), spiropyran (spiro to merocyanine form) (126), spirooxazine (spiro to merocyanine form) (127) and coumarin (photo-dimerzation and cleavage). (128)

I.6.1.2 Temperature as stimulus

Thermo-responsive polymers play a unique role in stimuli-responsive polymers, because temperature as stimulus can easily be applied from outside of the polymers. Generally, thermo-responsive polymer systems possess a critical solution temperature at which the polymer system undergoes a phase change within a small temperature range due to the disruption of intra- and/or inter- molecular interactions resulting in the expansion or contraction of polymer chains. (108) The typical thermo-responsive properties can be divided into lower critical solution temperature (LCST) and upper critical solution temperature (UCST). LCST polymer solution remains monophasic below LCST and turns into bi-phasic when increasing temperature above LCST. On the contrary, UCST polymer solutions have one phase at the temperature above UCST and become phase-separated below that temperature. Several thermo-responsive polymer systems have already been reported such as poly (N-alkyl substituted acrylamides) (129), poly(N-vinylalkylamides), (130) copolymers of acrylamide and acrylonitrile (131) and etc.

I.6.1.3 pH as stimulus

pH-responsive polymers can donate or accept protons according to the environmental change of pH. The adjustment of the pH value controls the protonation degree, which may trigger a solubility change of the polymer in aqueous solution. (112, 132) Typical pH-responsive polymers include polyacids, such as poly(acrylic acid) (133) and polybases such as poly(N,N-dimethyl aminoethyl methacrylate). (134) The polyacids are able to release their protons and swell under basic condition. The polybases can accept protons under acidic condition and expand due to coulomb repulsion. (109)

I.6.1.4 CO_2 as stimulus

Recently, CO_2-responsive polymers have attracted increasing interest. CO_2-responsive groups can be protonated by CO_2, an acid gas, and easily deprotonated by purging inert gases or heating to remove CO_2. Unlike pH-responsive polymers, this reversible process can be repeated for many cycles without the accumulation of byproducts. (119, 120) What's more, CO_2 is a non-toxic, inexpensive, benign and abundant gas which is very suitable for applications in industry. A series of CO_2-responsive polymers have been widely investigated including polymers bearing amidine, imidazole and amine groups.

I.6.2 Stimuli-responsive molecular structures used in this thesis

I.6.2.1 Coumarin

Coumarin is identified as a class of benzopyrone compounds, all of which consist a benzene ring fused to a pyrone ring which shows absorbance in the ultraviolet region and fluorescence

in the visible light range. (135) As a typical class of photo-active units, coumarin and its derivatives have been widely used in many functional polymeric materials due to their tunable photo-responsive properties including photo-dimerization and photo-cleavage. Upon irradiation over 300 nm, coumarin derivatives undergo [2+2] cycloaddition to yield cyclobutane dimer. (136) The cycloaddition reaction of coumarin is reversible when irradiation at a shorter wavelength (<300 nm). The reversible photo-dimerization reaction of coumarin has been observed both in solution and solid state. (Scheme 1) In addition, some coumarin derivatives such as esters or phosphates substituted at the 4 position undergo photo-cleavage under <300 nm UV irradiation due to the photolysis mechanism. (137) In addition, as a natural substance, most coumarin derivatives are biocompatible which become highly attractive for potential applications in biomedicine.

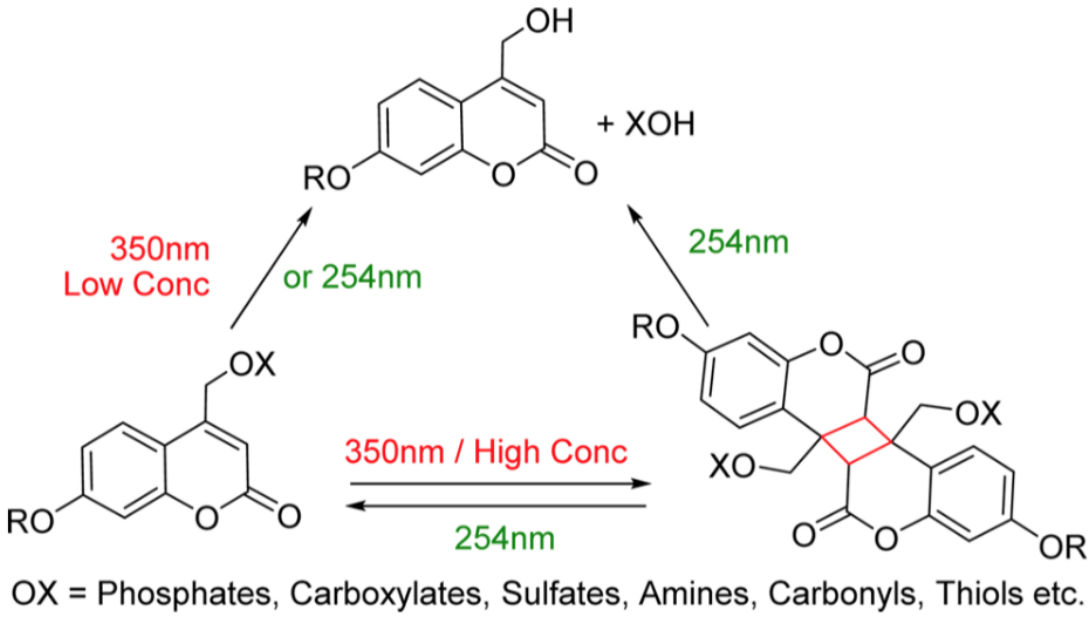

Scheme 1. Photochemical reactions of coumarin compound. [128]

I.6.2.2 Azobenzene

Azobenzene, a kind of diazene derivative where both hydrogens are replaced by phenyl groups can exist in either *cis*- or *trans*- conformation. (138) Generally, azobenzene and its derivatives undergo *trans*- to *cis*- isomerization under UV irradiation due to the π-π* transition of *trans* azobenzene. (139) The reverse *cis*- to *trans*- isomerization can be driven by visible light or heating in the dark due to n-π* transition of *cis*- azobenzene. (Scheme 2) As their photo-induced isomerization process is excellently reversible, azobenzene-containing polymers are highly interesting for various applications such as liquid crystal and shape memory materials. (125, 140, 141)

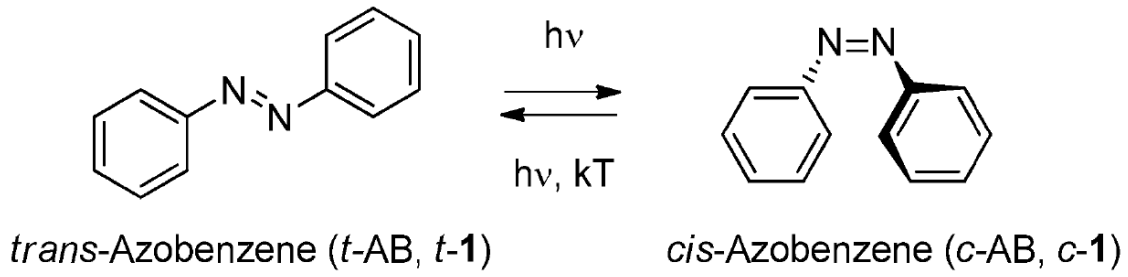

Scheme 2. Photoisomerization of azobenzene. [138]

I.6.2.3 2-(Dimethylamino)ethyl methacrylate (DMAEMA)

2-(Dimethylamino)ethyl methacrylate (DMAEMA) is a typical multi-stimuli-responsive functional group. Its homopolymer PDMAEMA has been found to have a cloud point in the range of 20-50 ºC in neutral aqueous solution. (142) In addition, increasing the pH can shift the LCST of PDMAEMA to higher values due to the protonation of the tertiary amine group. Interestingly, the protonation reaction can also occur after the addition of CO_2 which

increases the hydrophilicity of PDMAEMA. Meanwhile, this process is reversible, and PDMAEMA can be deprotonated by bubbling inert gases. (143) (Scheme 3) Due to their multi-stimuli-responsiveness (thermo-, pH- and CO_2-), DMAEMA has been widely used in many random copolymers and block copolymers to prepare functional materials including nanoparticles, (62) self-assemblies (144), hydrogels (143, 145) and so on.

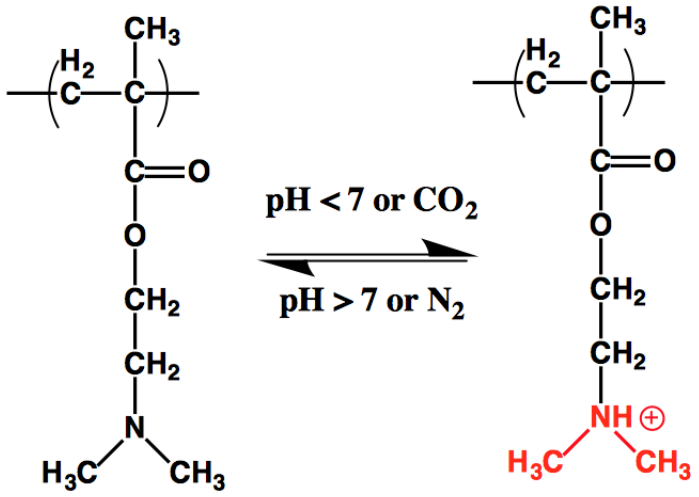

Scheme 3. Protonation/deprotonation of PDMAEMA by pH or gas stimulation.

I.7 Objective of the Thesis

The main objective of this thesis is to develop multi-functional polymeric SCNPs and expand their applications. To achieve this goal, we introduced various stimuli-responsive polymers as polymer precursor to prepare functional SCNPs. We hypothesized that the stimuli-responsive property should persist in the SCNPs system and these stimuli-responsive SCNPs can respond to external stimuli to perform different functions. We aim to find a general

approach to prepare functional SCNPs and expect to expand new potential applications. Therefore, we have designed three projects to confirm our hypothesis. Our accomplished research work can be divided into three parts presented in the following three Chapters.

In Chapter 1, we prepared a series of SCNPs based on photo-responsive main-chain coumarin-containing polyesters. We hope to introduce both of the photo-responsive properties of coumarin (photo-dimerization and photo-cleavage) in the SCNPs by incorporating coumarin moieties into the backbone of the polymer chain. Due to the photo-responsiveness of main-chain coumarin based polyester, several functions of this kind of SCNPs were studied including photo-degradablility and size-tunability. Finally, owing to the biocompatible and biodegradable nature of the polyesters, this kind of SCNPs have the potential to be exploited for biomedical applications.

In Chapter 2, we prepared a kind of SCNPs based on side-chain liquid crystalline azobenzene based polymers. On one hand, we aimed to answer two questions in this project. Firstly, by introducing azobenzene moieties into a SCNP system, we wanted to know whether or not the photo-isomerization of azobenzene still occurs in the SCNPs. Secondly, due to the liquid crystalline nature of the polymer precursor, we wanted to know whether the LC phase can retain in such tiny compact nanoparticles. We expect that both LC order and photo-isomerization of azobenzene properties can be retained inside the confined, crosslinked nanoparticles. On the other hand, similar with azobenzene-containing polymers and colloid particles, due to the photo-responsive properties of azobenzene, the SCNPs may exhibit a number of interesting and intriguing functions including solvent-sensitive fluorescence, photo-induced deformation and mechanically stretching-induced orientation which will provide new possible applications in the field of bio-imaging and LC materials.

In Chapter 3, to further introduce diverse stimuli-responsiveness in SCNPs, we chose a kind of multi-stimuli-responsive polymers P(DMAEMA-*co*-CMA) to prepare SCNPs and study their properties. Since the thermo-responsiveness of SCNPs based P(DMAEMA-*co*-CMA) had already been studied in the previous work, we mainly focused on their CO_2-responsiveness. First, the CO_2-responsiveness of SCNPs was found to result in LCST-shifting and reversible size change under CO_2 stimulation. The CO_2-responsive SCNPs can also be used to prepare gas-sensitive micelles which self-assembled by tadpole-like single-chain 'Janus' nanoparticles (SCJNPs) prepared by amphiphilic block copolymers of PS-*b*-P(DMAEMA-*co*-CMA). Furthermore, both CO_2-responsive SCNPs and their micelles of SCJNPs can be used as nano-reactors to prepare gold nanoparticles (AuNPs), and CO_2 stimulation allows for control in reaction rate and AuNP size.

Lastly, in Chapter 4, we make a further discussion for our studies and provide a number of ideas that are worth pursuing as future work.

CHAPTER 1 PHOTODEGRADABLE AND SIZE-TUNABLE SINGLE-CHAIN NANOPARTICLES PREPARED FROM A SINGLE MAIN-CHAIN COUMARIN-CONTAINING POLYMER PRECURSOR

1.1 Introduction

Functional polymer nanoparticles have attracted much attention because of their potential applications in many areas such as energy, biosensors and high performance materials. (1, 2) However, preparing well-defined polymeric nanoparticles with sizes below 20 nm is still challenging. In recent years, single-chain nanoparticles, being formed by one polymer chain *via* a unimolecular coil-to-particle transition, have gained increasing interest because their ultra-small sizes (1.5-20 nm) could lead to unique properties potentially useful for drug delivery, nano-reactor and bio-mimic systems. (3, 4, 15, 19, 49, 52, 61, 63, 67, 84, 94, 105, 107, 146-149) For instance, when employed as a drug carrier, such small sizes allow SCNPs to avoid uptake by the reticuloendothelial system and also prevent rapid renal exclusion. (146)

SCNPs are prepared *via* intramolecular crosslinking (42, 57) or collapse (65) and both covalent and non-covalent associations can be exploited to compress a single coil of polymer chain into a nanoparticle. (12) A number of SCNP preparation methods have been reported based on the use of various chemistries for intra-chain crosslinking, including photochemical reactions, (45, 62, 150) dynamic bonding, (59) polymerizations, (39) Diels-Alder reaction, (86) metal complexation, (98) click chemistry (34) and host-guest interactions. (77) In most cases, pendant reactive moieties were used for intra-chain crosslinking. In addition to developing efficient preparation methods, the ability to effectively control the size of SCNPs is also of major importance for practical applications. Obviously, the size of SCNPs can be

varied by changing the molecular weight of the used polymer precursor. (85) A study also showed the control of size by adjusting the content of crosslinkable units in a polymer chain, which determines the intra-chain crosslinking density. (44) In other words, the preparation of SCNPs of variable sizes requires the synthesis of various polymer precursors with either different molecular weights or different compositions. Notably, in a recent study of preparing SCNPs through photo-dimerization of pendant anthracene units, (45) Frank *et al.* showed a continuous shift of the size exclusion chromatography (SEC) peak towards longer retention times with increasing UV irradiation time, suggesting that SCNPs of varying sizes can be obtained from a single sample.

Herein we report a facile method that allows photodegradable SCNPs of variable sizes to be obtained from a single polymer precursor containing photo-crosslinkable units in the chain backbone. As shown in Figure 18, the method is based on the use of a polyester precursor bearing coumarin moieties in the main chain structure. We demonstrate that with the polymer dissolved in dilute solution, SCNPs can be obtained by the intra-chain photo-dimerization of coumarin groups upon >320 nm UV light irradiation, and that the size of SCNPs is tunable by varying the dimerization degree of coumarin moieties that is controlled by the UV irradiation time. Moreover, the polymer structure design also allows the photo-cleavage of coumarin to occur under 254 nm UV irradiation, which results in chain scission. (128) The latter photochemical reaction was utilized to impart the function of photo-degradability to SCNPs for the first time.

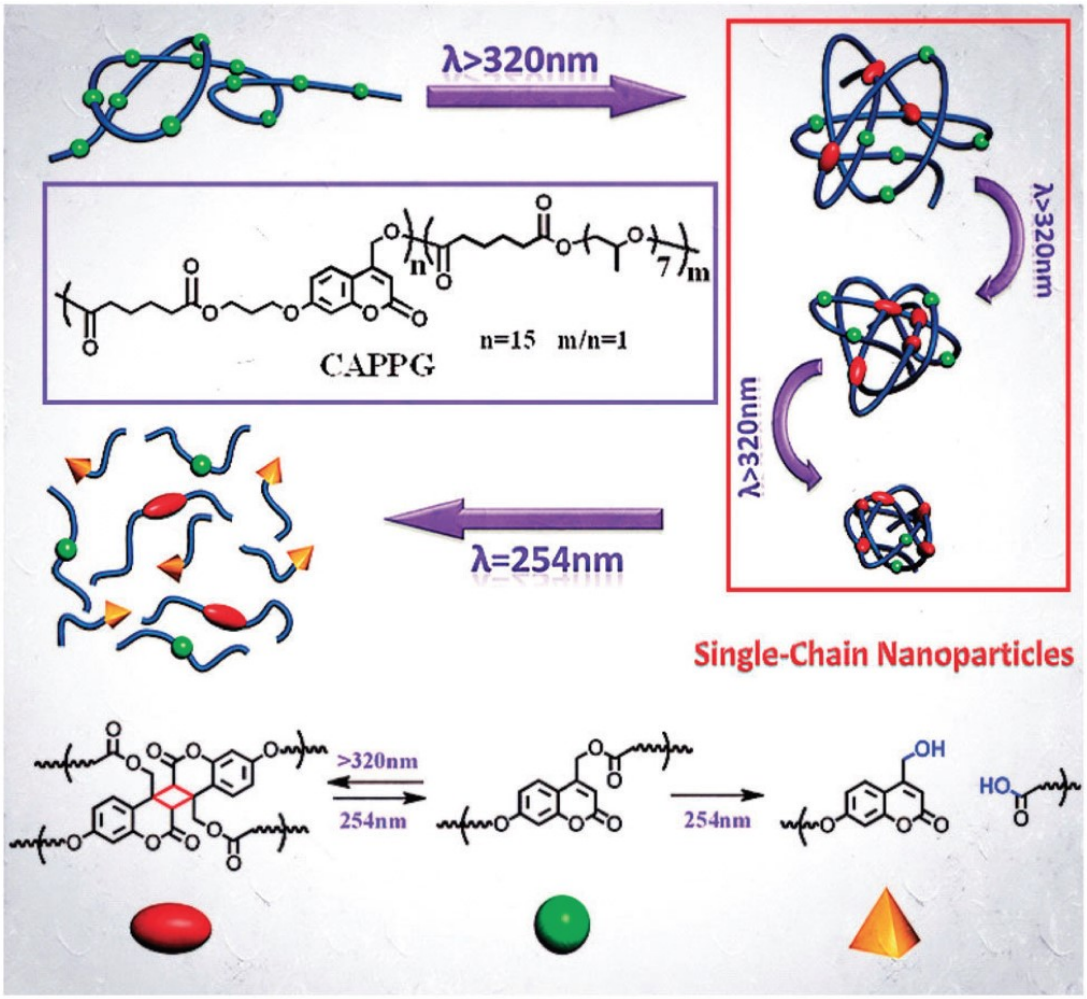

Figure 18. Schematic illustration for the preparation of variable-size SCNPs using a single polymer precursor based on intra-chain photo-dimerization of coumarin moieties and the photodegradable feature of the SCNPs.

1.2 Experimental Section

1.2.1 Materials

All chemicals were purchased from Aldrich and used as received unless otherwise noted.

Pyridinium-4-toluenesulfonate (DPTS) was synthesized using a literature method. (151)

1.2.2 Synthesis of the coumarin monomer

1.2.2.1 Synthesis of 7-hydroxy-4-(chloromethyl) coumarin (*a* in Scheme 4):

To a solution under stirring of resorcinol (10 g 91 mmol, 1 eq) and 4-chloromethyl acetoacetate (17 g, 103 mmol, 1.14 eq) in toluene (150 mL) was added p-toluene sulfonic acid (3.6 g, 19 mmol, 0.21 eq). The solution was connected to a Dean-Stark apparatus and heated to reflux at 110 ºC for 45 min. The reaction mixture was concentrated and purified by column chromatography (EtOAC:Hexane 1:9) to yield a white solid (***a***), (13.4 g, 70 % yield).

1.2.2.2 Synthesis of 7-hydroxy-4-4(hydroxymethyl) coumarin (*b*):

To water (350 mL) was added ***a*** (2.95 g, 14 mmol) under stirring. The reaction mixture was refluxed for 3 days, filtered while hot and cooled to room temperature over 12 h to yield off-white needles (***b***). The product was filtered and connected to vacuum overnight (2.67 g, 99 %). The product was used in the next step without purification.

1.2.2.3 Synthesis of 7-(hydroxypropoxy)-4-(hydroxymethyl) coumarin (c):

To a solution of anhydrous acetone (15 mL), ***b*** (1.0 g, 5.2 mmol, 1 eq), potassium carbonate (2.0 g, 14.5 mmol, 2.8 eq), 3-bromo 1-propanol (1.5 g, 10.8 mmol, 2.1 eq) was added 18-crown-6 (0.7 g, 2.65 mmol, 0.5 eq) in a N_2 atmosphere. The mixture was stirred for 30 min at room temperature and then was refluxed at 53 ºC for 18 h and filtered. The solvent was removed under reduced pressure to yield a light yellow solid. Purification by column chromatography (EtOAC:Hexane 4:1) yielded a white solid, (0.29 g, 22 %) (***c***).

1.2.3 Synthesis of the coumarin-containing polymer precursor CAPPG

A two neck round bottom flask was charged with ***c*** (62.5 mg, 0.25 mmol, 1 eq), poly (propylene glycol) (106.5 mg, 0.25 mmol, 1 eq), adipic acid (73 mg, 0.5 mmol, 2 eq) and DPTS (58.5 mg, 0.8 eq). The flask was vacuum backfilled three times with N_2. Dichloromethane (2.5 mL) was added while cooling the flask at 0 ºC. After 15 min, N, N-diisopropylcarbodiimide (DIC) (470 µL, 3 eq) was added and the reaction was allowed to take place at room temperature for 36-48 h. The polymer was precipitated three times in mixture of alcohols (MeOH:EtOH:PrOH 1:1:1). The polymer was collected, centrifuged, dried under vacuum to yield a white solid (208 mg, 87 % Mn=13223).

1.2.4 Preparation of single-chain nanoparticles of CAPPG

To fabricate the SCNPs of CAPPG, 10 mg of the copolymer was dissolved in 50 mL of $CHCl_3$ or THF and kept under stirring overnight. After being filtered with a 200 nm pore size Teflon filter, the solution was then exposed to >320 nm UV light (900 mW/cm^2, distance from the solution: 5 cm) for various times. The solution could be concentrated under vacuum distillation and polymer nanoparticles precipitated in hexane were then dried under vacuum overnight. Nanoparticles can be re-dispersed in THF or $CHCl_3$ to form a homogenous solution with a desired concentration.

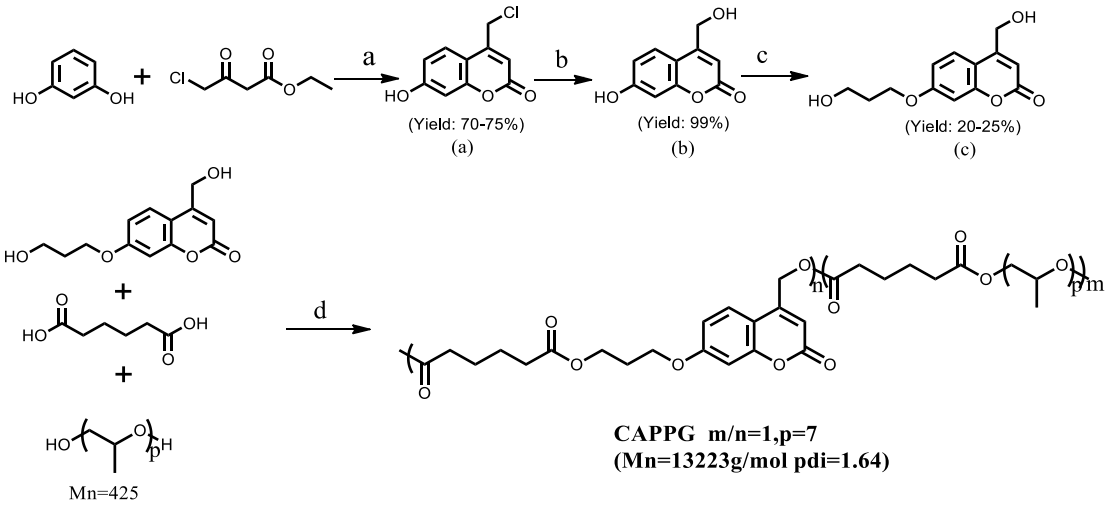

(a) p-Toluenesulfonic acid (PTSA), Toluene, Reflux, 45min

(b)H_2O, Reflux, 3 days

(c) K_2CO_3, 18-Crown-6, Acetone, 3-bromopropanol-1, 55°C, 18h

(d) Diisopropyl carbodiimide (DIC), Dimethylaminopyridinium-p-toluenesulfonate (DPTS), CH_2Cl_2, R.T., 48-72hrs

Scheme 4. Synthesis procedure for the CAPPG polymer precursor

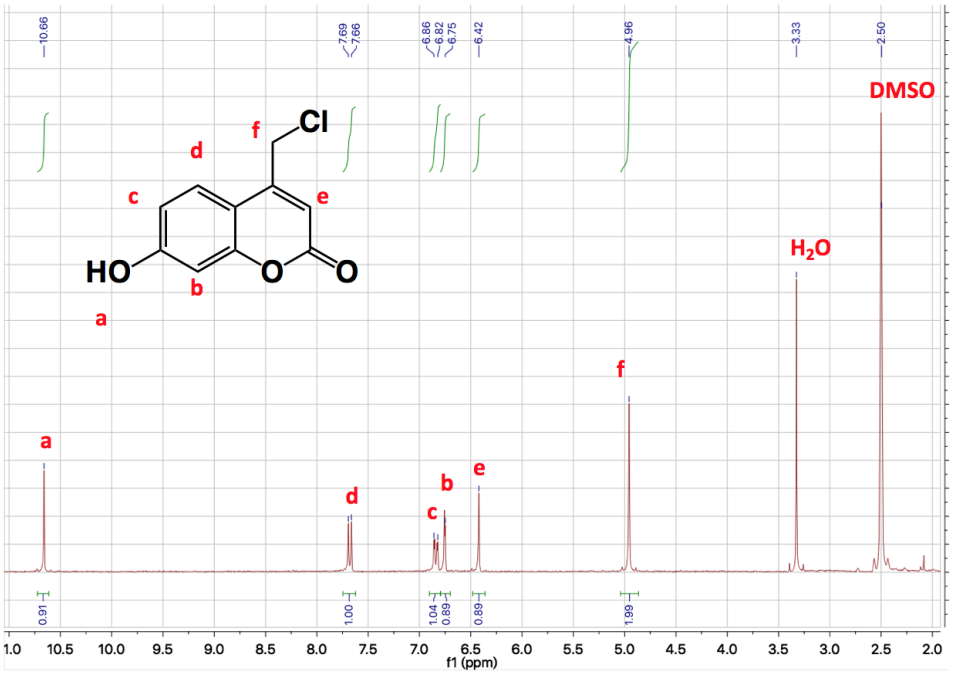

Figure 19. ^{1}H-NMR spectrum of 7-hydroxy-4-(chloromethyl) coumarin (***a***) (DMSO-d6).

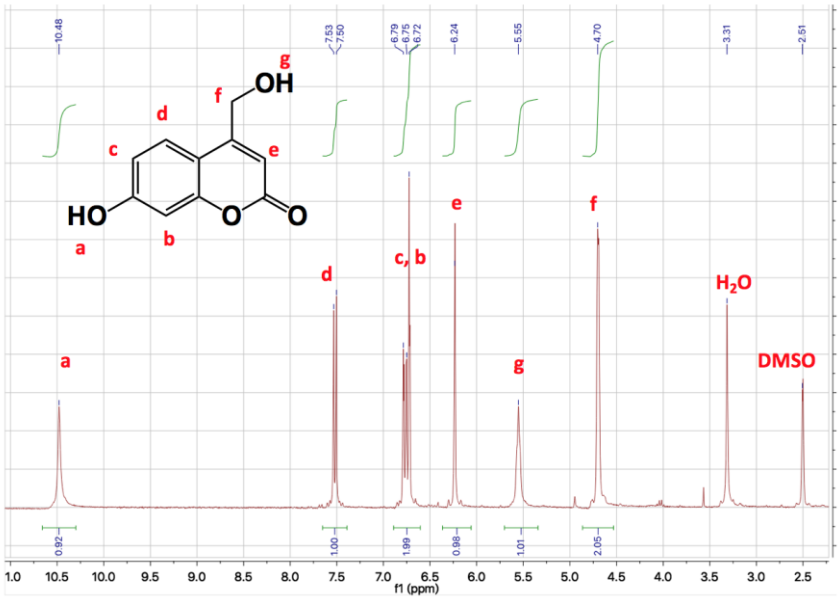

Figure 20. ^{1}H-NMR spectrum of 7-hydroxy-4-4(hydroxymethyl) coumarin (***b***) (DMSO-d6).

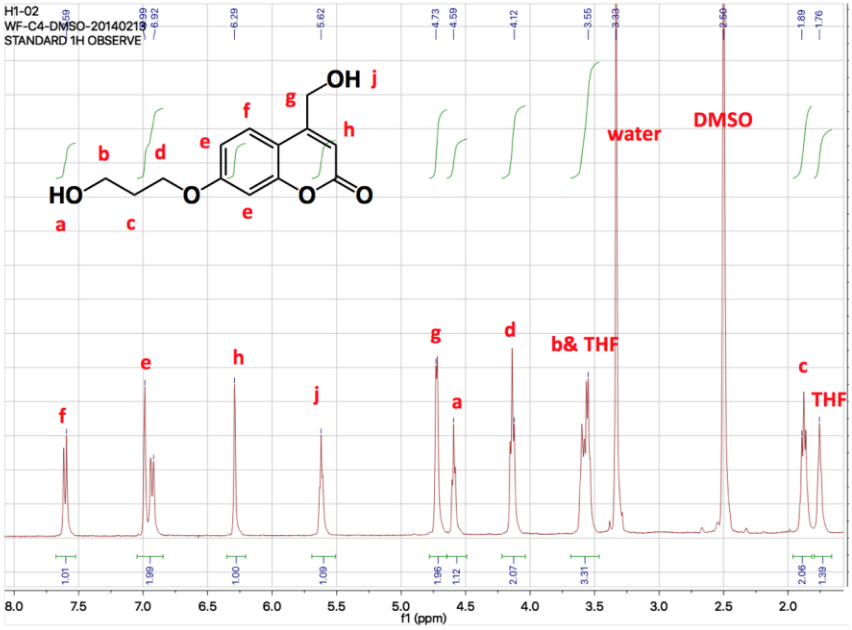

Figure 21. ^{1}H-NMR spectrum of 7-(hydroxypropoxy)-4-(hydroxymethyl) coumarin (***c***) (in DMSO-d6).

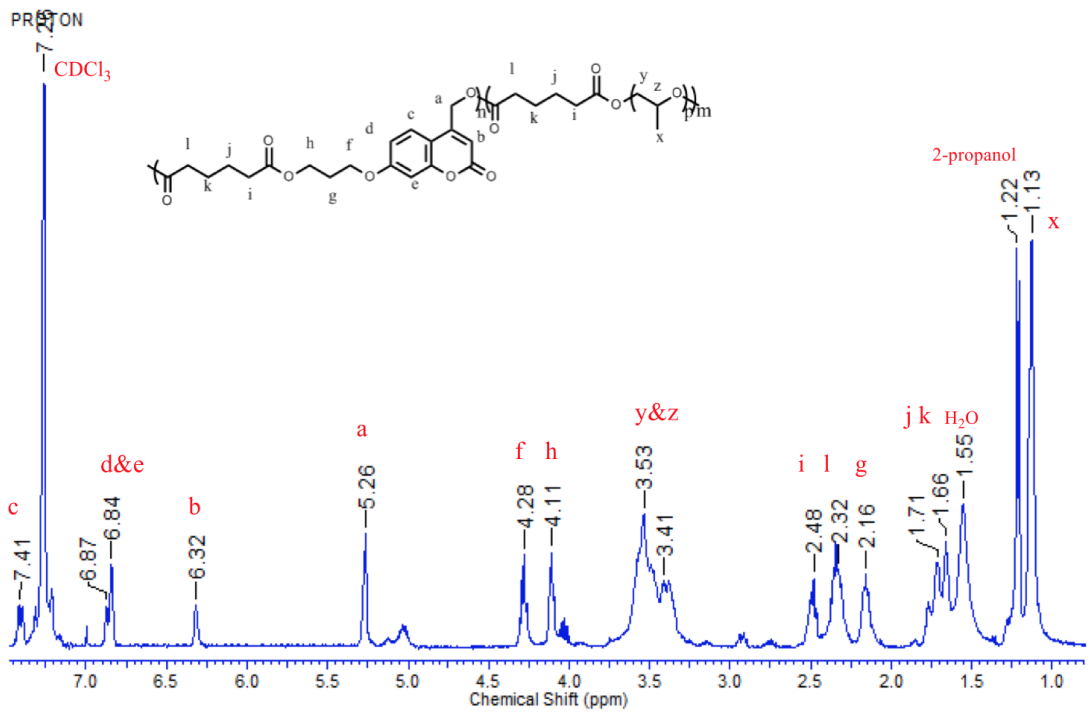

Figure 22. ^{1}H-NMR spectrum of the CAPPG polymer precursor (in $CDCl_3$).

1.2.5 SEC measurements of CAPPG polymer precursor, SCNPs and SCNPs after photo-degradation

CAPPG polymer (5 mg) was dissolved in THF (10 mL) and kept under stirring overnight. After being filtered with a 200 nm pore size Teflon filter, the solution was then exposed to > 320 nm UV light (900 mW/cm^2, distance from the solution: 5 cm) for a chosen time. In the case of photodegraded SCNPs, a THF solution of the SCNP prepared upon >320 nm UV irradiation for 120 min, was first prepared (5 mg SCNP in 10 mL THF). The solution was then sonicated for 10 min before being exposed to the 254 nm UV light (100 mW/cm^2, distance from the solution: 5 cm) for 3 h. In all cases, the SCNP solution was directly injected into SEC for the measurement.

1.2.6 Instruments and measurements

^{1}H NMR spectra were recorded on a Bruker AC 400 (400 MHz) spectrometer with DMSO-d6 and $CDCl_3$ as the solvent. Size exclusion chromatograph (SEC) measurements were performed on a Waters system equipped with a photodiode array detector (PDA 996) and a refractive index detector (RI 410). THF was used as the eluent at an elution rate of 1 mL/min, while polystyrene standards were used for calibration. Dynamic light scattering (DLS) measurements were performed on a Malvern Zetasizer Nano ZS ZEN3600 with a helium−neon laser (wavelength, λ= 633 nm). All measurements were carried out at a scattering angle of 173°. The polymer was crosslinked by UV irradiation by OmniCure@ Series 1000 UV lamp (approximately 900 mW/cm^2) with 320-480 nm filter. The SCNPs were degraded under short wavelength UV light from a UVS-28 EL Series UV lamp (254 nm, approximately 0.1 W/cm^2). The photo-dimerization degree of coumarin was monitored by recording UV-vis spectra on a Varian 50 Bio UV-vis spectrophotometer. The morphology of nanoparticles was examined using a Hitachi H-7500 transmission electron microscope (TEM) operating at 80 kV. Samples were prepared by casting 3-5 mL solution on a carbon-coated copper grid, followed by drying at room temperature. Atomic force microscopy (AFM) images were recorded on a Dimension Icon AFM instrument equipped with a NanoScope V controller (Veeco/Digital Instruments, Santa Barbara, CA). AFM topographical images were done under ScanAsyst mode at room temperature using a silicon nitride (force constant 0.4 N/m) cantilever tips.

1.3 Results and Discussion

Our main-chain coumarin-containing copolymer was synthesized by reacting a coumarin diol with adipic acid and polypropylene glycol (PPG, Mw = 425 g/mol) under carbodiimide/DPTS-catalyzed conditions. The coumarin diol was synthesized using a reported method. (128) The obtained polymer, abbreviated as CAPPG, has Mn = 13220 g/mol (about 15 repeating units) and a polydispersity index PDI (Mw/Mn) = 1.64 according the SEC measurements using polystyrene (PS) standards. With the polymer structure (Figure 18), the coumarin groups in the main chain can enable both UV light-induced chain cross-linking (>320 nm) and chain scission (254 nm) *via* photodimerization and photocleavage of the chromophore, respectively. (128, 152) Since a homopolymer prepared through condensation of the same coumarin diol and adipic acid was shown to be biodegradable and biocompatible, (128) CAPPG should behave the same way considering that it is basically a derivative of that polymer with the addition of the biocompatible PPG. (153)

SCNPs of CAPPG were obtained by the intra-chain photodimerization of coumarin groups, with a dilute polymer solution (0.2 mg/mL, in $CHCl_3$) exposed to >320 nm UV light (900 mW/cm^2). The occurrence of photo-dimerization could be observed by the decreasing absorbance of the coumarin groups at around 322 nm (Figure 23a); the increase of the dimerization degree (DD) of coumarin over irradiation time was monitored by UV-vis absorption spectra and calculated according to the equation $DD = 1-A_t/A_0$, with A_0 and A_t being the initial absorbance and the absorbance after irradiation time t at 322 nm, respectively. The results (inset of Figure 23a) show that in the dilute CAPPG solution and under the conditions used, the photo-dimerization of most coumarin groups occurs within the first 60 min of UV irradiation and prolonged times of up to 120 min further raise the dimerization

degree slightly, reaching an apparent maximum level of 87 %. The simple control of the photo-dimerization degree by changing the UV irradiation time offers the possibility of optically tuning the intra-chain crosslinking density and, consequently, the size of SCNPs. The nanoparticles formed by a single polymer chain of CAPPG were first proved by means of SEC that is sensitive to the changing hydrodynamic volume associated with the single chain coil-to-particle transition. As seen in Figure 23b, as compared with the CAPPG precursor without UV irradiation, the elution band of the polymer shifts continuously towards longer elution times upon increasing the >320 nm UV irradiation time, indicating a continuously increasing intra-chain crosslinking density and, consequently, reduced hydrodynamic volume. The absence of peaks at shorter retention times implies that only photo-induced intra-chain crosslinking takes place (SEC traces of the full retention time scale in Figure 24). Figure 23 c&d and Figure 25 show images of SCNPs (120 min UV irradiation) recorded by AFM and TEM, respectively. Well-separated nanoparticles, below 10 nm in diameter, were observable upon casting a very dilute polymer solution (0.02 mg/mL).

On the other hand, photo-degradability of SCNPs is an interesting feature that may find applications in light-controlled delivery. (154) Also shown in Figure 23b is the SEC trace of the SCNPs with the highest crosslinking density (DD=87 %) that was subsequently exposed to 254 nm UV light for 3 h. It is visible that the SCNPs are degraded into smaller fragments giving rise to a broad elution band at longer elution times corresponding to the lower molecular weight species (the apparent Mn value decreases from 13220 g/mol for the precursor to 1385 g/mol) after 254 nm UV irradiation. Photo-cleavage of the coumarin-4-yl methyl esters may be at the origin of the photo-degradation of SCNPs because it results in chain scission. (155, 156) The possible photo-cleavage of the cyclobutane functionality in the dimer can only diminish the intra-chain crosslinking density. (Scheme 5, Figure 26)

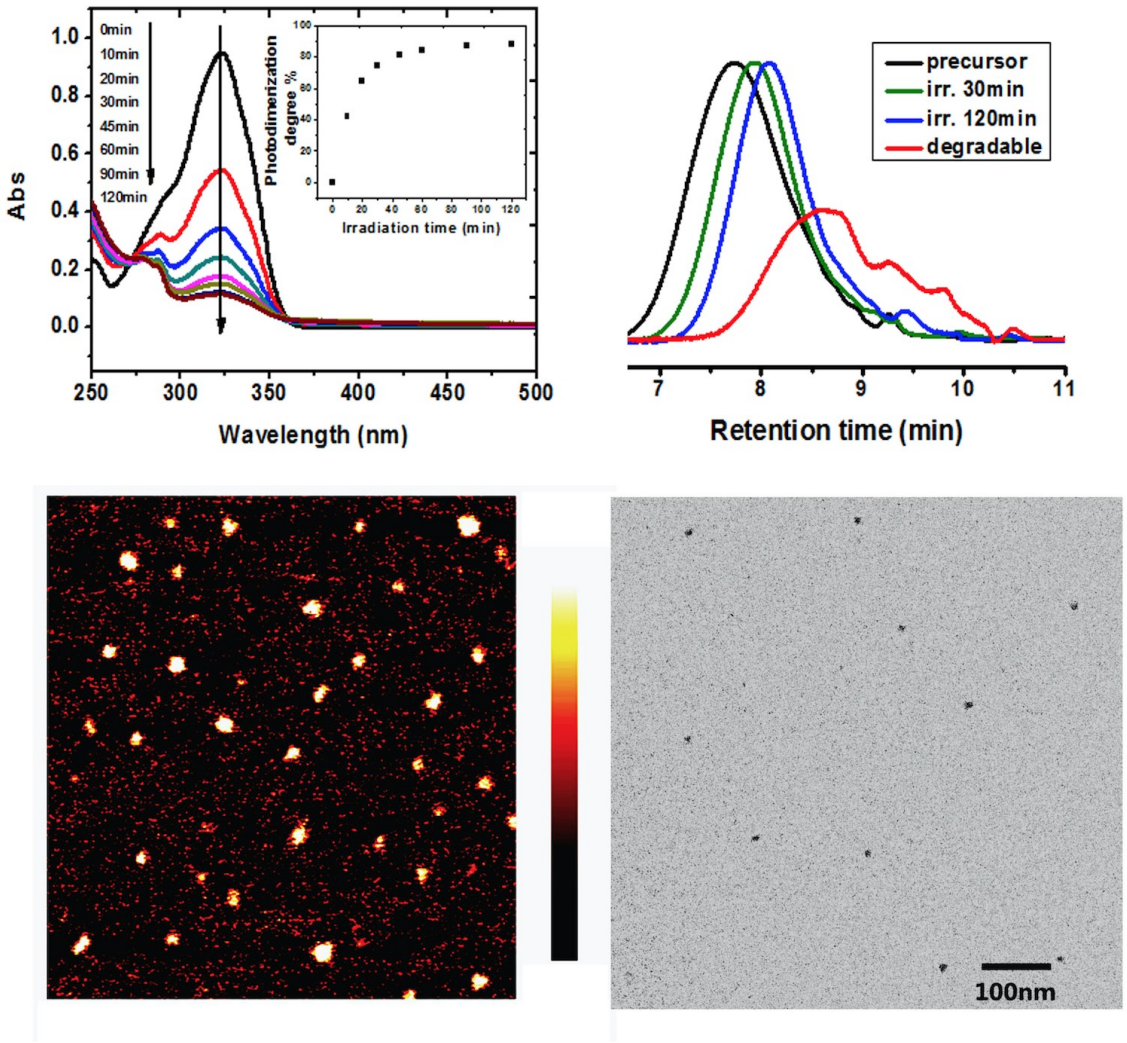

Figure 23. (a) Absorption spectra of CAPPG in $CHCl_3$ (0.2 mg/mL) recorded after different times of >320 nm UV irradiation showing intra-chain photodimerization (crosslinking). Inset is the plot of the photodimerization degree of coumarin *vs.* UV irradiation time. (b) SEC traces of the CAPPG precursor, SCNPs of varying photocrosslinking density obtained by exposing the same dilute CAPPG solution (0.2 mg/mL) to >320 nm UV light for different times, and SCNPs of the highest crosslinking density after subsequent 254 nm UV irradiation for 3 h. (c) AFM and (d) TEM image of the SCNPs with the highest crosslinking density, cast from a dilute polymer solution in $CHCl_3$ (0.02 mg/mL).

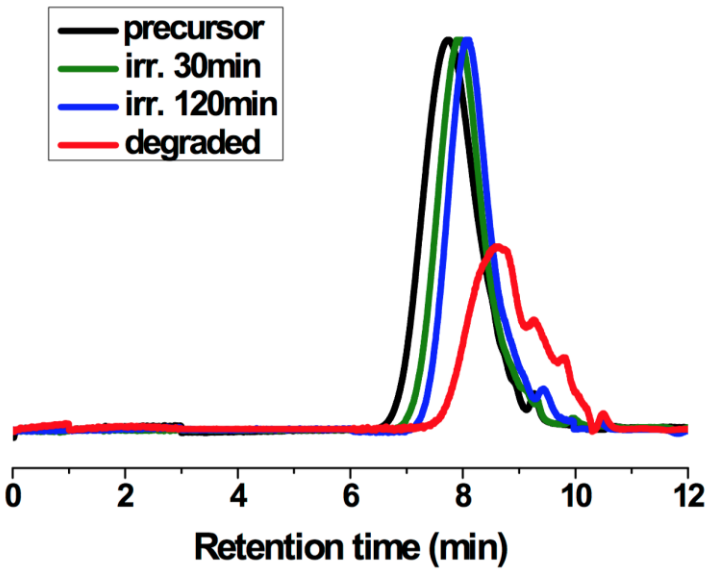

Figure 24. SEC traces over the full retention time scale for the CAPPG precursor, its SCNPs prepared upon 30 and 120 min >320 nm UV irradiation, respectively, and the photodegraded SCNP obtained after 254 nm UV irradiation.

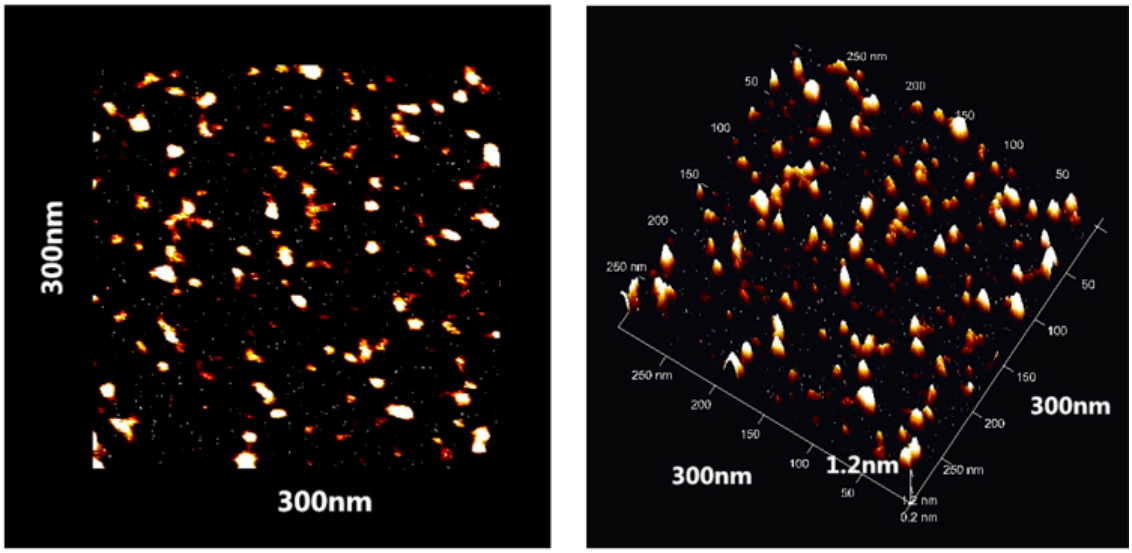

Figure 25. AFM images of SCNPs (after 120 min UV irradiation) dispersed in water.

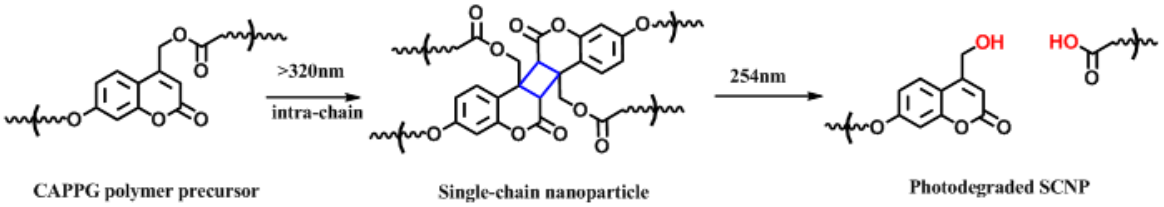

Scheme 5. Photo-crosslinking and photo-degradation of SCNP of the main chain coumarin-containing polymer. Under the 254 nm UV irradiation, cleavage of the coumarin-4-yl methyl ester, resulting in chain scission, can occur with coumarin in the monomeric form (as drawn in the scheme) or in the dimer form (not shown).

We further investigated the relationship between the photo-dimerization degree of coumarin and the size of SCNPs in solution by dynamic light scattering (DLS). Knowing that the photo-dimerization degree increases with increasing UV irradiation time (Figure 23a), SCNPs formed at various UV irradiation times were obtained and the characterization results are shown in Figure 27. Despite the scattering of data, the DLS results show a clear tendency for size decrease upon increasing the UV irradiation time (Figure 27a and b). The number-average hydrodynamic diameter decreases from 5.2 nm for uncrosslinked polymer coils to about 3 nm for SCNPs with 87 % photodimerization of coumarin. AFM images provide further evidence that as the photodimerization degree increases not only the SCNP reduces the size, but also becomes more compact and denser. While the nanoparticle formed after 30 min UV irradiation appears soft and deformable in contact with the mica surface, the one formed after 60 min UV irradiation becomes more solid. The nanoparticle subjected to 120 min UV irradiation is a smaller and tighter sphere on the surface. (Figure 28) Thus, within the limits of our SEC, DLS and AFM instrumentation used, the combined results suggest that

the nanoparticles were formed from single CAPPG chains, and that the size of those SCNPs could be controlled, to some extent, by adjusting the intra-chain photocrosslinking density that is determined by the photo-dimerization degree of the coumarin units in the main chain.

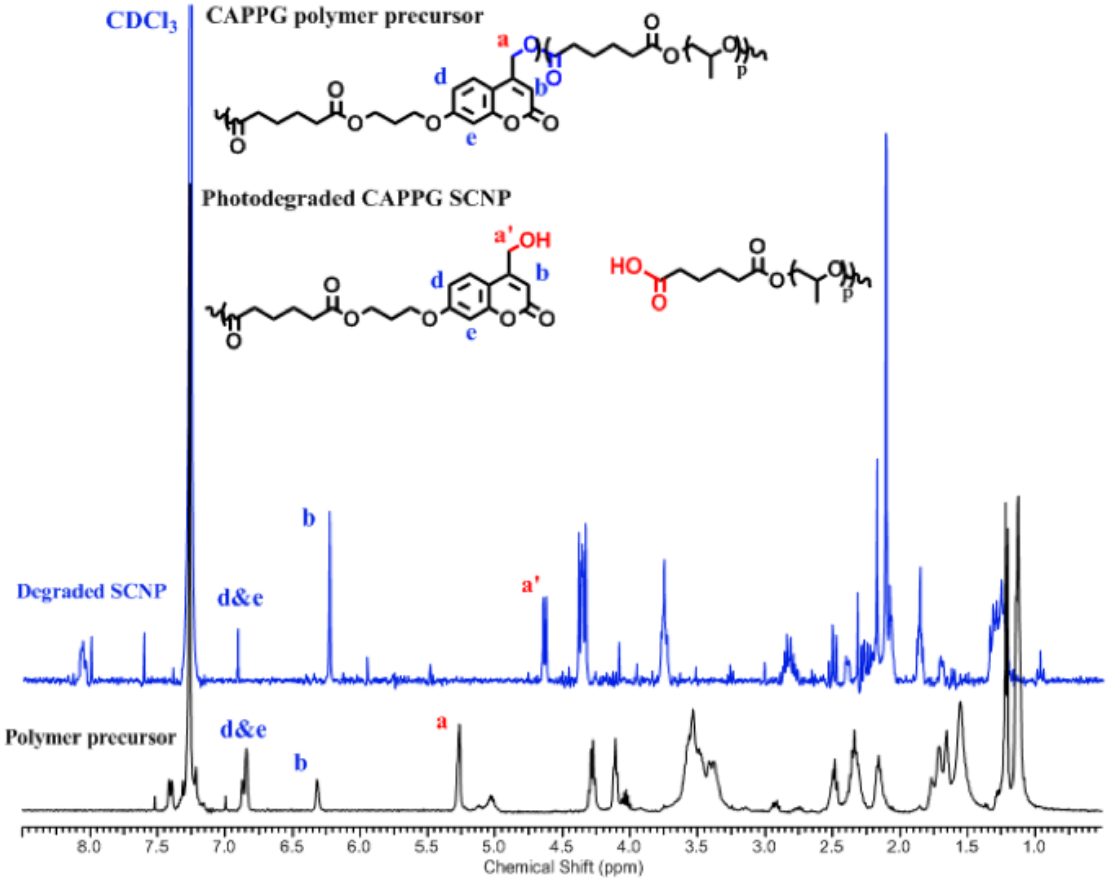

Figure 26. ^{1}H-NMR spectra of the CAPPG precursor and the SCNP after photo-degradation. The spectral changes upon 254 nm UV irradiation provide evidence for the photo-induced scission of chain backbone leading to the photo-degradation of SCNP: peak a in the polymer precursor being replaced by peak a' for the SCNP after photo-degradation.

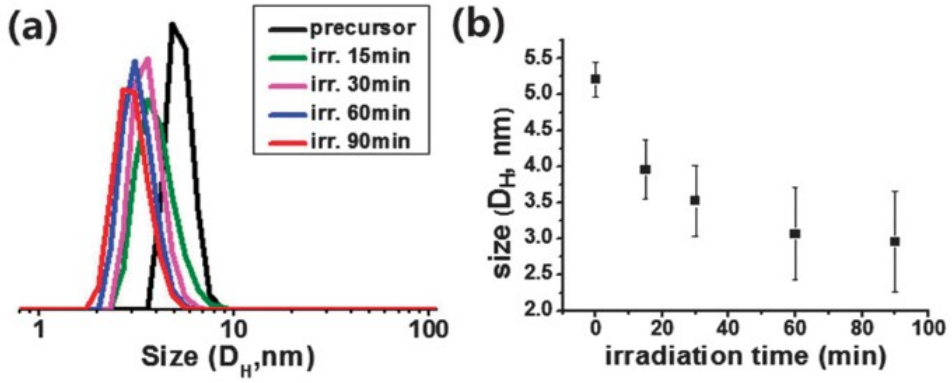

Figure 27. (a) Number-weighted size distribution of the precursor and SCNPs prepared with different >320 nm UV irradiation times. (b) Average hydrodynamic diameter, D_H, *vs.* UV irradiation time (from 8 measurements).

1.4 Conclusion

We have demonstrated a facile method that allows the use of a single polymer precursor to prepare photodegradable and size-tunable SCNPs. We showed that by incorporating coumarin moieties into the chain backbone of a polyester, photo-dimerization and photo-induced chain scissions, which occur at two different UV wavelengths, enable the preparation of sub-10 nm SCNPs through intra-chain photo-crosslinking (under >320 nm UV) and their subsequent photo-degradation (254 nm UV). SEC, DLS and AFM results show that the size of SCNPs decreases upon increasing the intra-chain photo-dimerization degree. We expect that insertion of coumarin moieties into the main chain of a given polymer represents a general approach for obtaining variable-size SCNPs possessing the function of photo-degradability, without the need for synthesizing different polymer precursors. Owing to the biocompatible and biodegradable nature of the polyesters, they have the potential to be exploited for biomedical applications.

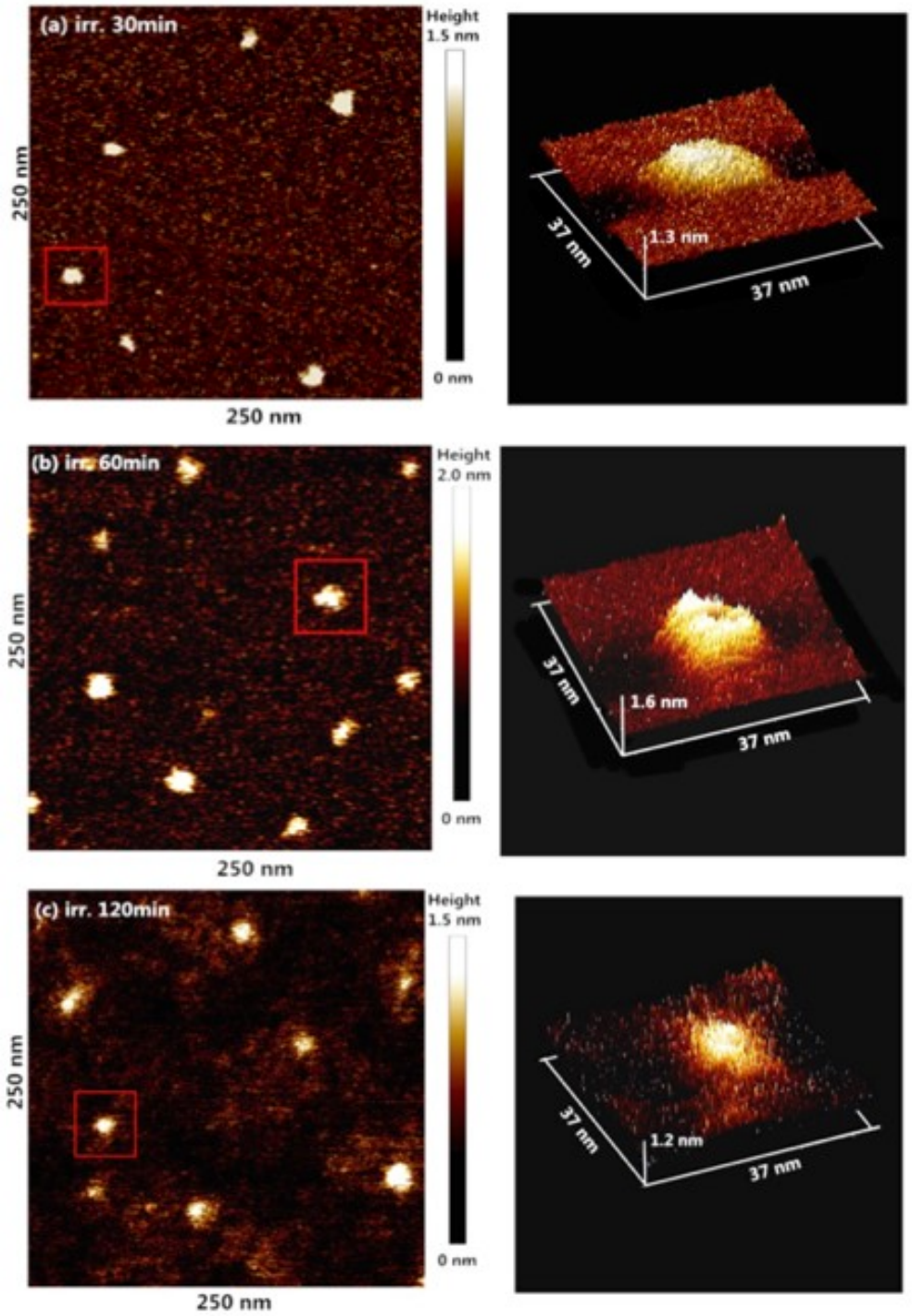

Figure 28. AFM images of SCNPs formed after different UV irradiation time (a: 30 min, b: 60 min, c: 120 min)

1.5 Statement of Contribution

Partial content of this project was published in *Chemical Communications* **2014**, *50*, 13492-13494. DOI: 10.1039/C4CC06629D. The paper is authored by Weizheng Fan, Xia Tong, Qiang Yan, Shangyi Fu and Yue Zhao. This research work was conducted in Université de Sherbrooke under supervision of Prof. Zhao. Xia Tong did the AFM measurements, Qiang Yan did the SEC measurements and Shangyi Fu helped for UV irradiation system. I synthesized all the samples and performed all the other characterizations reported in this publication. I wrote the first draft of the manuscript and Prof. Zhao finalized the manuscript.

CHAPTER 2 PHOTO-RESPONSIVE LIQUID CRYSTALLINE POLYMER SINGLE-CHAIN NANOPARTICLES

2.1 Introduction

The development of functional polymer nanoparticles has been a field of great scientific interest because of their potential applications in many areas such as energy, drug delivery and high performance materials. (1, 2) However polymer nanoparticles with typical sizes between 20-100 nm may not be best suited to certain specific application requirements. In recent years, polymer single-chain nanoparticles (SCNPs) prepared by intra-chain crosslinking or folding have attracted much attention because the preparation is simple and the ultra-small sizes, under 20 nm, may give rise to unique properties potentially useful for drug delivery, nano-reactor and low viscosity coating. (3, 15, 19-21, 49, 62, 67, 105, 107, 146, 148, 157) On the other hand, SCNPs based on controllable self-folding of single polymer chain could mimic the structure of folded enzymes. (158) Thus far, a variety of synthetic methodologies have been reported to fabricate SCNPs *via* both covalent and non-covalent bonding involving various chemistries such as photochemical reaction, (45, 62) dynamic bonding, (59) polymerization, (39) Diels-Alder reaction, (43) metal complexation, (72-74, 76, 98) click chemistry, (34, 159) host-guest interactions (77) and so on. In most cases, SCNPs were prepared through intra-chain crosslinking-induced collapse in a very dilute polymer solution to prevent inter-chain crosslinking. (13)

To expand the scope of applications, the development of functional SCNPs has become an important topic in recent years. Generally speaking, the preparation of SCNPs with specific functions is not trivial, because it may be challenging to incorporate the required functional

groups or moieties into such a tiny nanoparticle and to characterize it properly. Recently, a few reports described different functional SCNPs. For instance, Qiao and coworkers reported a type of biocompatible SCNPs *via* organocatalyzed ring-opening polymerization. (41) Barner-Kowollik *et al.* designed functional fluorescent SCNPs and used them as novel imaging agents. (44) Pu *et al.* reported a kind of voltage-responsive single-chain nanoparticles *via* host-guest interaction. (96) In our group, we designed a series of functional SCNPs based on coumarin-containing polymer precursors, which are thermo-responsive, size-tunable and photodegradable. (63, 160) Furthermore, in the area of bio-mimic systems, much effort has been made to control the folding of single polymer chain to prepare SCNPs of different morphologies. (161) Votes *et al.* reported the effect of the length of polymer chain and polymer concentration on the size and shape of SCNPs. (162) Pomposo *et al.* investigated the physical mechanism for the non-compact morphology of SCNPs. (163) In the latter case, they designed globular SCNPs by turning the solvent quality *via* simulation. Rationally designed polymer structures provide another approach to control chain folding and thus the morphology of SCNPs. To this regard, Chen and coworkers reported a kind of tadpole-like SCNPs by intramolecularly crosslinking P4VP block of a block polymer. (147) Lutz's group reported compartmentalization in SCNPs by stepwise intramolecular crosslinking of sequence-controlled macromolecules. (106) However, preparation of SCNPs with varying shape and specific functions remains a challenge because of the small size and crosslinked nature of SCNPs. (16)

Herein we report the preparation and characterization of a new class of functional SCNPs, namely, liquid crystalline polymer single-chain nanoparticles (LC-SCNPs). Liquid crystalline polymers (LCPs) are known for the combined processability of polymers with the anisotropic properties arising from molecular ordering of low-molar-mass liquid crystals

(LCs). The concepts of orientational order and cooperative molecular motion are recognized in bioscience, serving as model systems for cell membranes and muscles. In addition, LCs have found widespread use in information displays, sensing, photonic band gap structures as well as in optical elements such as controllable lenses and lasing. (164) Thus we envisioned that LC-SCNPs might exhibit interesting behaviors or functions. Among the many issues, it is of fundamental interest to know whether or not LC order can be preserved in SCNPs despite the severe confinement and crosslinked nature. Moreover, by choosing an azobenzene moiety as the mesogenic group in the polymer structure, the photoactivity related to the chromophore's *trans-cis* photo-isomerization can also be imparted to LC-SCNPs. Having these considerations in mind, a liquid crystalline random copolymer bearing two types of photoactive units was designed as the polymer precursor for the preparation of LC-SCNPs. As shown in Figure 29, the polymethacrylate is a random copolymer containing azobenzene side groups in majority for LC order and photo-isomerization as well as coumarin side groups in minority whose photo-dimerization can be used to prepare SCNPs *via* intra-chain photo-crosslinking. (128, 160)

As shown further on, this study allowed us to make several interesting findings on LC-SCNPs. In particular, despite the tiny size, severe confinement and intra-chain crosslinking in such LC-SCNPs, the LC order persists and the photo-isomerization of azobenzene mesogens occurs. Moreover, the LC-SCNPs exhibit two unexpected functions: they display a photoluminescence that varies according to the isomer state of azobenzene, and they can be deformed in different ways upon linearly polarized UV or visible light irradiation. Finally, to explore possible new applications of LC-SCNPs, they were used to prepare an all-polymer nanocomposite by dispersion in poly(methyl methacrylate) (PMMA) matrix. Thin film of the PMMA/LC-SCNP nanocomposite appears transparent due to the sub-15 nm size of the

nanoparticle, and upon mechanical stretching of the film in the LC phase, orientation of azobenzene mesogens along the stretching direction was observed.

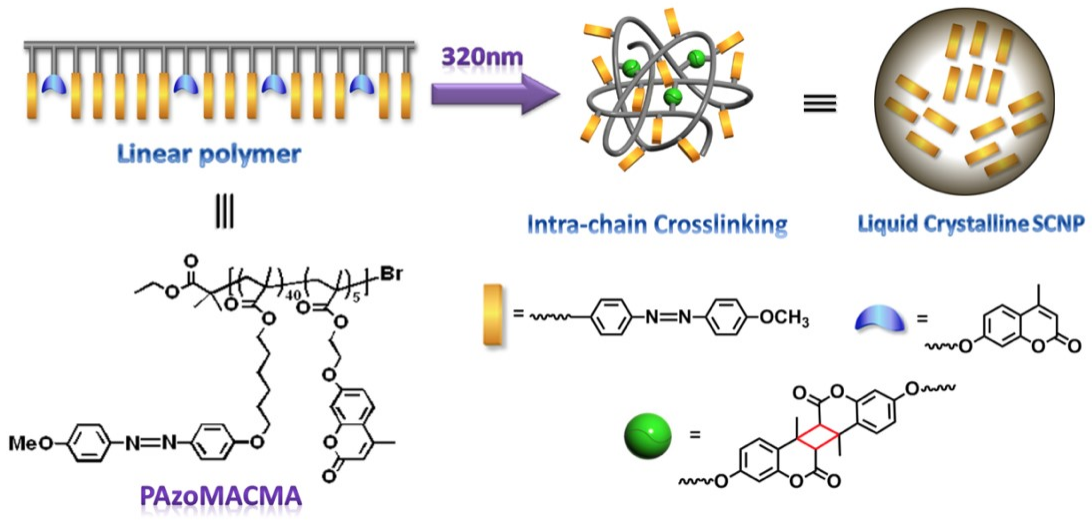

Figure 29. Schematic illustration for the preparation of liquid crystalline single-chain nanoparticles (LC-SCNPs) based on intra-chain photodimerization of coumarin moieties in the chemical structure of the used side-chain liquid crystalline polymer bearing azobenzene mesogens

2.2 Experimental Section

2.2.1 Materials

All chemicals were purchased from Sigma-Aldrich unless otherwise stated. The coumarin monomer (7-(2-Methacryloyloxyethoxy)-4-methylcoumarin) and azobenzene monomer (6-[4-(4-methoxyphenylazo)phenoxy]hexylmethacrylate) were synthesized according to the literature procedures. (165, 166)

2.2.2 Synthesis of polymer precursor PAzoMACMA

The polymer precursor PAzoMACMA was synthesized by typical atom transfer radical polymerization (ATRP) condition (Scheme 6). Ethyl-2-bromoisobutyrate (4.33 mg, 0.022 mmol), 6-[4-(4-methoxyphenylazo)phen-oxy]hexylmethacrylate (792 mg, 2 mmol), 4-methyl-[7-(methacryloyl)oxy- ethyloxy] coumarin (64 mg , 0.22 mmol), PMDETA (10 μL, 0.05 mmol), Cu(I)Br (7.15 mg, 0.05 mmol) and 2.5 mL of anisole were added under N_2 atmosphere into a round-bottom flask. Then, the mixture was degassed three times using the freeze-pump-thaw procedure and sealed under vacuum. After 30 min stirring at room temperature, the flask was placed in a preheated oil bath (80 ºC) for 6 h. The solution was passed through a neutral Al_2O_3 column with THF as eluent to remove the catalyst. The polymer was collected by precipitation twice into hexane. The product was collected and dried in vacuum oven at 25 ºC for 24 h, yielding 0.47 g yellow solid (yield: 55 %). Mn= 10900 g/ mol, Mw=13400 g/mol and PDI=1.2 (from SEC: size exclusion chromatograph).

2.2.3 Preparation of PAzoMACMA single-chain nanoparticles

To fabricate the liquid crystalline (LC) SCNPs, the copolymer PAzoMACMA (2 mg) was dissolved in THF (10 mL), and the solution was kept under stirring overnight. After being filtered with a 200 nm pore size Teflon membrane, the solution was exposed to 320-480 nm UV light for 30 min. The solution was concentrated under vacuum distillation and the polymer nanoparticles were then precipitated in hexane, collected and dried under vacuum overnight. The LC-SCNPs could be re-dispersed in THF or $CHCl_3$ to form a homogenous solution with a desired concentration. The photo-dimerization of coumarin in PAzoMACMA solution (0.2 mg/mL, THF), which is responsible for intra-chain crosslinking, was monitored

using UV-vis absorption spectra recorded from a solution upon 320-480 nm UV irradiation for varying times. The obtaining of LC-SCNPs was confirmed by using SEC. The dilute LC-SCNP solution was directly injected into the column of SEC for the measurement after photo-dimerization of coumarin groups.

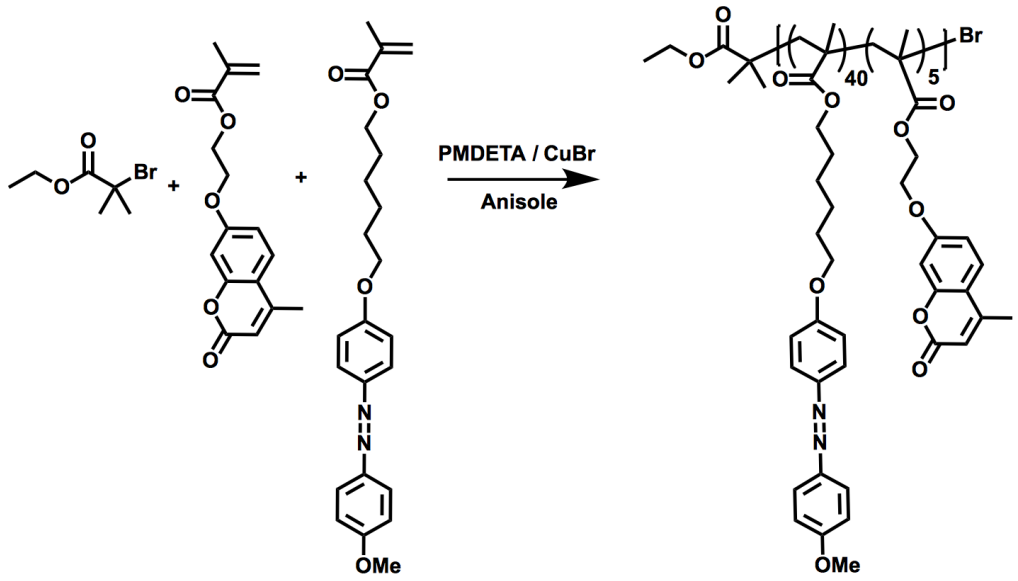

Scheme 6. Synthesis procedure of PAzoMACMA polymer precursor

2.2.4 Characterization of single-chain nanoparticles

The *trans-cis* photoisomerization of azobenzene mesogens in LC-SCNPs was investigated using UV-vis spectroscopy with a dilute solution in THF (0.2 mg/mL). Unless otherwise stated, the solution was exposed to 365 nm UV light for 5 min for the *trans-cis* isomerization and subsequently to 400-500 nm visible light for 5 min for the *cis-trans* back isomerization. In case $CHCl_3$ was used as the solvent, the LC-SCNP solution was irradiated under 365 nm UV light for 15 min to obtain the *cis* isomers of azobenzene and then heated to 75 ^{o}C for 1 h in water bath to

get the maximum azobenzene back to the *trans* form. The photoluminescence of LC-SCNPs in $CHCl_3$ was measured with azobenzene in different isomerization states and various excitation wavelengths (365 nm or 460 nm) were used for recording the emission spectra. The preservation of LC order in LC-SCNPs was investigated by means of differential scanning calorimetry (DSC) under a heating or cooling rate of 10 ºC/min and polarizing optical microscope (POM). The sample under POM observation was heated to 185 ºC, then decrease the temperature from 185 ºC to 110 ºC at 0.2 ºC/min and keep in 110 ºC for 72 h.

2.2.5 Photo-induced deformation of single-chain nanoparticles

Photo-induced deformation of LC-SCNPs was examined using atomic force microscopy (AFM). To prepare the sample, a THF solution was cast onto the surface of mica; after removing THF the LC-SCNPs were subjected to either of the two irradiation procedures. In the first one, the sample was heated at 115 ºC and was pretreated by unpolarized UV light (365 nm) irradiation for 15 min. Then the sample was irradiated under linearly polarized visible light (400-500 nm) for 15 min at 115 ºC in the isotropic phase for equilibrium and keep irradiation until being cooled to room temperature. In the second one, similarly the sample was first irradiated under unpolarized visible light (400-500 nm) for 15 min at 115 ºC, to reach the maximum amount of azobenzene *trans* isomers for pretreatment and then was exposed to linearly polarized UV light (365 nm) for 15 min at 115 ºC and continuously irradiation until being cooled to room temperature.

2.2.6 Nanocomposite preparation and characterization

To prepare thin films of the PMMA/LC-SCNP nanocomposite, PMMA dissolved in 1, 2-dichloroethane (0.5 g/mL, 10 mL) was mixed with LC-SCNPs dissolved in chloroform (5

mg/mL in 5 mL). The homogenous solution was then cast on a microscope slide to form a film after drying in a vacuum oven. To investigate the possibility of aligning the LC-SCNPs upon film elongation, the nanocomposite film was stretched at 113 ºC (above Tg of PMMA) to either 400 % strain at a rate of 25 mm/min, followed by rapid cooling under strain at room temperature. Polarized UV-vis spectroscopy was utilized to characterize the orientation.

2.2.7 Instruments and measurements

^{1}H NMR spectra were recorded on a Bruker (400MHz) spectrometer with $CDCl_3$ as the solvent at 293 K. The chemical shifts were referenced to residual peaks of solvent: $CDCl_3$ (7.26 ppm). Size exclusion chromatography (SEC) measurements were performed on an Agilent 1260 Infinity SEC system with MDS multi detectors (RI detector, Viscometer and Dual Angle LS detector: 15º and 90º). Tetrahydrofuran (THF) was used as the eluent at a flow rate of 0.4 mL/min at 30 ºC. The SCNPs were prepared *via* intra-chain crosslinking of polymer precursor under UV irradiation from an OmniCure@ Series 1000 UV lamp with 320-480 nm filter (240 mW/cm^2 at 350 nm, 5 cm distance). The photoisomerization of azobenzene were excited using the same lamp with 365 nm filter for UV light (65 mW/cm^2, 5 cm distance) and 400-500 nm filter for visible light (115 mW/cm^2 at 440 nm, 5 cm distance). The power of irradiation was measured by ORIEL 70260 Radiant Power Meter. The photodimerization of coumarin and photoisomerization of azobenzene were monitored by recording UV-vis spectroscopy on a Varian 50 Bio UV-vis spectrophotometer. Transmission Electron Microscopy (TEM) measurements were performed with a Hitachi H-7500 instrument at a voltage of 80 kV. The specimen was prepared by drop-casting the sample solution onto a carbon-coated copper grid, followed by drying at room temperature. Atom Forced Microscopy (AFM) measurements were performed on a Dimension Icon AFM

instrument equipped with a NanoScope V controller (Veeco/Digital Instruments, Santa Barbara, CA). AFM topographical images were done under ScanAsyst mode at room temperature using a silicon nitride (force constant 0.4 N/m) cantilever tips. The thermal phase transition behavior was investigated by Q-200 differential scanning calorimeter (DSC) from TA Instruments, using indium as the calibration standard. Polarizing optical microscopic (POM) observations were carried on a Leitz DMR-P microscope equipped with an Instec hot stage. Steady-state fluorescence emission and excitation spectra were recorded on a Varian Eclipse fluorescence spectroscopy. The PMMA/SCNP nanocomposite films were stretched by using an Instron 5965 universal testing system. A load cell of 500 N was fitted into the instrument and the tensile tests were performed at a speed of 25 mm/min in 113 ^{o}C.

2.3 Results and Discussion

2.3.1 Design of polymer precursor

To target the liquid crystalline property of SCNPs, a LCP precursor was chosen, being poly{6-[4-(4-methoxyphenylazo)phenoxy]hexylmethacrylate-*co*-4-methyl-[7-(methacrylo-yl)oxy-ethyl-oxy]coumarin} (PAzoMACMA). It contains two types of photoreactive groups: coumarin and azobenzene. On one hand, coumarin moieties, in minority in the polymer, are capable of photodimerization under 320 nm UV light that enables intra-chain crosslinking required for SCNP formation. On the other hand, azobenzene moieties, in majority, are side-group mesogens that not only form the LC phases but also render the polymer photoactive owing to the reversible *trans-cis* photo-isomerization. The polymer precursor PAzoMACMA was synthesized by means of atom transfer radical polymerization (ATRP) of two monomers, 6-[4-(4-methoxyphenylazo) phenoxy]hexyl methacrylate and 4-methyl-[7 (methacryloyl)

oxy-ethyloxy] coumarin, in a random copolymerization manner and at a molar ratio of coumarin to azobenzene of 1:9. The actual content of coumarin analyzed from the ^{1}H NMR spectrum is 12 mol% (Figure 30). The obtained polymer sample has an absolute Mw=13400 g/mol and PDI=1.2 (from triple detector SEC).

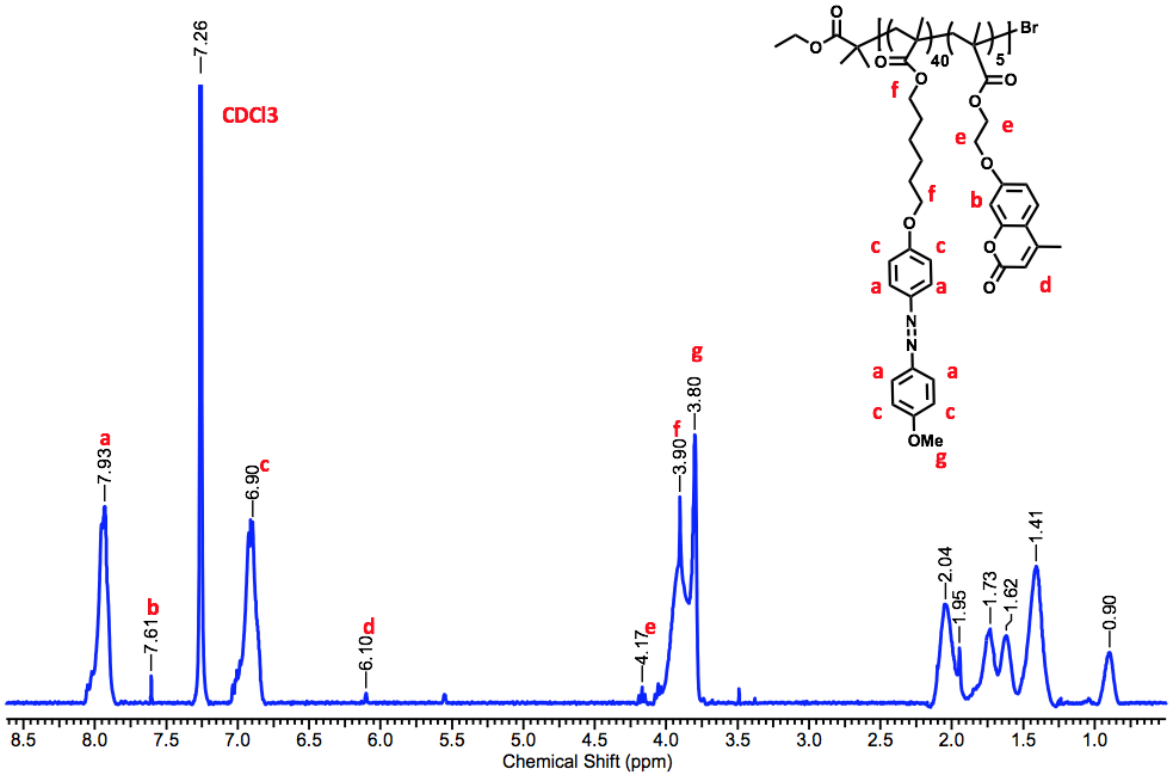

Figure 30. ^{1}H-NMR spectrum of PAzoMACMA in $CDCl_3$.

2.3.2 Single-chain nanoparticle preparation and characterization

The SCNPs of PAzoMACMA were obtained by using intra-chain photo-crosslinking of separate polymer chains through the photo-dimerization of coumarin groups. In order to avoid any inter-chain crosslinking, the photo-dimerization reaction was performed to occur in a dilute polymer solution (0.2 mg/mL, THF) exposed to 320-480 nm UV-vis light. Figure

31a shows the UV-vis spectra of the dilute PAzoMACMA solution before and after irradiation for various times. The peak intensity around 350 nm decreases with increasing the irradiation time, which indicates the occurrence of both the photodimerization of coumarins (absorption mostly below 350 nm) and the *trans-cis* photoisomerization of azobenzenes (absorption maximum near 360 nm). To better observe the change in photodimerization degree of coumarin, after the first irradiation over a given time, the polymer solution was further exposed to a UV light at 365 nm to convert essentially all azobenzene moieties remained in the *trans* form to the *cis* isomer. The UV-vis spectra recorded after the second UV irradiation are shown in Figure 31b. As can be seen, the 'removal' of the absorption of *trans* azobenzene centered at 360 nm makes the absorption peak of coumarins appear clearly at 320 nm. The decrease in peak intensity with increasing the first 320-480 nm irradiation time further confirms the intra-chain photodimerization of coumarin groups and thus the formation of SCNPs of PAzoMACMA.

The identity of SCNPs was further demonstrated by means of SEC which is sensitive to the change in the hydrodynamic volume. Figures 31c and 32 compares the SEC traces of PAzoMACMA polymer precursor before and after photo-crosslinking. It can be noticed that the elution band of the polymer after intra-chain photo-dimerization of coumarins shifts towards longer elution time, indicating reduced hydrodynamic volume of polymer chain as expected for SCNPs. The apparent absence of any peak from light scattering detection corresponding to the precursor or larger species at shorter exclusion times implies that only intra-chain crosslinking took place and no multi-chain aggregates existed. (45) The similarly absolute molecular weight and decrease of intrinsic viscosity are also consistent with the self-folding of SCNPs (Table 4). Furthermore, the decrease of hydrodynamic volume as revealed by both SEC and DLS can also be used to confirm the single-chain nature (Figure 33). Figure

31d shows a typical TEM image of the PAzoMACMA SCNPs prepared after 30 min photo-crosslinking. Well separated, sub-15 nm nanoparticles are observable upon casting a dilute SCNP solution (0.02 mg/mL) on the grid. The SCNPs could also be imaged using AFM (Figure 36a).

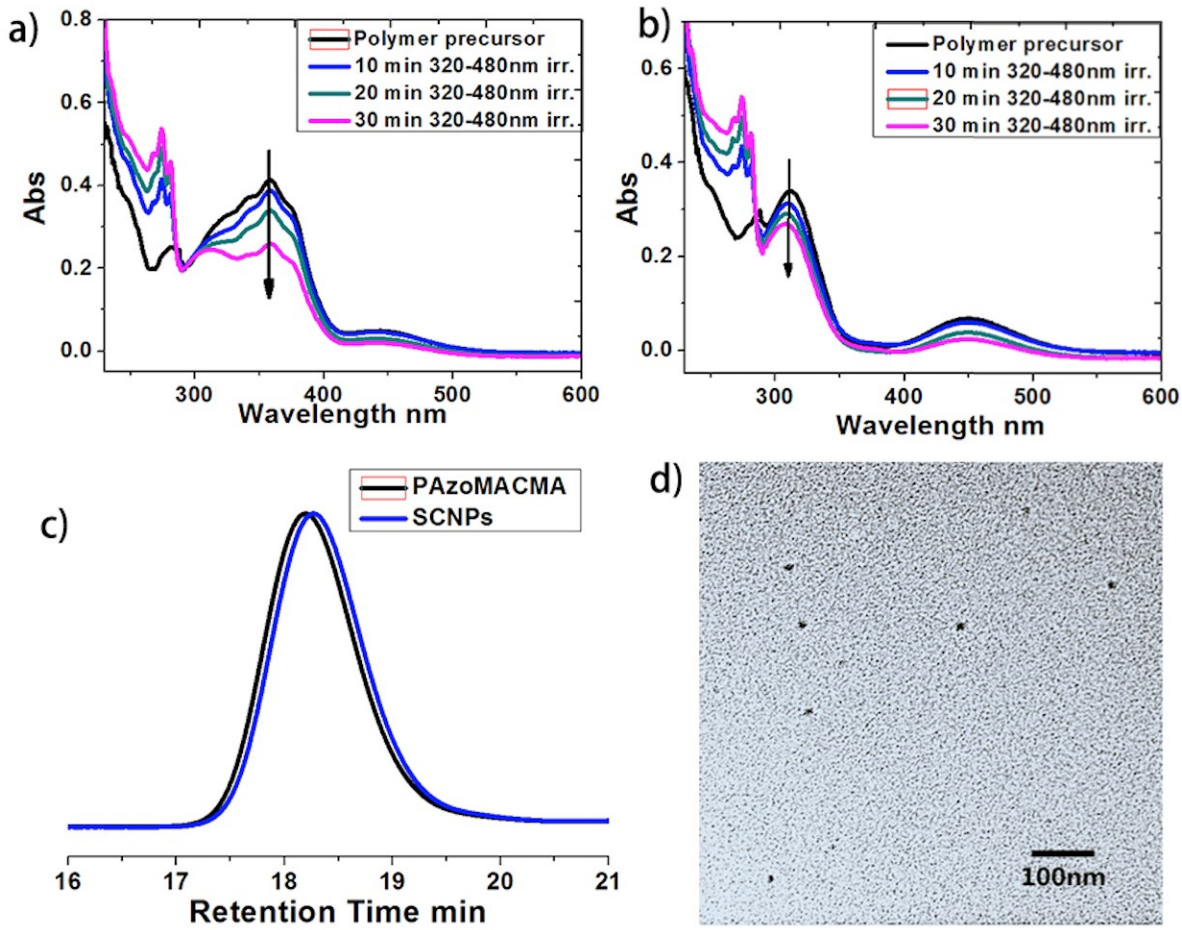

Figure 31. (a) UV-vis spectra of PAzoMACMA before and after 320-480 nm irradiation for different times (5 cm distance) (b) UV-vis spectra recorded after the solution in (a) was subjected to a second UV irradiation (365 nm) for 15 min. (c) SEC results from LS detection (90°) of linear polymer and SCNPs (d) TEM images of SCNPs.

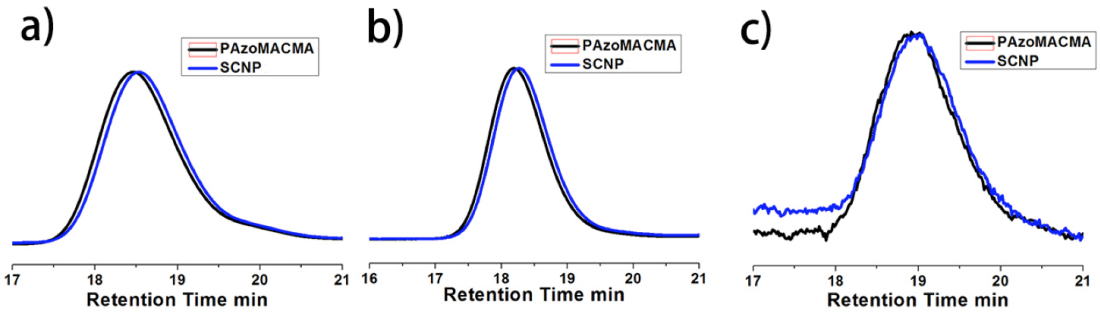

Figure 32. SEC traces of PAzoMACMA polymer precursor and SCNPs, a) Refractive Index (RI) detection traces. b) Light scattering (LS) detection traces (15°). c) Viscometric (VS) detection traces.

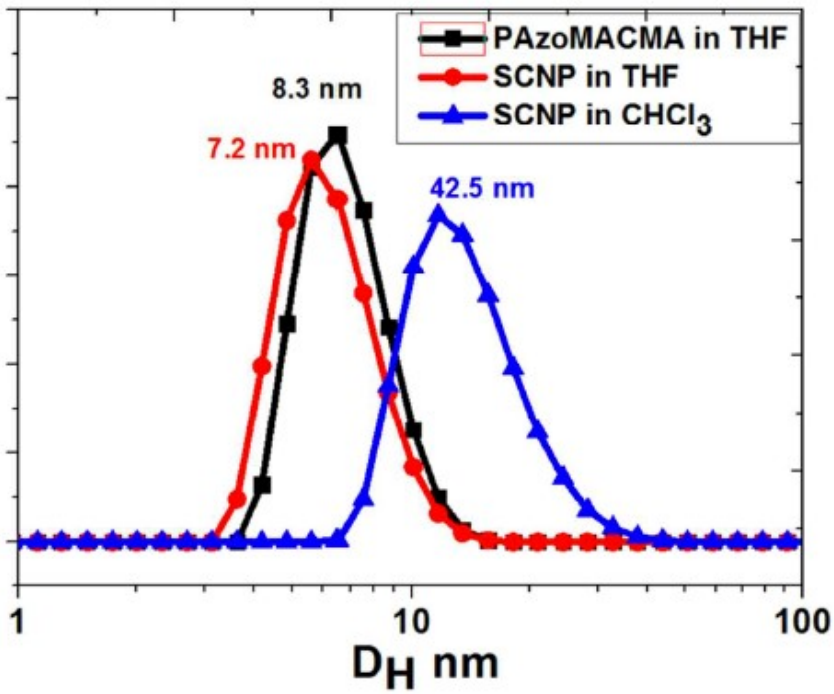

Figure 33. DLS results of linear polymer precursor of PAzoMACMA in THF and SCNPs in both THF and $CHCl_3$

Table 4. Triple detection SEC data of PAzoMACMA precursors and SCNPs

	Mn (g/mol)	Mw (g/mol)[a]	Đ	R_H (nm)[b]	[η] (mL/g)[b]
PAzoMACMA	10900	13400	1.2	2.5	5.3
SCNPs	10100	13100	1.3	2.3	4.7

a: Absolute Mw calculated from light scattering (LS) detection. b: calculated from viscometric detection results.

2.3.3 Liquid crystal order in PAzoMACMA SCNPs

As mentioned above, one of the interesting issues about SCNPs prepared using a LCP precursor is to know if the LC phases can persist in the nanoparticle under severe confinement and crosslinking effect. To have an answer to the question, a sample of PAzoMACMA SCNPs was collected by drying a THF solution of SCNPs, and used for DSC measurements. Figure 34a shows the obtained DSC heating curve of SCNPs and, for comparison, the curve of the polymer precursor. PAzoMACMA is known to display a smectic-nematic and a nematic-isotropic phase transition endothem on heating, which is visible at 76 ºC and 116 ºC. For SCNPs, despite the small amount of collected sample (1.5 mg), the two mesophase transitions remain noticeable, but the endotherms appear at lower temperatures and over a broader temperature range around 75 ºC and 107 ºC respectively.

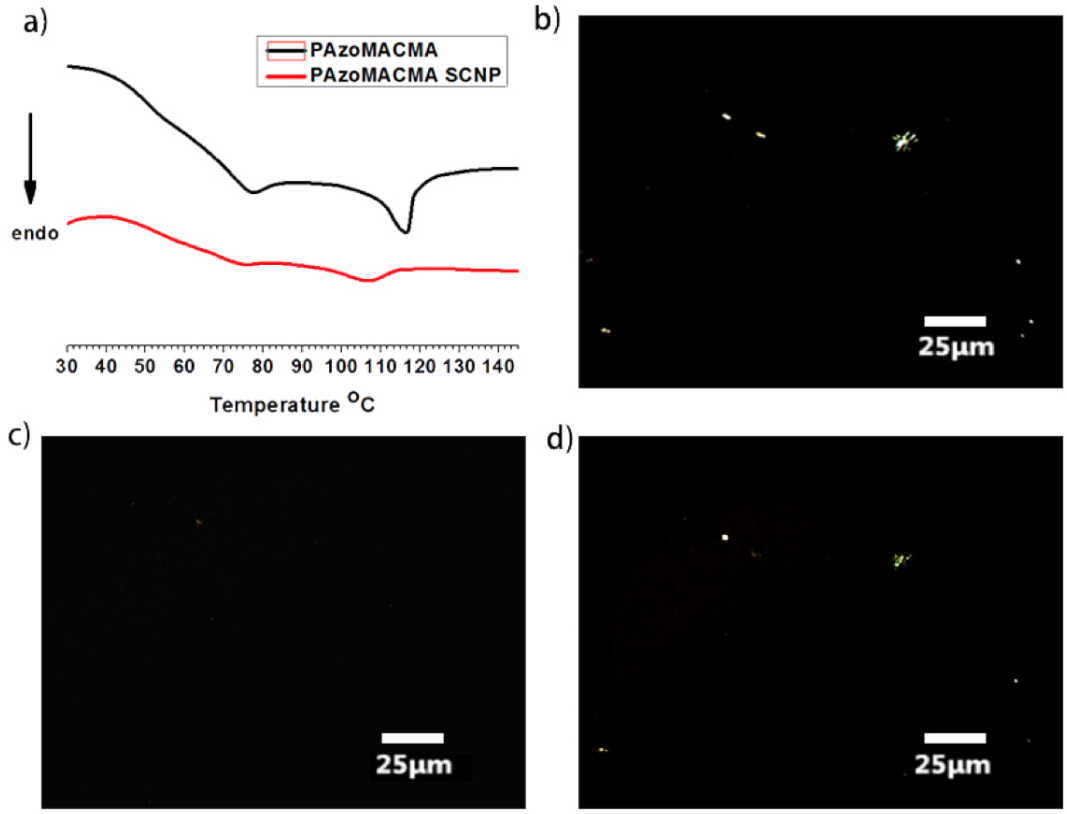

Figure 34. (a) DSC heating curves of polymer precursor and SCNPs. (b-d) Polarizing optical microscopy observation of SCNPs aggregates at room temperature (b), 185 ºC (c) and after annealing at 110 ºC (d).

The DSC results indicate that the LC phases of PAzoMACMA formed by the side-group azobenzene mesogens are preserved in SCNPs. However, the confinement and chain crosslinking (imposed chain topology) have as effect to reduce the LC orders as revealed by changes in mesophase transition temperatures. This is no surprise considering that the confinement and crosslinking could restrict the chain mobility as well as the motion of ordering mesogens.

The liquid crystal order in the PAzoMACMA SCNPs was further confirmed by polarizing optical microscopy (POM). Since dispersed nanoparticles are too small to be seen on POM, agglomeration of SCNPs was induced purposely by concentrating the SCNP solution and then casting on the microscopy plate. It is reasonable to assume that in an aggregate crosslinked chains could not interdiffuse, and that any observable anisotropy should come from 'collective' manifestation of SCNPs. Indeed, a number of bright aggregates can be spotted on the POM image in Figure 34b, indicating their birefringent nature that can only arise from the LC order in SCNPs. We note that on heating the sample into the isotropic phase (185 ^{o}C), the birefringence disappeared, while upon subsequent cooling the birefringent aggregates reappeared in the same regions. Annealing the SCNP to 110 ^{o}C for 72 h, the liquid crystal order of the SCNPs was formed and observed at the same position.

2.3.4 Optical behaviours of LC-SCNPs

After confirming the preservation of LC order formed by the azobenene mesogens in SCNPs, we wanted to know what are the possible effects of confinement and crosslinking on the optical property of the chromophores, mostly the photo-isomerization of azobenzene. Figure 35a shows a series of UV-vis absorption spectra of a solution of PAzoMACMA SCNPs in THF. After the initial solution was exposed to 365 nm UV light for 5 min, the absorption peak around 365 nm (π-π^* transition of *trans* azobenzene) disappeared while the absorption around 450 nm (n-π^* transition of *cis* azobenzene) raised in intensity, which indicates the conversion of basically all *trans* azobenzene into the *cis* isomer. Subsequently, when the solution of SCNPs with *cis* azobenzene was irradiated using a visible light (400-500 nm) for another 5 min, the absorption band of *trans* azobenzene reappeared as a result of the *cis*-*trans* back-isomerization. The apparent absorption of *trans* azobenzene is greater than the initial

solution, which implies the existence of a significant amount of *cis* azobenzene in the as-prepared SCNPs. The complete *trans-cis* isomerization occurred again under a second 365 nm UV irradiation. These results show that the confinement and intra-chain crosslinking does not hinder the reversible *trans-cis* photo-isomerization of azobenzene mesogens in the LC-SCNPs.

Interestingly, it was found that the optical behaviours of PAzoMACMA SCNPs could be affected by the solvent used. After removing THF, chloroform was added to re-disperse the dried SCNPs. Visually the obtained $CHCl_3$ solution of SCNPs shows little change with respect to the THF solution, its UV-vis absorption spectrum looks very different though. As seen in Figure 35b, in chloroform the absorption peaks are ill-resolved, likely caused by the rising spectral baseline with decreasing the wavelength, which is indicative of light scattering. It appears that chloroform is not as good a solvent as THF to disperse SCNPs and some aggregation of the nanoparticles occur in $CHCl_3$ according to the DLS result (Figure 33). When subjected to the same 365 nm UV irradiation, the *trans-cis* photo-isomerization could take place, but under subsequent visible light (400-500 nm) irradiation, the *cis-trans* back-isomerization was hardly discernible from the spectral change. The absorption spectrum of SCNPs with *trans* azobenzene was obtained by heating the solution to 75 ºC for 1h for thermal relaxation of *cis* azobenzene back to the *trans* form. Moreover, the difference in *trans-cis* photoisomerization of azobenzene mesogens in SCNPs between dispersion in THF and in chloroform was found to give rise to different fluorescence emissions. Generally, azobenzene and its derivatives are non-fluorescent, but exceptions are known in the literature for certain systems in which azobenzene moieties are under severe confinement effect that hampers the *trans-cis* photoisomerization. (167) With SCNPs in THF, no fluorescence was observable. By contrast, in $CHCl_3$, fluorescence emissions could be measured. Figure 35c

compares the emission spectra of SCNPs with azobenzene mesogens rich in either the *trans* or *cis* form and, in each case, using two excitation wavelengths at 365 nm and 460 nm corresponding to the maximum absorption of *trans* and *cis* azobenzene, respectively. It appears that the azobenzene *trans* and *cis* isomers in SCNPs fluoresce at different wavelengths. Under 365 nm excitation, the emission of the SCNP solution rich in *trans* azobenzene is peaked around 450 nm, while the solution rich in *cis* azobenzene exhibits dominant emission at longer wavelengths near 522 nm. Under 460 nm excitation, both samples show emission centered around 522 nm, but the emission of SCNPs rich in *cis* isomer is much more intense, further indicating that the longer-wavelength emission comes from *cis* azobenzene. From the above observation, it seems that intra-chain crosslinked PAzoMACMA was less soluble in chloroform than in THF, which results in a more compact SCNP structure in the former (also agglomeration to some extent) and, consequently, a more severe confinement that hinders somehow the photoisomerization of azobenzene mesogens and thus results in fluorescence emission. It should be noted that the used excitation wavelength of 365 or 460 nm is outside the absorption region of coumarin so that the observed fluorescence emission cannot arise from this chromophore in the polymer structure.

2.3.5 Photo-induced deformation of LC-SCNPs

One of the most interesting properties of azobenzene-containing polymers, especially LCPs, is that they can undergo a variety of photo-induced deformation as a result of the *trans-cis* photo-isomerization. For instance, films of liquid crystalline elastomers or networks bearing azobenzene mesogens can be bent towards or away from an actinic UV light depending on the orientation state of azobenzene mesogens, and unbent under visible light irradiation. (168-171) For azobenzene polymers in the form of colloidal particles, photo-induced

deformation under linearly polarized light (LPL), converting spherical particles to elongated shape, has long been reported. (172-174)

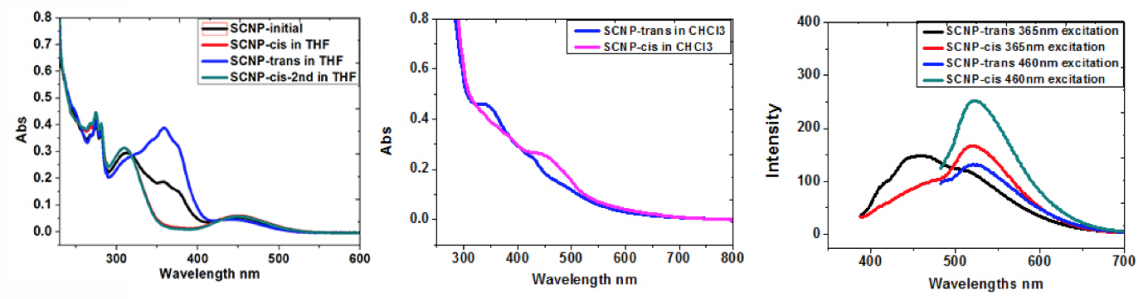

Figure 35. (a) UV-vis absorption spectra of SCNPs in THF (0.2 mg/mL) for initial solution and, subsequently, after 365 nm UV irradiation for 5 min, after 400-500 nm visible light irradiation for 5 min and after 365 nm UV irradiation for 5 min again). (b) UV-vis absorption spectra of SCNPs in chloroform (0.2 mg/mL) in the rich-in-*cis* state after 365 nm UV irradiation for 15 min and in the subsequent rich-in-*trans* state after thermal relaxation at 70 ºC for 1 h. (c) Fluorescence emission spectra of SCNPs in chloroform in both rich-in-*cis* and rich-in-*trans* state and, in each case, under excitation at 365 nm and 460 nm, respectively.

Since PAzoMACMA SCNPs are crosslinked LCP based on azobenzene mesogens, it is of interest to know if photo-induced deformation can also be observed for this type of nanoparticles. We carried out AFM observations by casting very dilute polymer solution (<0.01 mg/mL) on mica plates in order to deposit well separated nanoparticles. The results confirmed the occurrence of deformation of LC-SCNPs, being mostly circular before irradiation while becoming stretched after irradiation. Moreover, the experiments also revealed an unexpected phenomenon; that is, the stretching direction of the nanoparticles appeared to be dependent upon the wavelength of the LPL. In one case, the SCNP sample was first heated to 115 ºC (in the isotropic phase) for thermal equilibrium, then irradiated

under non-polarized visible light irradiation (400-500 nm) for 15 min to make all *trans*-state of azobenzene moieties in SCNPs, and finally exposed to linearly polarized 365 nm UV light at 115 ºC for 15 min before cooling to room temperature under the irradiation. As can be seen in Figure 36b (and Figure 37a), the nanoparticles appeared to stretch out in the direction perpendicular to the polarization of the actinic UV light. This is generally believed to be related to photo-induced orientation of azobenzene moieties in the direction perpendicularly to the polarization, as the increased amount of oriented *trans* azobenzenes in that direction could result in 'shrinkage' of the nanoparticle in the light polarization direction. (174)

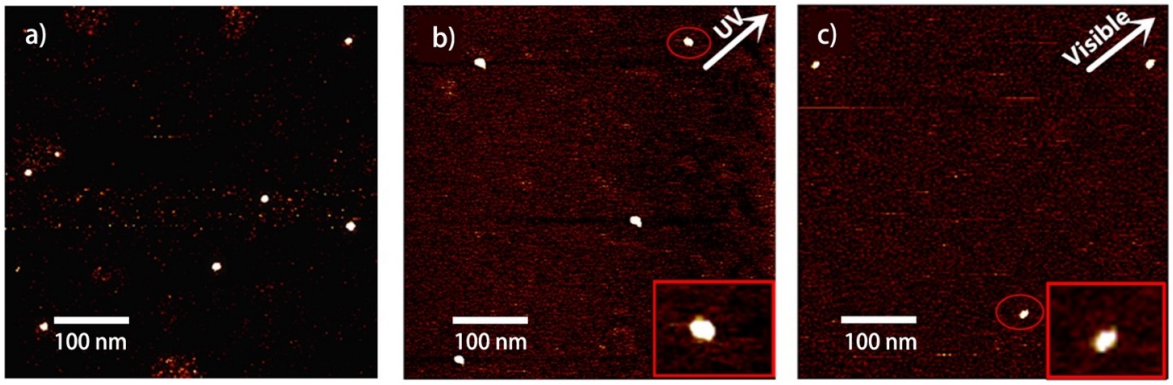

Figure 36. AFM images of LC-SCNPs: a) initial, b) after linearly polarized UV irradiation (365 nm), and c) after linearly polarized visible light irradiation (400-500 nm). The arrow indicates the light polarization direction and the insert shows an enlarged image of a single deformed nanoparticle.

The photo-induced deformation is different when the SCNP sample was subjected to the same treatment as above while only switching the wavelengths for the unpolarised pre-irradiation and the subsequent linearly-polarized irradiation. In this case, the sample was first exposed to unpolarized 365 nm UV before being irradiated with polarized visible light (400-500 nm)

and cooled under irradiation until room temperature. The AFM image shows stretching of the nanoparticles along the polarization direction (Figure 36c and Figure 37b). At this point, the mechanism leading to the stretching parallel to the visible light polarization is unclear, it is likely to be caused by photo-induced anisotropic mass transportation though. It is noticed that similar 'parallel' elongation of colloidal particles of an azobenzene LCP was reported by the groups of Wang and Zhu. (175, 176) Regardless of the irradiation conditions, the shape change of LC-SCNPs is not prominent, because the intra-chain crosslinking could restrict chain mobility and hamper mass transport inside the nanoparticles.

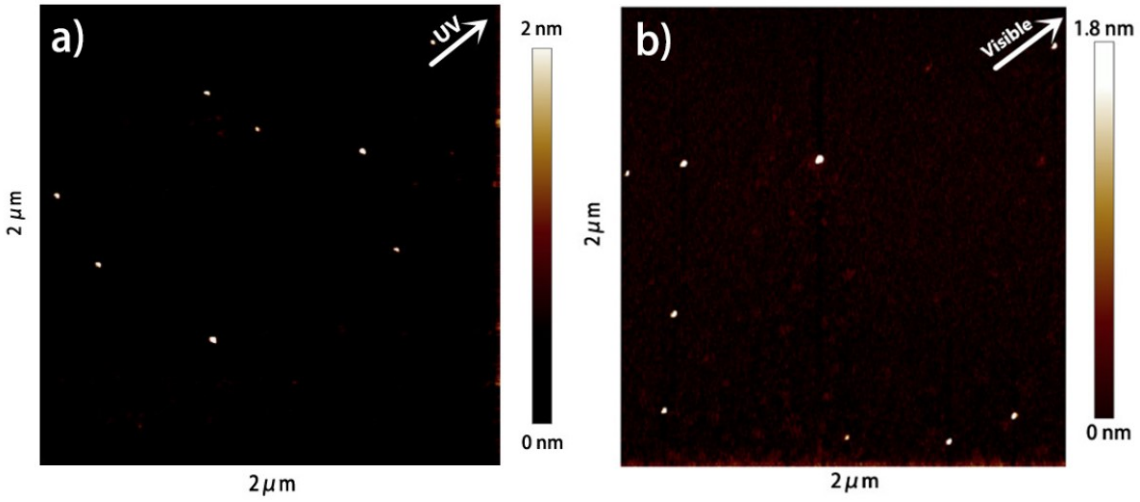

Figure 37. AFM images of deformed SCNPs under linearly polarized UV (365 nm) (a) and visible light (400-500 nm) irradiation (b). The arrow indicates the light polarization direction.

2.3.6 Stretching-induced orientation in a nanocomposite with LC-SCNPs

An all-polymer nanocomposite of poly(methyl methacrylate) (PMMA) loaded with LC-SCNPs was prepared and investigated. It contains 0.5 % of the nanoparticles in weight. Figure 38a shows a photo of the nanocomposite film. It appears transparent, indicating good

dispersion or compatibility of LC-SCNPs in the PMMA matrix, and slightly yellowish due to the presence of azobenzene mesogens in the material. The film was stretched at 113 ºC (above Tg of PMMA) to 400 % strain, followed by cooling to room temperature to retain the film in the elongated state for polarized absorption spectral measurements. As can be noticed from Figure 38b, the stretched film displays a strong parallel dichroism for the absorption peaks of azobenzene moieties, indicating that the mesogens are preferentially oriented along the stretching direction inside LC-SCNPs. The order parameter *S* calculated at 365 nm is about 0.2, according to $S=(A_{//}-A_{\perp})/(A_{//}+2A_{\perp})$ where $A_{//}$ and $A_{\perp}$ are the absorbances with the spectrophotometer's light polarized parallel and perpendicular to the stretching direction, respectively. The stretching-induced orientation of azobenzene moieties confined in the SCNPs is reminiscent of side-chain LCPs, of which the side-group mesogens can be effectively aligned upon deformation of the polymer. This result implies that in the PMMA/LC-SCNP nanocomposite, the nanoparticles could be deformed by mechanical stretching resulting in orientation of azobenzene mesogens.

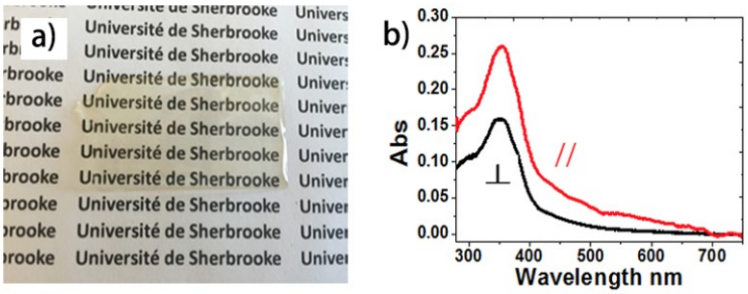

Figure 38. (a) Photograph of a PMMA/LC-SCNP nanocomposite film. (b) Polarized UV-vis spectra of the PMMA/LC-SCNP film stretched at 113 ºC to 400 % strain followed by cooling to room temperature, being recorded with the spectrophotometer's beam polarized parallel and perpendicular, respectively, to the film stretching direction.

2.4 Conclusion

We have designed and synthesized new sub-15 nm LC-SCNPs with multiple functions. They were prepared using a side-chain liquid crystalline polymer PAzoMACMA bearing two types of photoactive moieties: coumarin in minoriy for intra-chain crosslinking and azobenzene in majority as mesogens for liquid crystalline state. Despite the tiny size and severe confinement of SCNPs, LC order was found to persist and the *trans-cis* photoisomerization of azobenzene occurs. More interestingly, such LC-SCNPs exhibited a number of interesting properties. First, when re-dispersed in a less good solvent like chloroform, they displayed significant fluorescence emission that is dependent upon the isomer state of azobenzene mesogens. Secondly, when exposed to linearly polarized irradiation, those LC-SCNPs could undergo photo-induced deformation, changing from initially spherical form to stretched shape. The AFM observation proved that the photo-deformation of LC-SCNPs depends on the excitation wavelength, the stretching of nanoparticles being perpendicular to the light polarization under 365 nm UV light while becoming parallel to the light polarization under 400-500 nm visible light. Finally, the LC-SCNPs could be well dispersed in PMMA matrix leading to a new type of all-polymer nanocomposite. Their LC nature was further revealed by the preferential orientation of azobenzene mesogens induced by stretching the nanocomposite film above Tg of PMMA followed by cooling to room temperature. We hope these ultra-small liquid crystalline, multi-functional SCLCPs will provide new possible applications in such areas as bio-imaging and LC materials.

2.5 Statement of Contribution

This work was published in *Polymer Chemistry* **2017**, *8*, 3523-3529**.** DOI: 10.1039/C7PY00668C. The paper is authored by Weizheng Fan, Xia Tong, Guo Li and Yue Zhao. This research work was carried out in the Université de Sherbrooke under the supervision of Prof. Zhao. Xia Tong did the AFM measurements and Guo Li helped for stretching the nano-composited film by Instron. I performed all the other experiments and characterizations. I wrote the first draft of the manuscript and Prof. Zhao finalized the manuscript.

CHAPTER 3 CO_2-RESPONSIVE POLYMER SINGLE-CHAIN NANOPARTICLES FOR GAS-SENSITIVE SELF-ASSEMBLY AND NANOREACTORS

3.1 Introduction

Polymer nanoparticles have long been a topic of active research in the fields of nanoscience and nanotechnology due to their ease of fabrication and applications in many areas. (1, 2) Over the past decade or so, fabricating nanoparticles based on collapsing or folding one single polymer chain has emerged as an important technology. The growing interest in the so-called polymer single-chain nanoparticles (SCNPs) stems from their tunable small sizes and size-enabled unique properties useful for a wide range of applications such as nanoreactor, sensor, catalytic system, low viscosity coating, bio-imaging and drug delivery applications. (4, 12, 15, 18-20, 79, 90, 100, 101, 146, 177, 178) Generally, SCNPs are prepared *via* intra-chain crosslinking using either covalent or noncovalent bonding, requiring well-separated macromolecules in a dilute solution (<1 mg/mL) to avoid inter chain coupling. (13, 16, 21, 25, 65, 104, 107, 179-181) Studies reported by many groups have now shown that a variety of chemistries can be utilized for efficient intra-chain crosslinking leading to SCNPs. (34, 36, 39, 41, 45, 62, 63, 72, 75-77, 86, 95, 98, 99, 182) In recent years, research effort has been increasingly focused on a more challenging issue, namely, how to make functional SCNPs that target a specific application. (16) A few examples include fluorescent SCNPs as imaging agents, (44, 89, 183) biocompatible SCNPs, (41) bio-mimicking SCNPs, (158) and tadpole-like amphiphilic 'Janus' SCNPs capable of self-assembling into hierarchical structures like proteins. (52, 91, 94, 147, 184, 185)

Stimuli-responsive SCNPs represent one class of functional SCNPs since they can respond to external stimuli, such as variation in pH or temperature, exposure to redox species, light or ultrasound and so on, by undergoing certain change either in structure or morphology or property. (59, 94) For example, Pu's group reported voltage-responsive SCNPs *via* host-guest interaction to control the folding and unfolding of polymer chains. (96) Loinaz *et al.* prepared thermo-responsive SCNPs whose solution displayed gradual decrease in transmittance around the lower critical solution temperature (LCST) of the linear polymer precursor. (84) As for our group, we demonstrated a type of photo-degradable SCNPs using coumarin chemistry. (160) One convenient way to render SCNPs responsive to a particular type of stimulation obviously is to prepare SCNPs using a polymer precursor that is responsive to that stimulus. To this regard, CO_2, a gaseous stimulus, has not been explored for SCNPs yet. Being a non-toxic and inexpensive gas as well as a physiological stimulus, development of CO_2-switchable polymers and related materials has gained momentum in recent years, and many possible applications have been demonstrated. (118-120, 122, 144, 145, 186-190) Among the notable advantages, the stimulation intensity of CO_2 can readily be tuned by controlling the bubbled or injected amount of the gas in aqueous solution; and by using tertiary amines or amidines as CO_2-reactive moieties in the polymer structure, CO_2 can also be easily removed by purging the solution with an inert gas (N_2 or Ar) or heating. This feature makes the reversible switching process robust and repeatable over many cycles without any chemical contamination, in contrast to pH-change induced switching, for which the alternating acid/base addition in solution results in salt accumulation.

In the present study, we investigated the first CO_2-responsive SCNPs and their application as gas-sensitive nanoreators for the synthesis of gold nanoparticles (AuNPs). As will be shown further on, on one hand, SCNPs were prepared through intra-chain photocrosslinking

of a random copolymer precursor of N, N-dimethylaminoethylmethacrylate (DMAEMA) in majority and coumarin methacrylate in minority, referred to as P(DMAEMA-*co*-CMA). The nanoparticles could undergo repeated swelling/shrinking in aqueous solution upon alternating CO_2/N_2 bubbling, as a result of the protonation/ deprotonation of tertiary amine groups (Figure 39a). On the other hand, amphiphilic, tadpole-like 'Janus' single-chain nanoparticles (SCJNPs) were prepared using a diblock copolymer precursor of PS-*b*-P(DMAEMA-*co*-CMA), with the polystyrene (PS) block acting as a 'tail' (Figure 39b). In this case, SCJNPs could further self-assemble into micelles of larger sizes, which could also exhibit gas-controlled reversible expansion and contraction upon CO_2/N_2 bubbling. Both SCNPs and micelles of SCJNPs were utilized as gas-sensitive nanoreactors to synthesize AuNPs in aqueous solution. The rate of AuNP formation and the size of AuNPs or their aggregates were found to be adjustable by controlling the passage of CO_2 or N_2 in the reactive solution. Furthermore, we show that with the controlled aggregation of AuNPs resulting from the large micellar reactor of SCJNPs, the surface plasmon resonance (SPR) absorption underwent red shift. This allowed us to the use a long-wavelength red light (635 nm), sought for biomedical applications, to generate a sufficient photo-thermal effect for optically inducing the sol-gel transition of a thermo-responsive block copolymer.

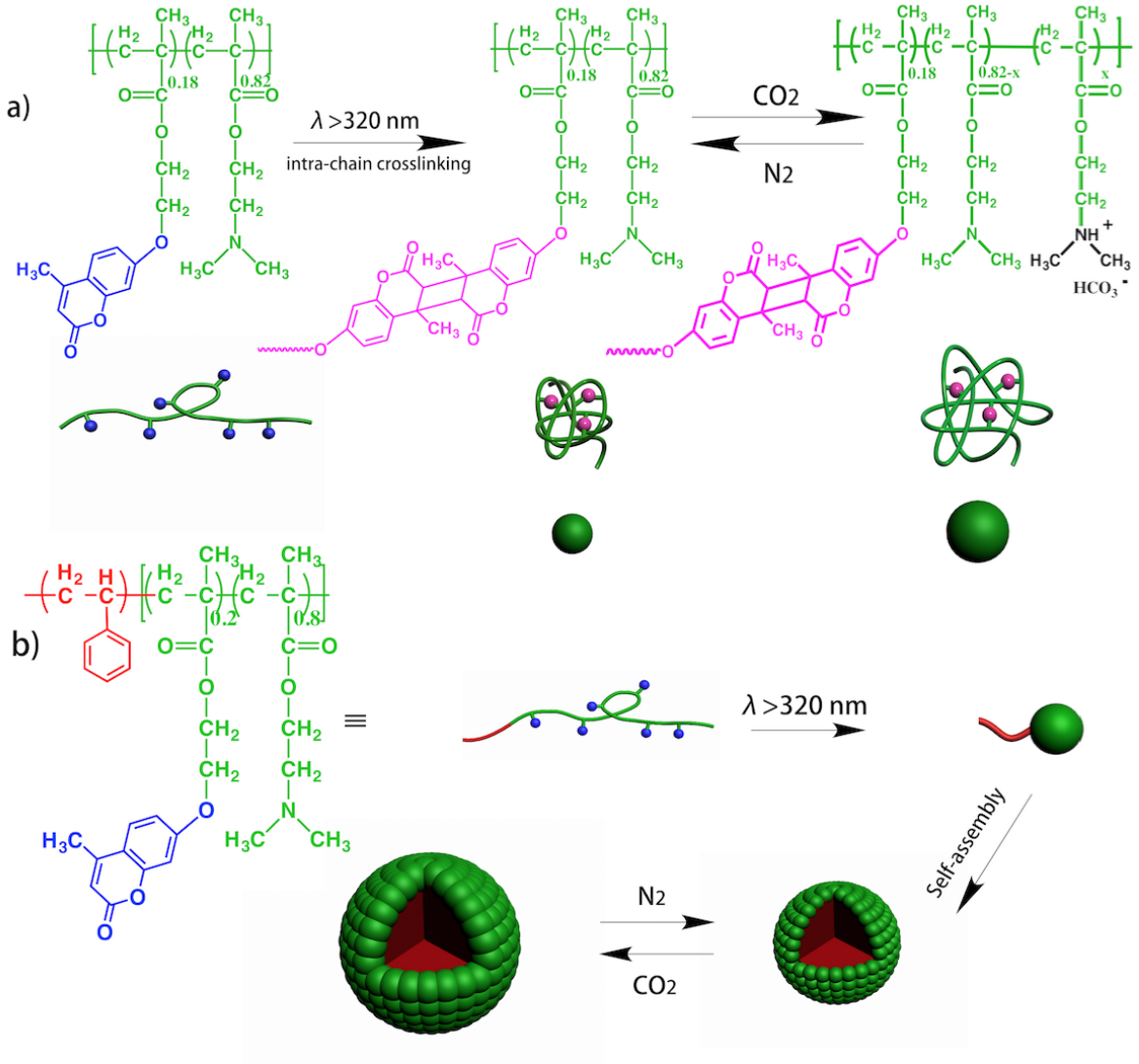

Figure 39. Schematic illustration for: (a) preparation of P(DMAEMA-*co*-CMA) single-chain nanoparticles (SCNPs) through intra-chain photo-crosslinking (*via* photo-dimerization of coumarin groups) and the gas-switchable size change of SCNPs in aqueous solution; and (b) preparation of amphiphilic, tadpole-like PS-*b*-P(DMAEMA-*co*-CMA) single-chain 'Janus' nanoparticles (SCJNPs) and their gas-responsive self-assembled micellar aggregates.

3.2 Experimental Section

3.2.1 Materials

All chemicals were purchased from Aldrich and used as received unless otherwise noted. N, N-dimethylamino-ethyl methacrylate (DMAEMA, 98 %) was passed through a basic aluminium oxide column and distilled under vacuum prior to use. 4-Methyl-[7-(methacryloyl)oxy-ethyl-oxy] coumarin (coumarin methacrylate, CMA) was synthesized by using a previously reported method. (165) 2, 2'-Azobis(isobutyronitrile) (AIBN) was recrystallized twice from ethanol before use. The chain transfer agent, 2-(2 cyanopropyl) dithiobenzoate (CPDB), was synthesized according to literature methods. (191) The synthesis of the ABA-type triblock copolymer P(MEO_2MA-*co*-MAA)-*b*-PEO-*b*-P(MEO_2MA-*co*-MAA) (Mn=146000, PDI=1.23) was reported previously. (143) The middle block is water-soluble poly(ethylene oxide) (PEO) and the end blocks are a random copolymer of 2-(2-methoxyethoxy)ethyl methacrylate and methacrylic acid (P(MEO_2MA-*co*-MMA). (Scheme 7)

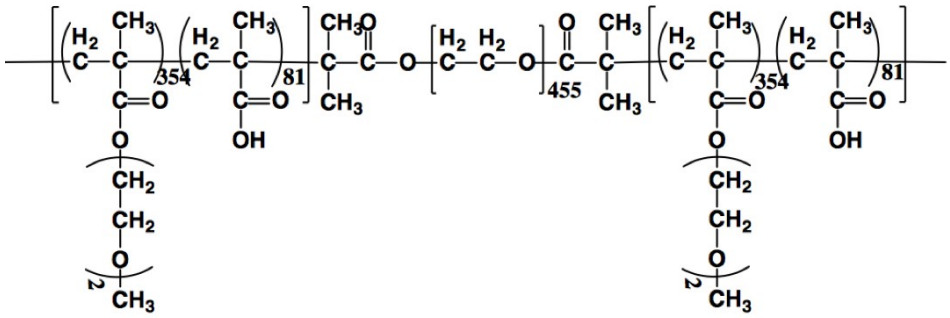

Scheme 7. Chemical structure of P(MEO_2MA-*co*-MAA)-*b*-PEO-b P(MEO_2MA-*co*-MAA)

3.2.2 Synthesis of P(DMAEMA-*co*-CMA)

The P(DMAEMA-*co*-CMA) was synthesized by 2-(dimethylamino)ethyl methacrylate (DMAEMA) and 4-methyl-[7-(methacryloyl)oxy-ethyl-oxy] (CMA) in a random copolymerization manner and at a molar ratio of coumarin to DMAEMA of 1:6.6 *via* reversible addition-fragmentation chain-transfer polymerization (RAFT). DMAEMA (1.57 g, 10 mmol), CMA (432 mg, 1.5 mmol), CPDB (11 mg, 0.05 mmol) and AIBN (3.3 mg, 0.02 mmol) were dissolved in 4 mL anisole (99 %, anhydrous) in a 10 mL flask. The reaction mixture was degassed under vacuum and refilled with nitrogen for 30 min. Then, the flask was placed in a pre-heated oil bath at 65 ^{o}C for 24 h. After polymerization, the reaction mixture was cooled to room temperature; the polymer was collected after three times of precipitation in hexane, and dried under vacuum for 24 h, obtaining 1.2 g white solid product (yield: 60 %). The obtained polymer has a number-average molecular weight Mn=18200 g/mol, Mw=21900 g/mol and a polydispersity index PDI (Mw/Mn)=1.2 according to SEC measurements in THF using polystyrene (PS) standards. The actual content of coumarin analyzed from the ^{1}H NMR spectrum is 17.8 %. (Figure 40)

3.2.3 Synthesis of PS-*b*-P(DMAEMA-*co*-CMA)

To fabricate amphiphilic tadpole-like single-chain 'Janus' nanoparticles and prepare the SCJNPs self-assemblies, the amphiphilic copolymer with addition polystyrene hydrophobic block, PS-*b*-P(DMAEMA-*co*-CMA), was synthesized by typical atom transfer radical polymerization (ATRP) condition.

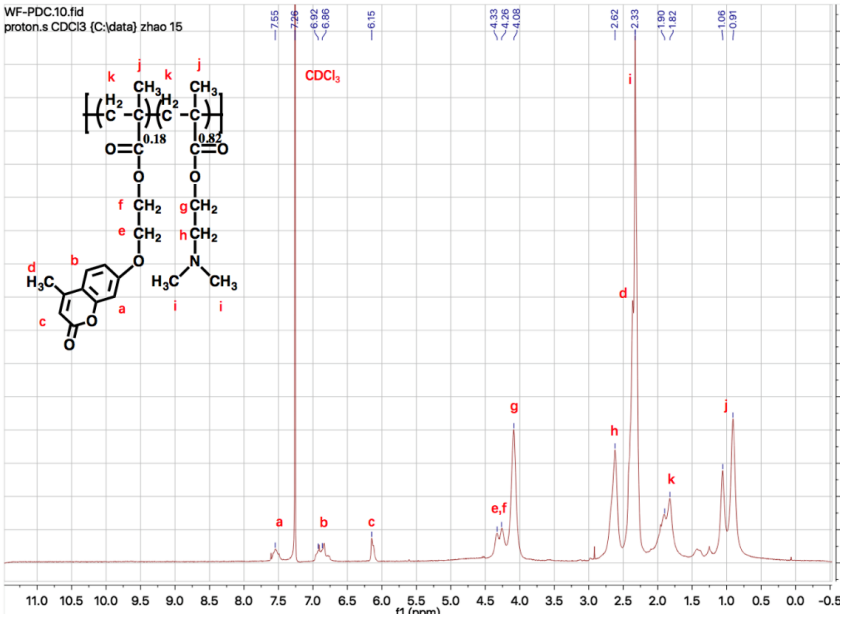

Figure 40. ^{1}H-NMR spectra of P(DMAEMA-*co*-CMA) polymer precursor in $CDCl_3$

3.2.3.1 Synthesis of PS macro-initiator

Ethyl α-bromoisobutyrate (39 mg 0.2 mmol), styrene (2.08 g, 20.0 mmol), CuBr (14 mg, 0.1mmol) and PMDETA (20 μL, 0.1 mmol) were added into a round bottom flask, followed by three freeze-pump-thaw cycles. The flask was reacted at 110 ºC with magnetic stirring. After reaction for 4h, the resulting solution was immersed to liquid nitrogen in order to stop the radical polymerization. Then the solution was diluted to 30 mL of THF and passed through a neutral alumina column twice to remove the copper catalyst. The filtrate was concentrated to 5 mL, and then precipitated into 200 mL of cold hexane for three times. The product was collected and dried in vacuum oven at room temperature for 24 h, yielding 0.74 g product (conversion: 36 %). The polystyrene block polymer has a number-average molecular weight Mn=3300 g/mol and a polydispersity index PDI (Mw/Mn) 1.17 according to SEC measurements in THF using polystyrene (PS) standards.

3.2.3.2 Synthesis of PS-*b*-P(DMAEMA-*co*-CMA).

The above product (PS-Br, 0.175 g, 0.05 mmol), DMAEMA (1.57 g, 10.0 mmol), CMA (432 mg, 1.5 mmol), CuBr (7 mg, 0.05 mmol), PMDETA (10 μL, 0.05 mmol), and 4 mL of anisole were added into a round bottom flask, followed by three freeze-pump-thaw cycles. The flask was reacted at 70 ºC with magnetic stirring. After reaction for 24 h, the resulting solution was immersed into liquid nitrogen so as to deactivate the free radical. Then the solution was added 30 mL of THF and then passed through neutral alumina column twice to remove the copper catalyst off. The filtrate was concentrated to 3 mL and then precipitated into 100 mL of cold hexane for three times. The product was collected and dried in vacuum at room temperature for 24 h, obtaining 1.4 g product (yielding 64 %). The PS-*b*-P(DMAEMA-*co*-CMA) has a number-average molecular weight Mn=13000 g/mol and a weight-average molecular Mw=17700 g/mol and a polydispersity index PDI (Mw/Mn)=1.36. The actual content of polystyrene, coumarin and PDMAEMA analyzed from the ^{1}H NMR spectrum is 32 %, 13.6 % and 54.4 % respectively. (Figure 41)

3.2.4 Preparation of single-chain nanoparticles of P(DMAEMA-*co*-CMA).

To fabricate the SCNPs, 5 mg of P(DMAEMA-*co*-CMA) was dissolved in 10 mL of THF and kept under stirring overnight. After being filtered with a 200 nm pore size Teflon filter, the solution was exposed to 320-480 nm UV-visible light for 30 min (achieving about 60 % dimerization degree for coumarin groups). The solution was concentrated by solvent evaporation under vacuum, and polymer nanoparticles were then precipitated in hexane, collected and dried under vacuum. The obtained SCNPs could be re-dispersed in water or THF to form a homogenous solution with a desired concentration for further characterization.

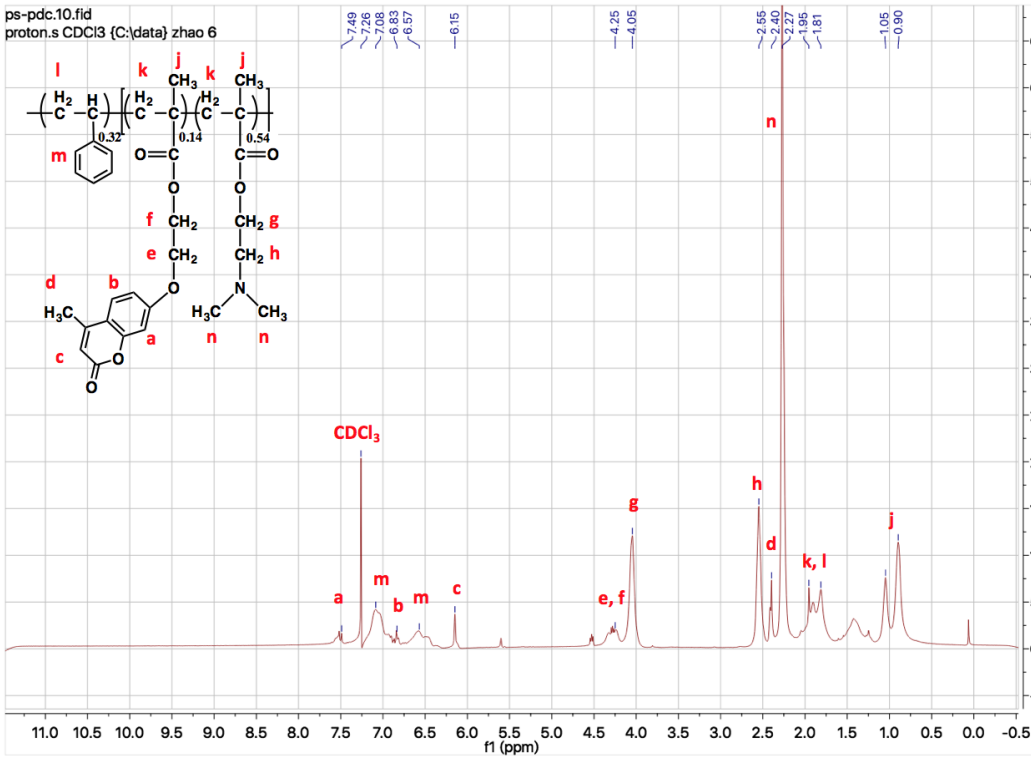

Figure 41. ^{1}H-NMR spectra of PS-*b*-P(DMAEMA-*co*-CMA) polymer precursor in $CDCl_3$

3.2.5 Preparation of tadpole-like single-chain 'Janus' nanoparticles and self-assembly.

Basically the same method as described above was used to prepare the amphiphilic SCJNPs, that is, 5 mg of PS-*b*-P(DMAEMA-*co*-CMA) diblock copolymer was dissolved in 10 mL of THF and the dilute solution was then subjected to 320-480 nm light exposure for 20 min to achieve about 60 % dimerization degree of coumarin moieties, yielding collapsed nanoparticles After being collected and dried, due to the presence of hydrophobic PS tail of the tadpole nanoparticle, SCJNPs could not be directly re-dispersed in water; instead they could be re-dispersed in THF, which is a good solvent for both PS and P(DMAEMA-*co*-CMA), to form a homogenous solution. To induce self-assembly of the amphiphilic SCJNPs,

typically, 6 mL deionized water was added under a slow rate (1 mL/h) into 1 mL SCJNPs THF solution (5 mg/mL) with mild stirring. In the end, THF in the solution was removed by slow evaporation under ambient conditions. The resulting aqueous solution with self-assembled micellar aggregates of SCJNPs was used for study.

3.2.6 Synthesis of gold nanoparticles (AuNPs) using CO_2-responsive nano-reactors of SCNPs or SCJNP micelles.

The synthesis of AuNPs was conducted in water solution using both P(DMAEMA-*co*-CMA) SCNPs and PS-*b*-P(DMAEMA-*co*-CMA) SCJNP micelles as CO_2-responsive nanoreactors. Table 5 summarizes the conditions used for the reduction reaction leading to AuNPs. The CO_2 bubbling time determines the amount of CO_2 injected into the aqueous solution and affects the size and morphology of the nanoreactors. Using SCNP3 and SA3 samples as examples, details are as follows. For SCNP3, 9 mg P(DMAEMA-*co*-CMA) SCNPs were dissolved in 9 mL deionized water, and the solution was bubbled with CO_2 at a rate of 50 mL/min for 2 min. Afterward, 1.5 mL of $HAuCl_4$ water solution (1 mg/mL) was added into the 9 mL of CO_2-bubbled water solution of SCNPs (1 mg/mL) for reaction. As for SA3, 9mL micellar solution of PS-*b*-P(DMAEMA-*co*-CMA) SCJNPs (1 mg/mL) in deionized water was bubbled with CO_2 for 2 min, then 1 mL $HAuCl_4$ water solution (1 mg/mL) was added into the CO_2-bubbled SCJNP micellar solution for reaction. The reduction reaction was carried out under stirring at room temperature and the amount of formed AuNPs was monitored by UV-vis spectroscopy.

Table 5. Conditions for the synthesis of AuNPs in water using nanoreactors of either P(DMAEMA-*co*-CMA) SCNPs or micelles of PS-*b*-P(DMAEMA-*co*-CMA) SCJNPs.

Sample	Polymer	Au/N[a]	Time of CO_2 bubbling [b]	pH[c]
SCNP1	P(DMAEMA-*co*-CMA) SCNPs	1/11	0 min	8.44
SCNP2	P(DMAEMA-*co*-CMA) SCNPs	1/11	0.5 min	5.37
SCNP3	P(DMAEMA-*co*-CMA) SCNPs	1/11	2 min	4.96
SA1	PS-*b*-P(DMAEMA-*co*-CMA) SCJNP micelles	1/13	0 min	7.82
SA2	PS-*b*-P(DMAEMA-*co*-CMA) SCJNP micelles	1/13	0.5 min	5.53
SA3	PS-*b*-P(DMAEMA-*co*-CMA) SCJNP micelles	1/13	2 min	4.69

(a) N was calculated from the number of tertiary amine groups in the polymer. (b) CO_2 bubbling rate was 50 mL/min. (c) pH of the solutions was measured after CO_2 bubbling and before addition of $HAuCl_4$.

3.2.7 Instrumentation and characterization methods.

^{1}H NMR spectra were recorded on a Bruker AC400 (400MHz) spectrometer with $CDCl_3$ as the solvent. Size exclusion chromatograph (SEC) measurements were performed on a Waters system equipped with a photodiode array detector (PDA 996) and a refractive index detector (RI 410). THF was used as the eluent at an elution rate of 1 mL/min, while polystyrene standards were used for calibration. The dilute SCNP solutions were directly injected into the column of SEC for the measurement after photodimerization. Dynamic light scattering (DLS) measurements were performed on a Malvern Zetasizer Nano ZS ZEN3600 with a

helium-neon laser (λ= 633 nm), using a scattering angle of 173Å. The polymer was photocrosslinked using an OmniCure@ Series 1000 UV lamp with 320-480 nm filter (280 mW/cm^2 at 350 nm, distance from the sample set at 5 cm). The photodimerization degree of coumarin groups as well as the appearance of AuNPs were monitored by recording UV-vis spectra on a Varian 50 Bio UV-vis spectrophotometer. The morphologies of SCNPs, self-assemblies of SCJNPs and AuNPs were examined using a Hitachi H-7500 transmission electron microscope (TEM) operating at 80 kV. The samples of SCNPs and AuNPs were prepared by casting a drop of their dilute solution on a carbon-coated copper grid, followed by drying at room temperature. In the case of SCJNP self-assembly, samples were prepared by drop-casting the solution onto a carbon-coated copper grid, which was then stained by 0.2 % phosphotungstic acid and freeze-dried before observation. Atomic force microscopy (AFM) images were recorded on a Dimension Icon AFM instrument equipped with a NanoScope V controller (Veeco/Digital Instruments, Santa Barbara, CA). AFM topographical images were obtained under ScanAsyst mode at room temperature using a silicon nitride cantilever tip (force constant 0.4 N/m). The cloud point of a given polymer solution was taken as the inflection point of the transmittance vs temperature curve. The solution transmittance was measured at 700 nm using a Carry 6000i UV-vis-NIR spectrometer. The solution pH was measured using a pH-meter (Fisher Scientific accumet AB 15 pH-meter with 13-620-223A accumet glass pH electrode). The sol-gel transition was observed under 635 nm irradiation (1 W/cm^2) (using a CNI model with PSU-H-LED laser from Changchun New Industries Optoelectronics Technology Co., Ltd.). CO_2 and N_2 were bubbled by inserting a needle in the solution at a flow rate of 50 mL/min.

3.3 Results and Discussion

3.3.1 Preparation and characterization of P(DMAEMA-*co*-CMA) SCNPs

To aim the single-chain nanoparticles with CO_2-responsive functions, the polymer structure contains two functional groups: DMAEMA and coumarin. The coumarin methacrylate provide the crosslinkers of the intra-chain crosslinking system to form the single-chain nanoparticles by using '2+2'dimerization reaction under 320-480 nm UV-light irradiation. DMAEMA provide CO_2-responsive functional groups, of which the tertiary amine can be protonated by CO_2. The SCNPs of DMAEMA containing polymer can be expected to exhibit CO_2-responsive that the reversible hydrophilicity adjustable by CO_2 and N_2 bubbling.

Single-chain nanoparticles of P(DMAEMA-*co*-CMA) were prepared by intra-chain crosslinking *via* photo-dimerization of coumarin groups, as reported previously. (62) To avoid intermolecular crosslinking, the solution was diluted to 0.5 mg/mL before exposure to light, presuming the absence of chain aggregation. Collected in Figure 42 are the usual characterization results used to confirm the formation of SCNPs. Under 320-480 nm irradiation, the photodimerization was observed from the decreasing absorption of coumarin groups at around 320 nm (Figure 42a). The inset shows the increase in dimerization degree (DD) of coumarin over irradiation time, calculated according to $DD = 1 - A_t/A_0$, with A_0 and A_t being the absorbances at 320 nm before and after irradiation for time t, respectively. In this study, SCNPs used for characterizations were prepared with a 30 min irradiation time, reaching about 60 % dimerization of coumarin moieties. As will be shown, this level of intra-chain crosslinking is high enough to build a collapsed single chain structure while still leaving room for volume change in solution under stimulation of CO_2. The absence of inter-

chain crosslinking could be revealed by comparing the SEC traces of P(DMAEMA-*co*-CMA) polymer precursor before and after irradiation (Figure 42b). While no elution peak appears at shorter retention time than the precursor, implying no occurrence of inter-chain crosslinking that would lead to larger aggregates, the elution peak shifted to longer retention time after irradiation indicates smaller hydrodynamic volume associated with the transition from single chain coil to a more compact particle structure. Moreover, the formation of SCNPs was clearly observable on either AFM or TEM (Figures 42c and d). By casting dilute polymer solution (0.02 mg/mL), well separated nanoparticles below 20 nm in diameter are visible on the AFM and TEM images. The size of SCNPs is about 10 nm in diameter from TEM images which is similar to the DLS results. However, AFM images show apparently larger size (about 17 nm), which is likely caused by the used AFM tips.

3.3.2 Preparation and characterization of PS-*b*-P(DMAEMA-*co*-CMA) SCJNPs

The amphiphilic copolymer PS-*b*-P(DMAEMA-*co*-CMA) can be used to prepare single-chain 'Janus' nanoparticles with a hydrophilic and CO_2-responsive 'head' and a hydrophobic 'tail' which are expected to self-assemble to ordered aggregation. The preparation conditions for SCJNPs of the copolymer were the same as for SCNPs of P(DMAEMA-*co*-CMA): with the diblock copolymer dissolved in THF (a good solvent for both polymers) and the dilute solution subjected to irradiation for intra-chain photo-crosslinking of the P(DMAEMA-*co*-CMA) block. Similarly, the usual characterization results for SCJNPs are reported in Figure 43. The photo-dimerization of coumarin groups could be monitored by recording the absorption spectra over irradiation time (Figure 43a). The dimerization of coumarin is visible from the decreasing absorption around 320 nm and at lower wavelengths that results in an apparent decrease of the PS absorption near 280 nm. And the formation of a compact particle

structure (with 60 % dimerization of coumarin moieties) was also revealed from the SEC measurements (Figure 43b). Figure 44 shows the image of SCJNPs recorded by TEM.

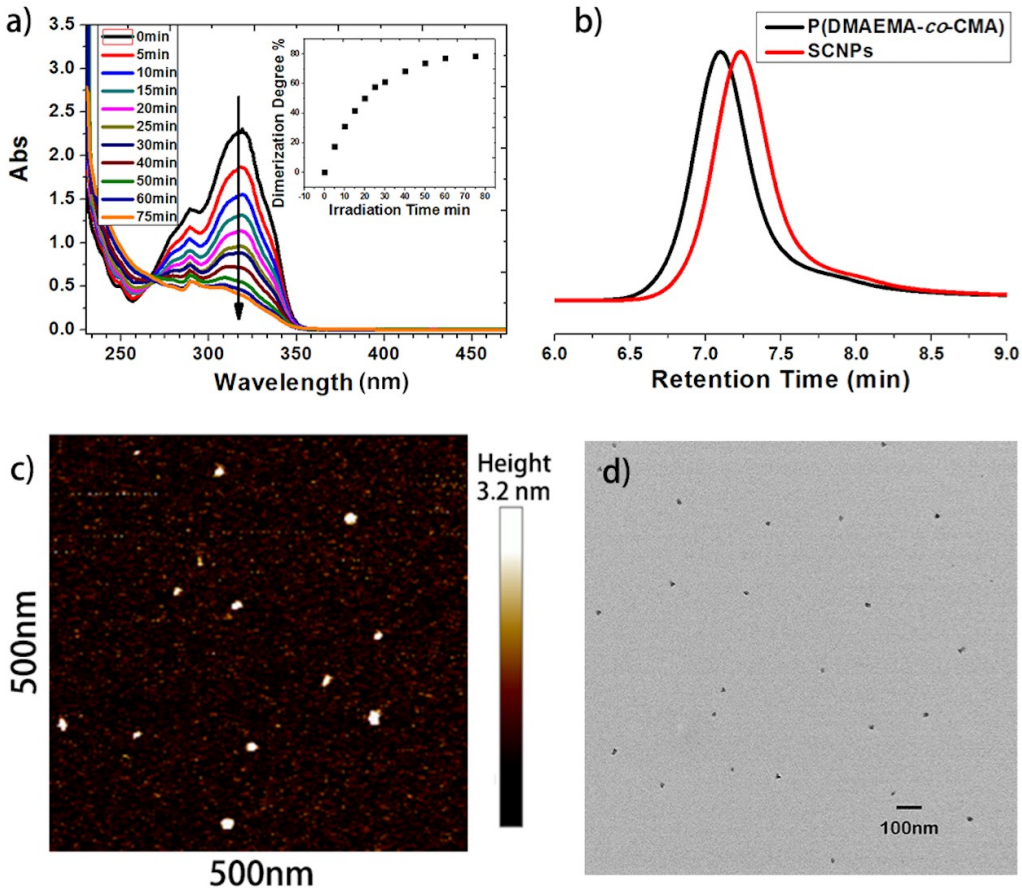

Figure 42. (a) Absorption spectra of P(DMAEMA-*co*-CMA) in THF (0.5 mg/mL) recorded before and after 320-480 nm light irradiation for different times, showing photodimerization of coumarin moieties. Inset is the plot of photodimerization degree *vs.* irradiation time. (b) SEC traces of P(DMAEMA-*co*-CMA) in THF (0.5 mg/mL) before and after 30 min irradiation, indicating the transition from coil to a more compact particle structure (SCNP) upon photodimerization of coumarin. (c) AFM and (d) TEM image of SCNPs obtained by casting a dilute polymer solution in THF (0.02 mg/mL).

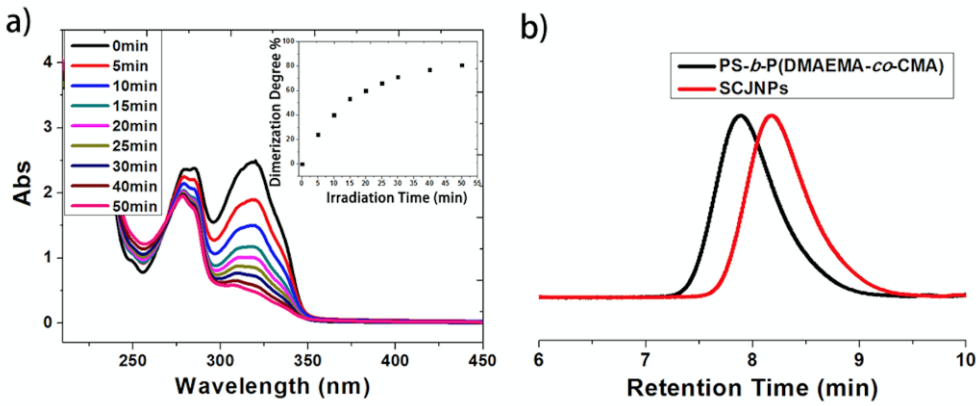

Figure 43. (a) Absorption spectra of PS-*b*-(DMAEMA-*co*-CMA) in THF recorded before and after 320-480 nm light irradiation for different times, showing intra-chain photodimerization of coumarin moieties. Inset is the plot of photodimerization degree *vs.* irradiation time. (b) SEC traces of PS-*b*-P(DMAEMA-*co*-CMA) in THF (0.5 mg/mL) before and after 20 min irradiation, indicating the transition from coil to a more compact particle structure (SCJNP) upon photo-dimerization of coumarin.

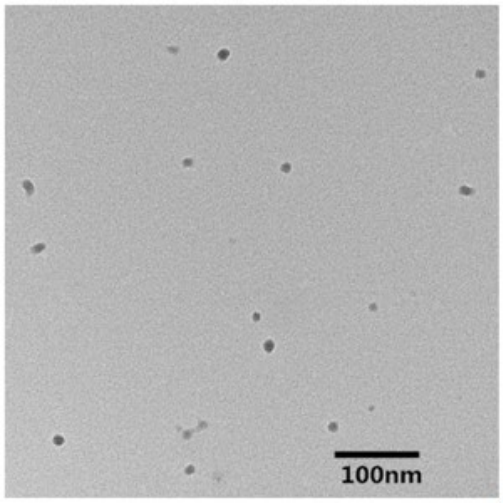

Figure 44. TEM image of the PS-*b*-P(DMAEMA-*co*-CMA) SCJNPs cast from a dilute polymer solution in THF.

3.3.3 CO_2-responsive single-chain nanoparticles of P(DMAEMA-*co*-CMA).

The CO_2-responsive behaviors of P(DMAEMA-*co*-CMA) SCNPs were investigated and the results are shown in Figure 45. First, with SCNPs dispersed in water, DLS measurements found that their average hydrodynamic diameter D_H increased from 7.7 nm to 10 nm after passing CO_2 for 10 min, and then decreased to the initial size after subsequently bubbling N_2 for 10 min (Figure 45a). The reversible size change under alternating CO_2/N_2 bubbling could be repeated (Figure 45b). This result indicates that despite the highly crosslinked nature of SCNPs, bubbling CO_2 results in protonation of tertiary amine groups in P(DMAEMA-*co*-CMA), which makes the nanoparticles more hydrophilic (increase in hydration degree) and swell by absorbing water. Bubbling N_2 removes CO_2 and deprotonates tertiary amines, and the return to the initial hydration degree shrinks the nanoparticles. Since the gas-controlled protonation/deprotonation is reversible, the size of P(DMAEMA-*co*-CMA) SCNPs can be switched, between swelling and shrinking, by passing CO_2 and N_2, respectively, through the aqueous solution.

Moreover, the CO_2-responsive property of P(DMAEMA-*co*-CMA) SCNPs was also revealed from their thermo-sensitivity change. As a matter of fact, PDMAEMA is known to have lower critical solution temperature (LCST) that can be switched by CO_2/N_2 bubbling. (145) Figure 45c shows the plots of transmittance (measured at 700 nm) *vs.* temperature for aqueous solutions of P(DMAEMA-*co*-CMA) polymer precursor and SCNPs before CO_2 bubbling, after CO_2 bubbling and after subsequent N_2 bubbling. The cloud point of SCNPs increased from 25 ^{o}C to 36 ^{o}C comparing with the polymer precursor, because the nanoparticles can reduce chain entanglements which renders their agglomeration more difficult and thus shifts the cloud point to higher temperature. After CO_2 bubbling for 30 s,

the cloud points of both polymer precursor and SCNPs increased to about 75 ºC, as a result of the protonation which enhances their solubility in water. After bubbling N_2 for 2 min, the cloud points went down to the initial temperatures. It was observed that bubbling CO_2 for over 1 min, no cloud point could be detected before water evaporation, which implies that the increase in cloud point was sensitive to the protonation degree of tertiary amines in the polymer or SCNPs. Therefore, P(DMAEMA-*co*-CMA) SCNPs dispersed in water respond to the presence of CO_2 by swelling in size and enhancing the thermal stability of dispersion (no aggregation up to 80 ºC).

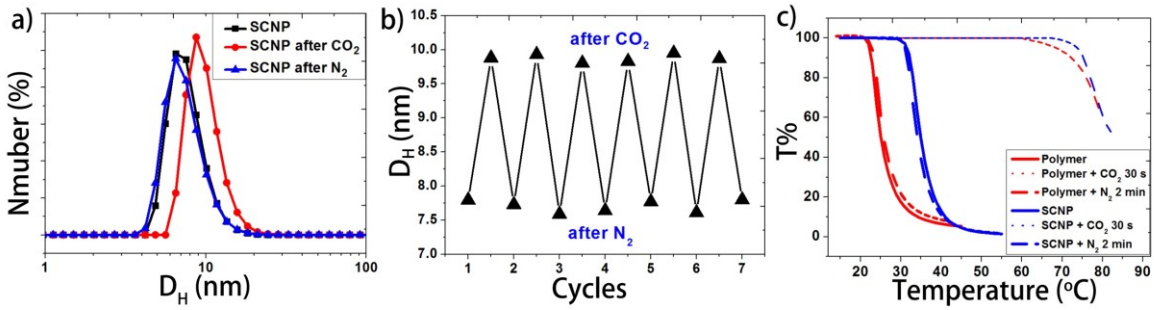

Figure 45. (a) Number-weighted size distribution for P(DMAEMA-*co*-CMA) SCNPs before CO_2 bubbling, after bubbling CO_2 for 10 min and after subsequent N_2 bubbling for 10 min. (b) Reversible change in average hydrodynamic diameter, D_H, of P(DMAEMA-*co*-CMA) SCNPs upon repeated cycles of alternating CO_2/N_2 bubbling. (c) Transmittance *vs.* temperature for aqueous solutions of P(DMAEMA-*co*-CMA) polymer precursor and SCNPs (3 mg/mL), with both solutions subjected to 30 s CO_2 and 2 min N_2 bubbling.

3.3.4 CO_2-responsive micellar aggregates of single-chain 'Janus' nanoparticles of PS-*b*-P(DMAEMA-*co*-CMA).

We envisioned that the CO_2-responsive property of SCNPs can manifest not only individually in a well dispersed state but also collectively if they are self-assembled into a larger structure. To investigate such gas-sensitive self-assemblies, we prepared a kind of tadpole-like 'Janus' single chain nanoparticles (SCJNPs) using a diblock copolymer of PS-*b*-P(DMAEMA-*co*-CMA) (Figure 39b). Since the PS tail is hydrophobic and the P(DMAEMA-*co*-CMA) SCNP head is water-soluble (good dispersion over a wide range of temperature), SCJNPs are amphiphilic and expected to be able to self-assemble in aqueous solution.

By adding water into THF solution of PS-*b*-P(DMAEMA-*co*-CMA) SCJNPs, the tadpole nanoparticles could self-assemble into spherical core-shell micellar aggregates, with PS 'tails' in the core and P(DMAEMA-*co*-CMA) 'heads' constituting the shell. A stable dispersion of SCJNP micelles in water was then obtained by removing THF, and used for characterization. The micelles of SCJNPs were found to respond to alternating CO_2/N_2 bubbling in a similar manner as SCNPs. DLS measurements found that the average size, D_H, of SCJNP micelles increased from 28 nm to 80 nm after CO_2 bubbling for 10 min and decreased almost to the original size after subsequent N_2 bubbling (Figure 46a). The gas-induced swelling and shrinking could be repeated upon cycles of alternating CO_2/N_2 bubbling (Figure 46b). TEM observations further confirmed the gas-switchable sizes of the micelles of SCJNPs (Figure 46c-e). These results are no surprise. The micelle shell contains a number of P(DMAEMA-*co*-CMA) SCNPs, the swelling of all nanoparticles upon CO_2 bubbling collectively amplifies the expansion of the micellar aggregate. Figure 46b shows that in average D_H of the micellar

aggregates switches between 30 nm (after N_2 bubbling) and 75 nm (after CO_2 bubbling), which corresponds to a hydrodynamic volume expansion of more than 10 times in the presence of CO_2.

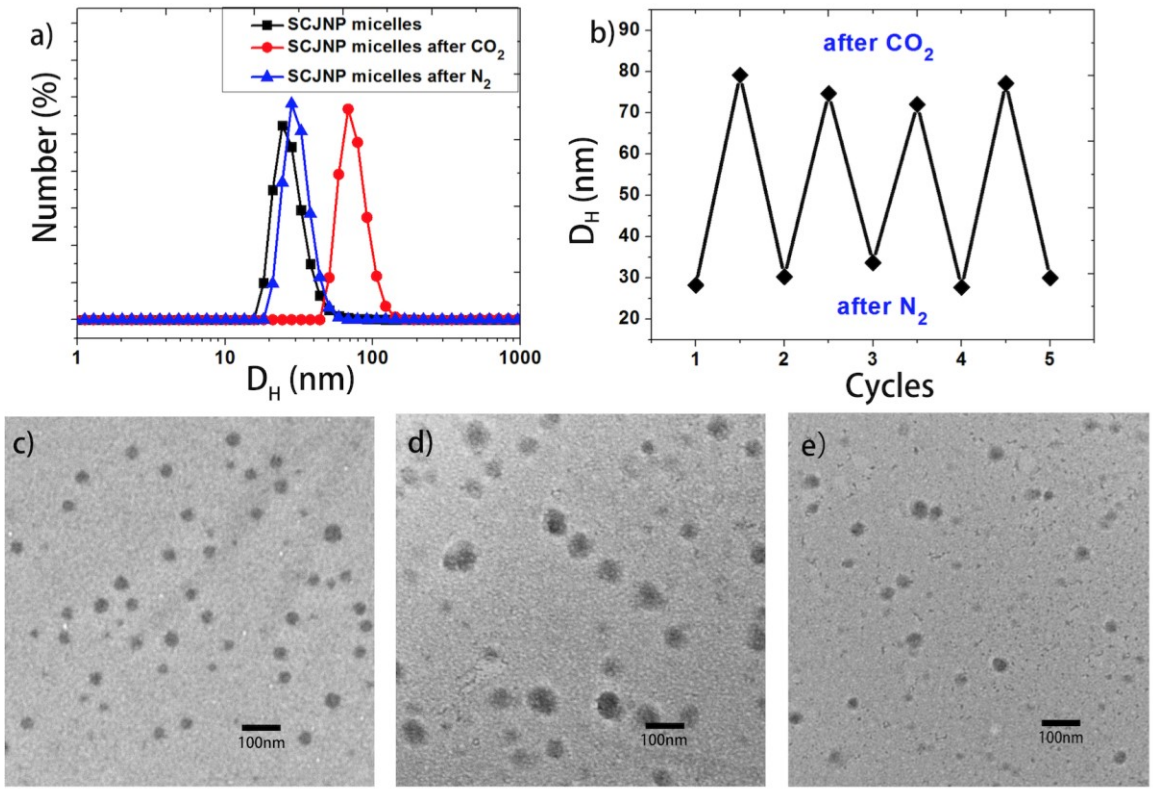

Figure 46. (a) Number-weighted size distribution for PS-*b*-P(DMAEMA-*co*-CMA) SCJNP micellar aggregates before CO_2 bubbling, after bubbling CO for 10 min and after subsequent N_2 bubbling for 10 min. (b) Reversible change in average hydrodynamic diameters, D_H, for PS-*b*-P(DMAEMA-*co*-CMA) SCJNP micellar aggregates upon repeated alternating CO_2/N_2 bubbling. TEM images of the micellar aggregates (c) before CO_2 bubbling, (d) after CO_2 bubbling for 10 min and (e) after subsequent N_2 bubbling for 10 min.

3.3.5 Gas-tunable formation rate of AuNPs using SCNPs as nanoreactors.

As reported previously, P(DMAEMA-*co*-CMA) SCNPs can be used as nanoreactors to prepare AuNPs in both water and THF. (62) In the present study, we wanted to know if the CO_2-responsiveness of the SCNPs could make them a kind of gas-tunable nanoreactors for AuNP synthesis. To do this, three SCNP solutions were prepared under the same conditions except for the CO_2 bubbling time (SCNP1-3 in Table 5). After addition of $HAuCl_4$, the formation of AuNPs was monitored by recording the absorption spectra of the three reaction solutions. Even visually, it became evident that the reaction to CO_2 of SCNPs has a significant effect on the speed at which the reduction of Au ions proceeded, leading to AuNPs. Figure 47a shows the pictures of the three solutions at different times of reaction. It can be seen that the solution turned red after 0.5 h for SCNP3 (2 min CO_2 bubbling), after 1 h for SCNP2 (30 s CO_2 bubbling) and only after 2 h for SCNP1 (without CO_2 bubbling). This observation already points out that bubbling CO_2 into the SCNP solution has as effect to speed up the formation of AuNPs. This was further confirmed by comparing the absorption spectra recorded over reaction time for the three solutions (Figure 47b-d). Without CO_2, the surface plasmon resonance (SPR) peak of AuNPs appeared only after 90 min, while it became visible after 30 min and less than 20 min with SCNP solution bubbled with CO_2 for 0.5 min and 2 min, respectively. The CO_2-sensitive kinetics of AuNP formation can also be noticed by plotting the absorption intensity at 530 nm, which is related to the amount of formed AuNPs, as a function of reaction time (Figure 47e). CO_2 bubbling even for 0.5 min accelerated the reaction drastically. The further increase in the reaction rate with a longer time of CO_2 bubbling can be better appreciated from the inset in Figure 47e (enlarged region of the early reaction period). The increasing rate of AuNP formation using SCNPs subjected to CO_2 is likely the result of a more hydrophilic SCNPs and their CO_2-induced swelling may

provide easier access of $AuCl_4^-$ counterions into the nanoreactors for association with protonated amine groups and residual non-protonated tertiary amine groups lead to their *in-situ* reduction to zerovalent gold. (192, 193)

Since the hydrophilicity, and thus the swelling, of P(DMAEMA-*co*-CMA) SCNPs can be reversibly changed by CO_2 and N_2 bubbling, it would be possible to tune the rate of AuNP formation using the two gases. This rate tuning was examined by conducting the experiment shown in Figure 48, where the amount of formed AuNPs over time in a solution subjected to alternating CO_2/N_2 bubbling was monitored by measuring the absorbance at 530 nm, which was compared to the same reaction solution with only CO_2 bubbling for 30 s at the beginning of the reaction. It started with 30 s CO_2 bubbling, the reaction rate followed the profile of the reference solution. However, upon N_2 bubbling for 30 s, the reaction was slowed down. Such speed up and down (reaction on and off) was observed for another cycle of 30 s CO_2 and N_2 bubbling. The AuNP formation was fast following CO_2 bubbling and became slow after N_2 bubbling. Of course, in the late stage of reaction (after about 30 min in the present case), the reaction rate can no longer be tuned by the gases, because most Au ions have already been reduced and the reaction reaches the end. The on/off switching of the AuNP formation rate stems from the reversible swelling/shrinking under CO_2/N_2 bubbling. This observation is significant because it shows that the CO_2-responsive nanoreactor of P(DMAEMA-*co*-CMA) SCNPs provides an ability to tune or adjust the rate of AuNP formation simply by passing gases through the reaction solution.

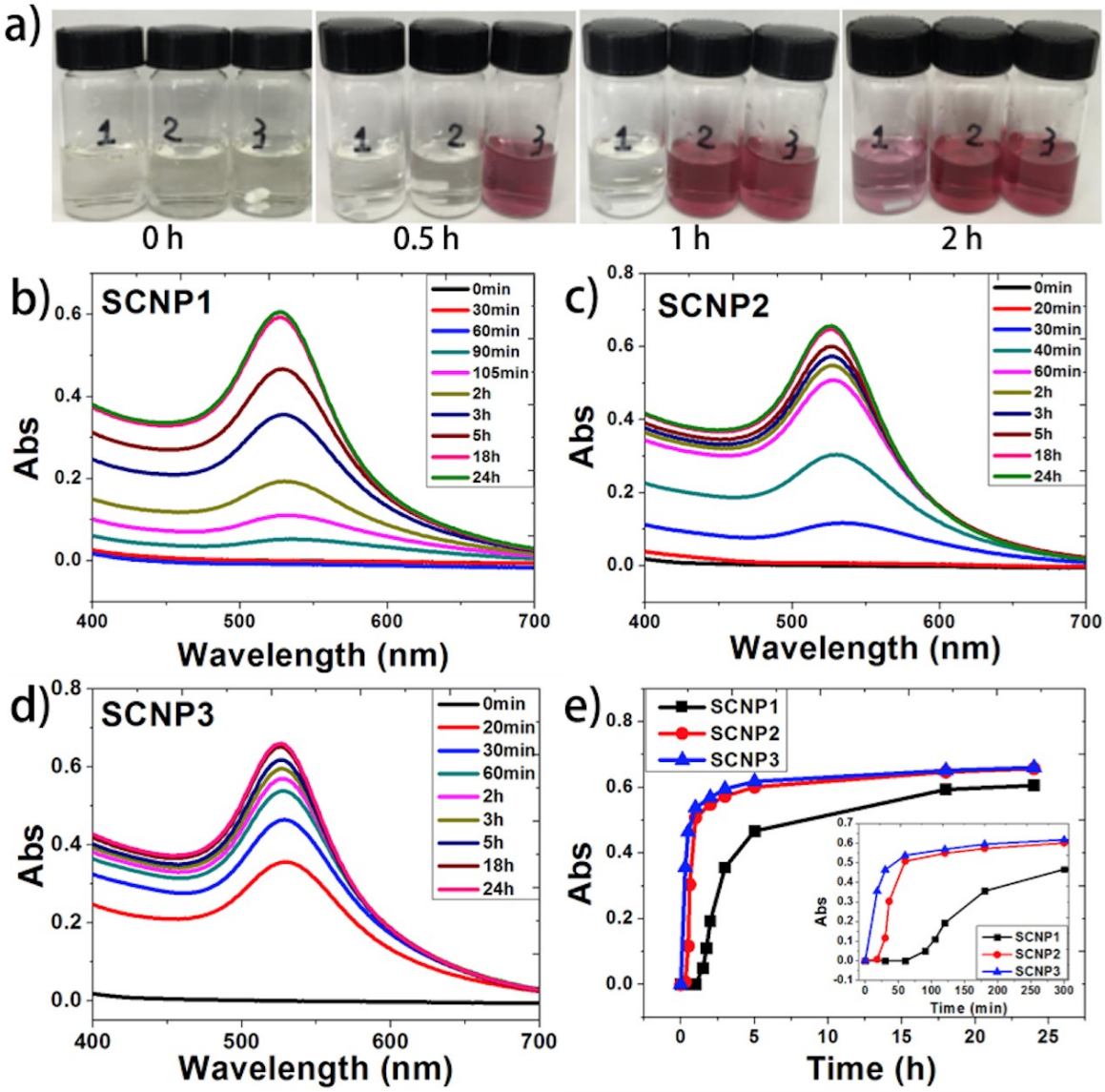

Figure 47. (a) Photos of three reaction solutions for AuNP formation at different times with SCNP1 (solution 1, with no CO_2), SCNP2 (solution 2, 30 s CO_2 bubbling) and SCNP3 (solution 3, 2 min CO_2 bubbling). (b)-(d) Absorption spectra of SCNP1, SCNP2 and SCNP3 solutions over reaction time, respectively. (e) Absorbance of AuNPs at 530 nm *vs.* reaction time for the three solutions. Insert is a zooming for the first 5 h of reaction.

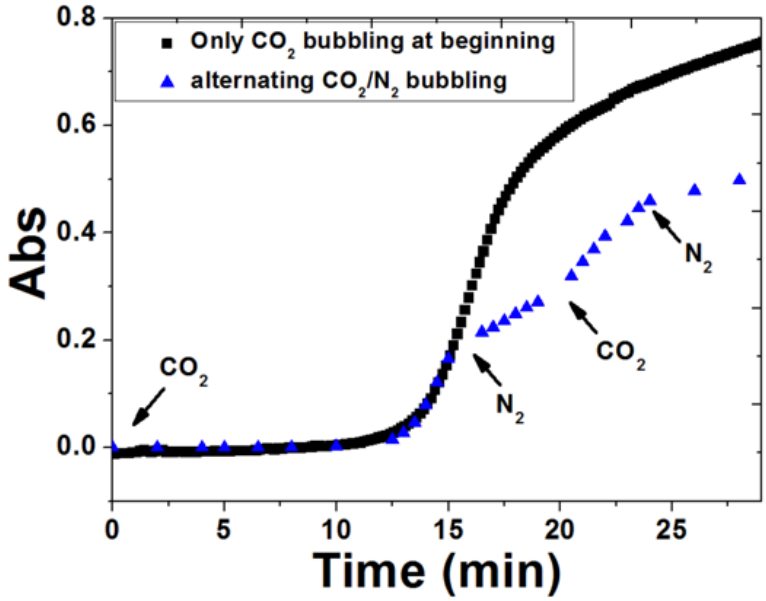

Figure 48. Absorbance of AuNPs at 530 nm *vs.* reaction time for a solution bubbled with CO_2 for 30 s at first and then subjected to alternating CO_2/N_2 bubbling (each for 30 s) and, for comparison, the same solution only bubbled with CO_2 for 30 s at the beginning of reaction.

3.3.6 Gas-tunable size of AuNPs using micelles of SCJNPs as nanoreactors.

Micelles of PS-*b*-P(DMAEMA-*co*-CMA) SCJNPs can undergo much larger volume change under CO_2/N_2 stimulation than SCNPs of P(DMAEMA-*co*-CMA); their use as gas-controlled nanoreactors for AuNPs was also investigated. Similarly, three micellar solutions subjected to CO_2 bubbling of different times were utilized for the reduction reaction of Au ions under otherwise the same conditions, being denoted as SA1 (no CO_2), SA2 (0.5 min CO_2 bubbling) and SA3 (2 min CO_2 bubbling), respectively (Table 5). Figure 49 shows the absorption spectra recorded for the three reaction solutions over time as well as the plots of absorbance of AuNPs at 530 nm *vs.* time. It can be noticed that the rate of AuNPs formation also increased by bubbling CO_2 into the micellar solution. This effect on the reaction speed is

similar to that observed with P(DMAEMA-*co*-CMA) SCNPs and should originate from the CO_2-induced expansion of the micelles of SCJNPs. There is a clear difference though. With increasing the amount of bubbled CO_2, the SPR peak of AuNPs shifted to longer wavelength, from 531 nm with SA1 to 540 nm with SA2 to 556 nm with SA3, and, in the same time, the SPR peak became broader (Figure 49e). This result implies that larger AuNPs or aggregates were formed in the micellar solution subjected to longer time of CO_2 bubbling, which was indeed confirmed by TEM observations. Figure 50 shows TEM images of AuNPs obtained with the three micellar solutions as well as, for comparison, with SCNP3 (SCNPs with 2 min CO_2 bubbling). AuNPs prepared using micelles of SCJNPs not only are much larger than those obtained with SCNPs, but their size can also be tuned between 30 nm and 120 nm by varying the CO_2 bubbling time between 0 and 2 min. These results indicate that size-tunable AuNPs could easily be obtained by adjusting the size of SCJNP micelles using CO_2 bubbling.

AuNPs aggregates of increasingly larger size can be prepared by increasing the volume of SCJNPs micellar nanoreactors upon bubbling more CO_2 into the solution. A possible utility of tuning the SPR of AuNPs into the red light region (over 600 nm) is the photo-thermal effect, as demonstrated by the test in Figure 51. An ABA-type triblock copolymers, namely, poly{[2-(2-methoxyethoxy)ethyl methacrylate]-*co*-methacrylic acid}-*b*-poly(ethylene oxide)-*b*-poly{[2-(2-methoxyethoxy)ethyl methacrylate]-*co*-methacrylic acid} (P(MEO_2MA-*co*-MAA)-*b*-PEO-*b*- P(MEO_2MA-*co*-MAA), is known to undergo sol-gel transition in aqueous solution at temperatures above LCST of the end blocks (hydrogel formed by an assembled network of flower-micelles). (143) (Figure 52) AuNPs prepared with SCNP3 and SA3, respectively, were added in aqueous solution of P(MEO_2MA-*co*-MAA)-*b*-PEO-*b*-P(MEO_2MA-*co*-MAA) (10 wt% of triblock copolymer and 0.12 wt% of AuNPs), and the solutions were exposed to a 635 nm laser at room temperature for 10 min. As seen from

the photos (Figure 51), while no sol-gel transition occurred in the solution with AuNPs prepared with SCNP3, the gelation took place for the solution containing AuNPs prepared with SA3. For the former solution, the 635 nm light is far from the maximum SPR peak of AuNPs, but for the latter solution, the SPR of AuNPs at 635 nm is strong (Figure 49e), which can generate much more heat to bring the triblock copolymer solution temperature above LCST of the end blocks (solution temperature measured to be 60 ^{o}C after 10 min irradiation). Such photo-induced gelation using long-wavelength 635 nm red light suggests potential use in biomedical applications.

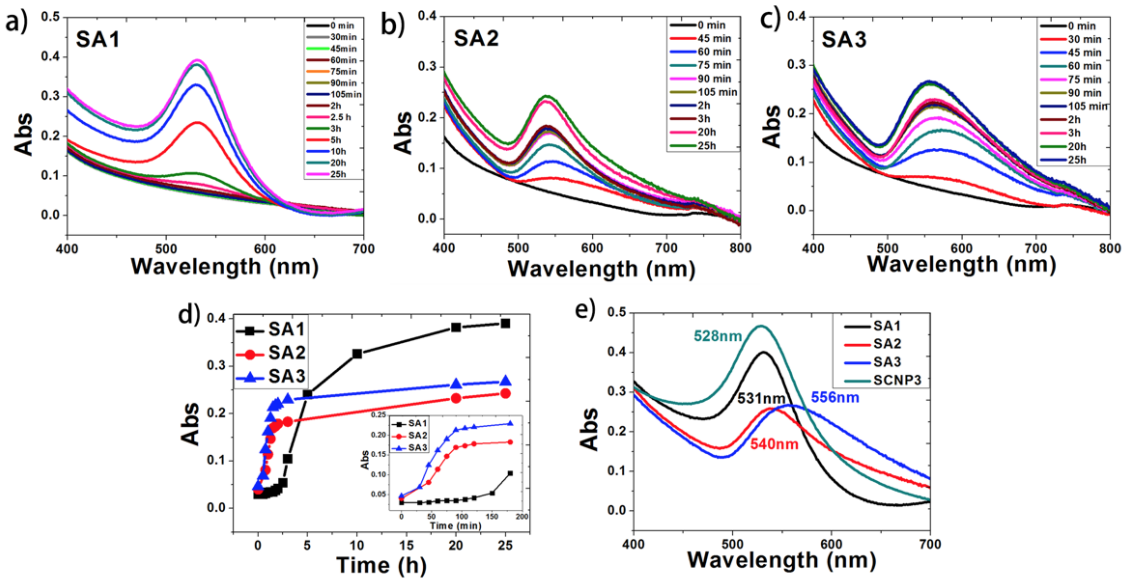

Figure 49. Preparation of AuNPs using micelles of PS-*b*-P(DMAEMA-*co*-CMA) SCJNPs subjected to different CO_2 bubbling through the solution. (a)-(c) Absorption spectra of SA1 (no CO_2), SA2 (30 s CO_2 bubbling) and SA3 (2 min CO_2 bubbling) solutions over reaction time, respectively. (d) Absorbance of AuNPs at 530 nm *vs.* reaction time for the three solutions. Insert is a zooming for the first 3 h of reaction. (e) Absorption spectra of AuNPs solutions of SCNP3, SA1, SA2 and SA3, respectively, after 48 h of reaction.

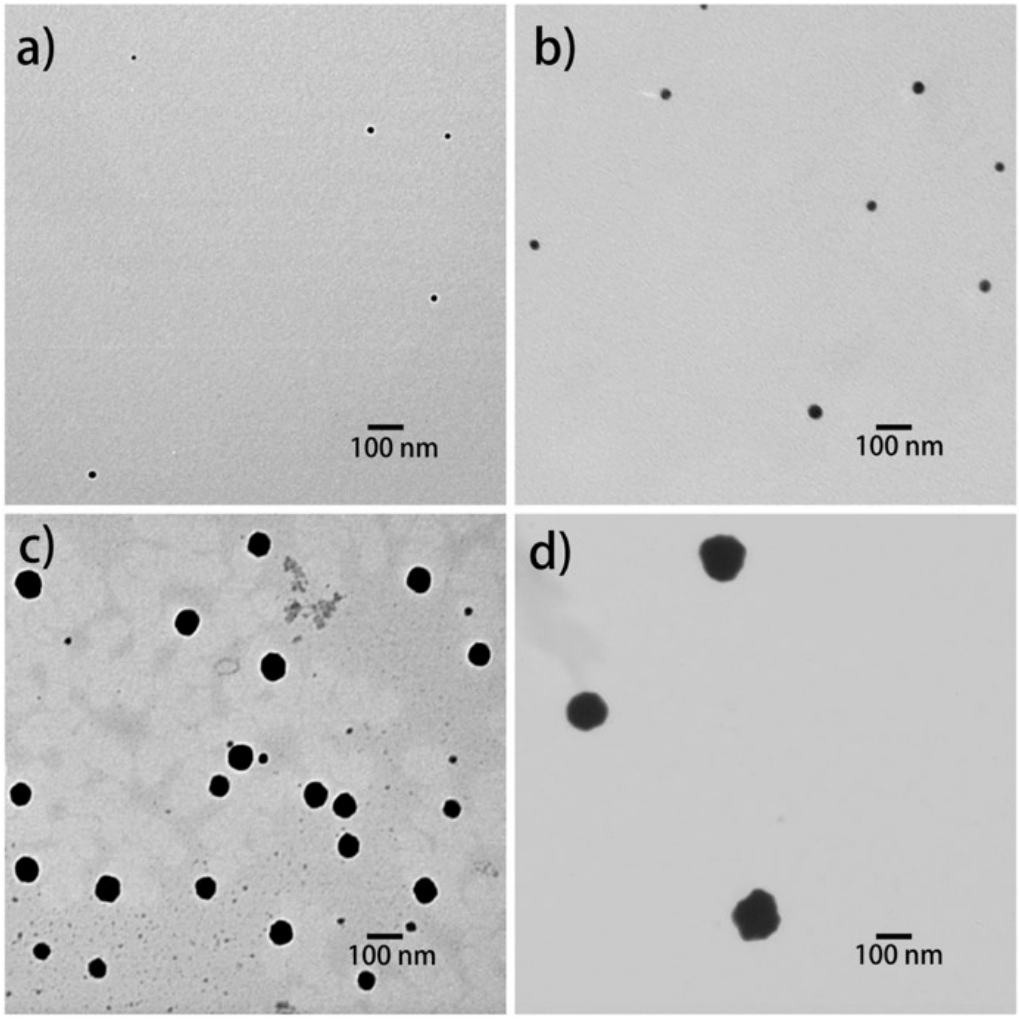

Figure 50. TEM images of AuNPs prepared using (a) SCNP3, (b) SA1, (c) SA2 and (d) SA3 (see Table 5 for different samples).

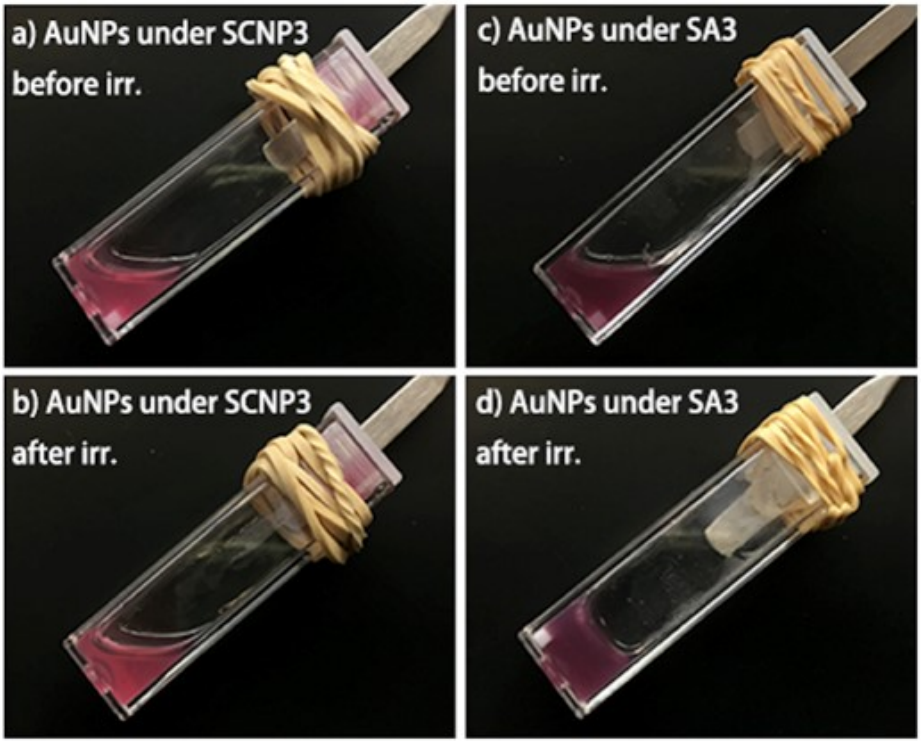

Figure 51. Photos for aqueous solutions of P(MEO_2MA-*co*-MAA)-*b*-PEO-*b*-P(MEO_2MA-*co*-MAA) (10 wt%) containing AuNPs (0.12 wt%) prepared using SCNP3 (a, b) and SA3 (c, d) respectively, showing the gelation only occurred in the latter solution after exposure to 635 nm red light at room temperature for 10 min.

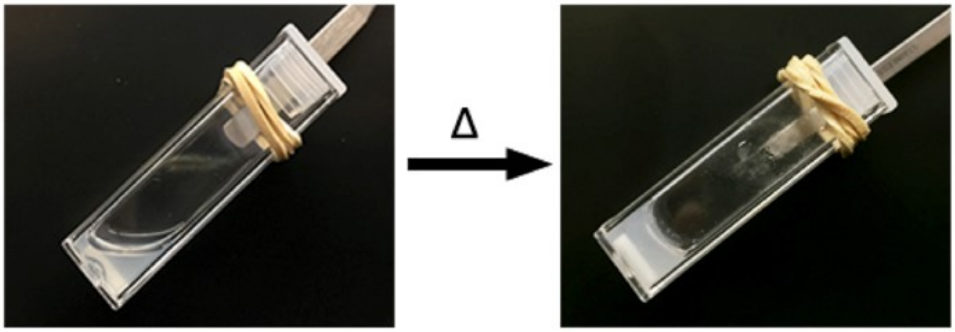

Figure 52. Photographs of thermal-induced of sol-gel transition of pure P(MEO_2MA-*co*-MAA)-*b*-PEO-*b*-P(MEO_2MA-*co*-MAA).

3.4 Conclusion

We have prepared and investigated CO_2-responsive SCNPs of P(DMAEMA-*co*-CMA) as well as micelles self-assembled from amphiphilic tadpole SCJNPs of PS-*b*- P(DMAEMA-*co*-CMA). We showed that under CO_2 stimulation, as a result of increased hydration due to protonation of tertiary amine groups, the nanoparticles can respond either individually (for P(DMAEMA-*co*-CMA) SCNPs) or collectively (in micelles of PS-*b*-P(DMAEMA-*co*-CMA) SCJNPs) to undergo a volume increase in aqueous solution. While the swelling of individual SCNPs is limited, the collective swelling of self-assembled SCJNPs results in large expansion of the micelles in the presence of CO_2. In both cases, the size change is reversible and can be reversed under N_2 bubbling that removes CO_2 and deprotonates tertiary amine groups. Furthermore, we explored the gas-controlled swelling/shrinking property for using both P(DMAEMA-*co*-CMA) SCNPs and PS-*b*-P(DMAEMA-*co*-CMA) SCJNP micelles as gas-tunable nanoreactors for synthesizing AuNPs. The rate of AuNP formation was found to increase under CO_2 stimulation, which is likely caused by the swelling of the nanoreactor that facilitates access of $AuCl_4^-$ counterions, their association with protonated amines and their *in-situ* reduction to zerovalent gold by non-protonated amines. We further showed that the reaction could be tuned to speed-up or slow-down (on/off switching) by bubbling CO_2 or N_2, respectively, through the reaction solution, which provides a means of gas-controllable kinetics of AuNP formation. Equally interesting, tunable-size nanoreactors of AuNPs were demonstrated using the micelles of SCJNPs. Starting with the same aqueous solution of micelles, bubbling different amounts of CO_2 could control the size of the nanoreactor and result in different sizes of AuNPs or, more likely, their aggregates. By shifting the SPR of AuNPs into long-wavelength region through the size or aggregation control, we also showed the possibility of using 635 nm red light-generated photo-thermal effect to induce sol-gel

transition of thermosensitive block copolymers in aqueous solution.

3.5 Statement of Contribution

This work was published in *Chemistry of Materials* **2017**, *29*, 5693-5701. DOI: 10.1021/acs.chemmater.7b01656. The paper is authored by Weizheng Fan, Xia Tong, Farhad Farnia, Bing Yu and Yue Zhao. This research work was carried out in the Université de Sherbrooke under the supervision of Prof. Zhao. Xia Tong did the AFM measurements and Farhad Farnia helped for CO_2 bubbling system and pH-meter. Bing Yu synthesized the ABA triblock copolymer P(MEO_2MA-*co*-MAA)-*b*-PEO-*b*-P(MEO_2MA-*co*-MAA). I performed all the rest of experiments and characterizations. I wrote the first draft of the manuscript and Prof. Zhao finalized the manuscript.

CHAPTER 4 GENERAL DISCUSSION AND PERSPECTIVE

4.1 General Discussion

We prepared three multi-functional SCNP systems from stimuli-responsive polymer precursors. According to previous studies from our group, coumarin as crosslinker provides a facile method to fabricate SCNPs. All of our multi-functional SCNPs were formed by intramolecular crosslinking under >320 nm UV irradiation *via* photo-dimerization reaction of coumarin. The functionalization of SCNPs is achieved by introducing stimuli-responsive properties and properly designing the chemical structures of the polymer precursors. On the other hand, we developed a universal modular polymer structure to transfer stimuli-responsive properties from polymer precursor to SCNP system.

In the first project (Chapter 1), we successfully prepared multi-functional SCNPs by introducing dual-photo-responsive properties of coumarin (photo-cleavage and photo-dimerization) and properly designing the main-chain coumarin containing polyesters. The main contribution for the first work is twofold. On one hand, by incorporating coumarin moieties into the chain backbone of polymer precursor, they not only act as crosslinkers for fabricating SCNPs (photo-dimerization of coumarin under >320 nm UV irradiation), but also endow the SCNPs with the photo-degradability (photo-cleavage of coumarin leading to chain scission of polymer precursor under 254 nm UV irradiation). On the other hand, the study shows a simple method to prepare SCNPs with varying size from one polymer chain. Before that, SCNPs with different sizes can only be prepared by synthesizing polymer precursors with different molecular weight or crosslinker contents. Herein, the size of SCNPs can be varied by adjusting the degree of dimerization which can be controlled by the irradiation time.

Obtaining variable-size SCNPs with no need for synthesizing different samples of the polymer precursor is an appealing advantage of this method that, in principle, can be applied to most stimuli-responsive SCNPs due to easy control of the crosslinking degree. Later reports on other SCNP systems prove the universal use of this method. (45, 161, 179) Finally, considering the photo-degradability of SCNPs combined with the known biocompatible and biodegradable properties of the polymer precursor, we expect this type of SCNPs have a possibility for biomedical applications, especially as drug carriers for stimuli-controlled drug delivery.

The contribution for the second project (Chapter 2) is also of fundamental significance. We demonstrated the first liquid crystalline SCNPs. Again, following the approach of translating a given functionality from the polymer precursor to SCNPs, a liquid crystalline polymer bearing azobenzene mesogenic groups was utilized. We show that under certain intra-chain crosslinking degrees, the photo-isomerization of azobenzene as well as the liquid crystalline order can persist in SCNPs despite the severe confinement. Moreover, due to the LC order, photo-isomerization properties of azobenzene and confinement effect, the SCNPs exhibit several functions and properties, some of which are unexpected, such as solvent-selective photoluminescence and excitation wavelength-dependent photo-induced deformation. First, the fluorescence of SCNPs is only found in $CHCl_3$ due to the less solubility of SCNPs which results in a more compact structure or aggregation. Secondly, the deformation of SCNPs occurs under both linearly polarized UV and visible light. Although the photo-induced deformation property has already been reported for colloidal particles of azobenzene-containing polymers, the observation on SCNPs is still quite surprising. While the deformation of colloidal particles can be observed on optical microscope, the ultra-small size of SCNPs makes the characterization difficult. We tried hard to find sample preparation

conditions that allowed the photo-induced deformation of SCNPs to be observed by AFM. However, this cannot be done *in-situ* due to the limitation of the AFM measurements. The effect of the excitation wavelength on the stretching deformation direction with respect to the light polarization needs further studies to be understood. Finally, the preparation of SCNP nanocomposite and mechanical-induced orientation of SCNPs provide an idea of application. As a matter of fact, this is the first all-polymer nanocomposite material reinforced by SCNPs. The compatibility between organic polymers favors the dispersion of SCNPs in the polymer matrix, which results in good transparency of the nanocomposite. In essence, our liquid crystalline SCNPs are new. And the new findings and knowledges from this study may instigate interest on this type of functional nanoparticles. Through this project, we successfully prepared multi-functional SCNPs by introducing photo-responsive properties of azobenzene and designing a random polymethacylate with pendant groups of azobenzene (as stimuli-responsive unit) and coumarin (as crosslinkable unit). This polymer structure can be considered as a modular structure to prepare multi-functional SCNPs.

The third work conducted in the thesis (Chapter 3) focuses on yet another totally new system of functional SCNPs, namely, CO_2-responsive SCNPs. In order to prove our modular polymer structure can be suitable for various stimuli-responsive units, we introduce a class of multi-stimuli-responsive (thermo-, pH- and CO_2-responsive) units, PDMAEMA, in our modular structure to prepare multi-functional SCNPs. Since the protonation/deprotonation of tertiary amine units in PDMAEMA lead to the reversible hydrophilicity change under CO_2/N_2 stimulation, the size of SCNPs and their LCST-type aggregation temperature in aqueous solution can be reversibly tuned by the gases. In addition, we show that the reaction to CO_2 of the individual SCNPs can manifest collectively with their self-assembled, larger-scale structures. Indeed, the reversible expansion/shrinking property under CO_2/N_2

stimulation was observed in the micelles of 'Janus' single-chain nanoparticle prepared from amphiphilic block copolymers. Another contribution of this project is that we demonstrated a gas-controlled, rate- and size-tunable nanoreactors for preparing gold nanoparticles (AuNPs). Due to the CO_2-responsiveness of SCNPs and micelles from SCJNPs, the rate of AuNP reduction reaction was found to be tunable and on/off-switchable by using CO_2 and N_2. In addition, using SCJNP micelles as nanoreactors and adjusting the CO_2 stimulation strength, variable-size AuNPs or their aggregates can be obtained with continuous redshift of the surface plasmon resonance (SPR) into the long-wavelength visible light region.

From the above three projects, we successfully functionalized SCNPs by using stimuli-responsive polymers. Through rational design of chemical structure and position of stimuli-responsive moieties in the polymer precursor, the resulting SCNPs can perform a variety of functions. Moreover, we have established a simple method for introducing stimuli-responsive properties to SCNPs, that is, using random copolymers comprising stimuli-responsive units and crosslinkable units as polymer precursors. Most stimuli-responsive properties of polymer precursors will be retained in the corresponding SCNPs and make them functional or multi-functional to satisfy a diversity of requirements for applications. This approach is general and easily expandable to many stimuli-responsive polymers.

4.2 Perspective

Although we have reported convincing examples of multi-functional SCNPs prepared from stimuli-responsive polymers and demonstrated some possible applications, further studies are still necessary. Described below are a couple of ideas on this topic that are worth being investigated.

4.2.1 Compartmentalized 'Janus' single-chain nanoparticles with multi-functions

Although stimuli-responsive SCNPs can be prepared from polymers with stimuli-responsive groups and crosslinking units, specific design of polymer structure is necessary to achieve multi-functions. Certainly, we can prepare multi-functional or multi-stimuli-responsive SCNPs by random copolymers incorporating more functional groups in their structures, but this approach has its limitations. For example, if we want to set both LCST and UCST properties in SCNPs, simply incorporating LCST and UCST functional groups in random copolymer may not be achieved due to their obstructing mutual. Therefore, new methods of preparation need to be developed to further expand the scope of multi-functional SCNPs.

'Janus' particle is a type of materials with dual- or multi-functionality which provide a possibility for relatively compartmentalized multi-functional SCNPs, that is 'Janus' single-chain nanoparticles. Figure 53 illustrates the preparation of Janus SCNPs. Two different stimuli-responsive diblock polymer precursors can be used to prepare two tadpole-like SCNPs, and subsequently be connected (e.g., azide-alkyne click coupling) to form Janus SCNPs. These 'Janus' SCNPs are composed of tadpole-like SCNPs with any stimuli-responsiveness (thermo-, pH-, gas- or photo-responsive) or functions (fluorescent and etc.). Such compartmentalized 'Janus' SCNPs can perform multi-functions independently and have multiple combinations to satisfy the requirement of practical applications.

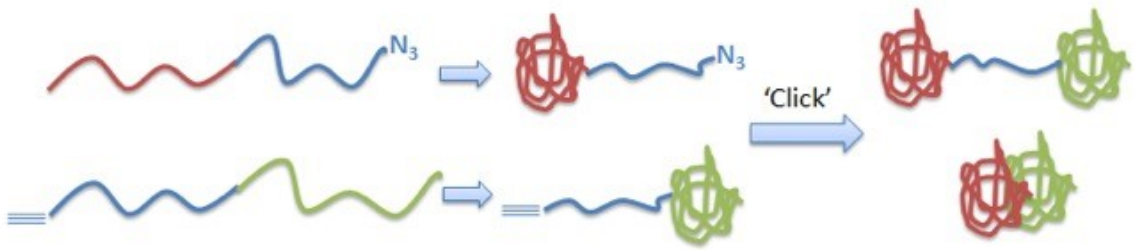

Figure 53. Preparation procedure of Janus SCNPs

4.2.2 Stimuli-responsive single-chain nanoparticles in drug delivery system

The 1.5-20 nm size of SCNPs is very suitable as nano-carrier for drug delivery system, because this range of size can avoid accumulation in the liver and spleen, as well as unwanted immunogenic reactions. Therefore, designing a stimuli-responsive SCNP system for drug delivery applications is interesting. Considering the potential difficulty of drug loading due to the ultra-small size of SCNPs, directly linking drug molecules to the SCNPs with covalent bonding is preferred. Scheme 8 shows an idea of SCNPs for drug delivery application. We designed a random copolymer with pendant groups of coumarin as crosslinkers and aldehyde groups. A class of drug with amine groups (eg: doxorubicin (DOX) for cancer treatment) can be connected with polymer precursor *via* a Schiff base reaction between an aldehyde group and an amine group. The SCNPs with drugs can be prepared *via* photo-dimerization reaction of coumarin under >320 nm UV irradiation. The drug can be released with the cleavage of the Schiff's base in acidic environment, such as in tumor cells (pH=5-6.8).

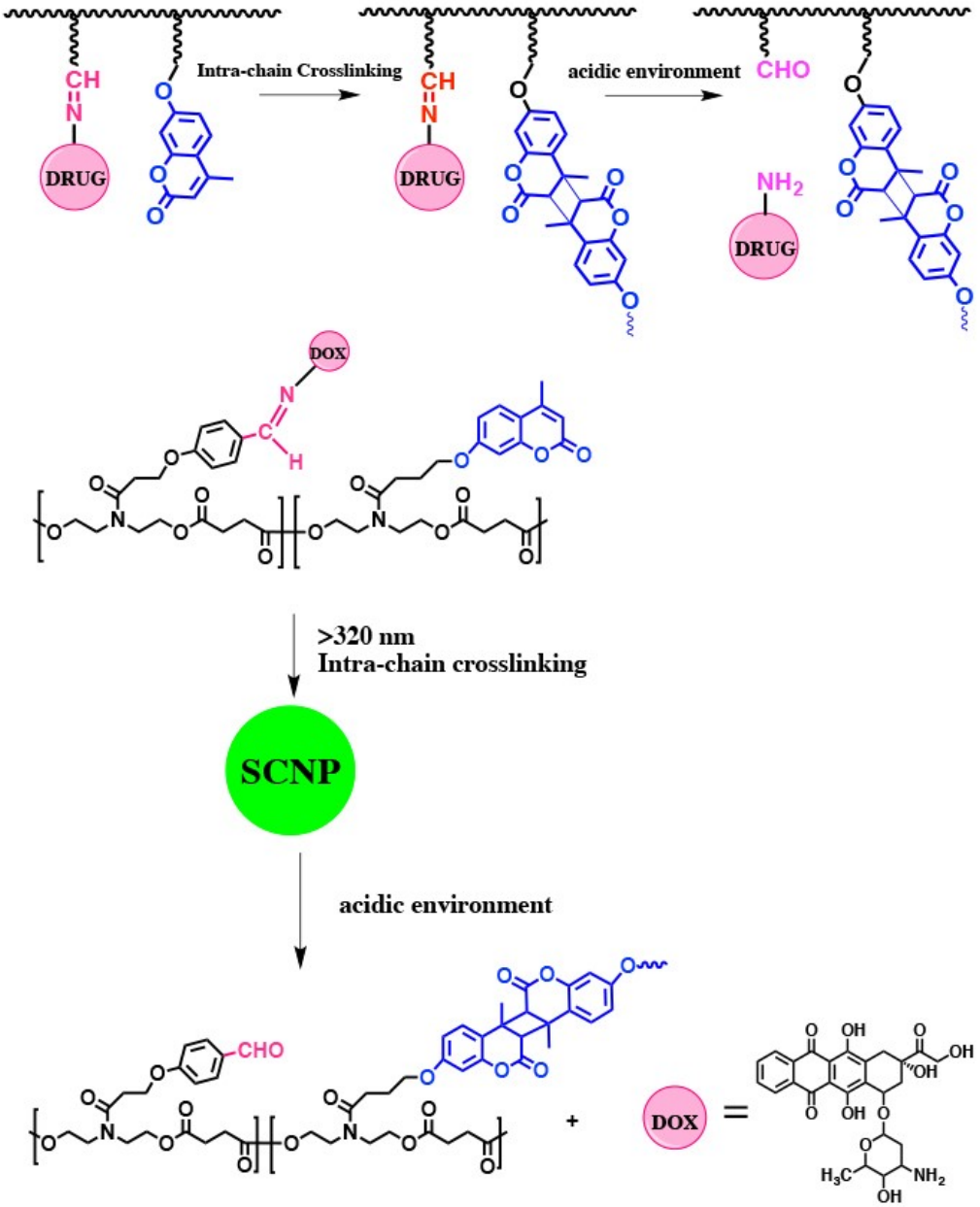

Scheme 8. Schematic illustration of SCNPs for drug delivery applications.

CONCLUSION

In this thesis, we have developed three systems of multi-functional polymeric single-chain nanoparticles and demonstrated some of their possible applications. These multi-functional SCNPs were prepared by introducing various stimuli-responsive properties from stimuli-responsive polymers as precursors. Through rational precursor polymer design, in terms of chosen stimuli-responsive moieties and their positions in the polymer precursors, each class of SCNPs exhibits multiple functions, such as being photodegradable, size-tunable, photo-induced deformable, photoluminescent and gas-tunable self-assembled, and can be exploited for diverse applications, such as biomedicine, liquid crystalline nanocomposites and gas-tunable nanoreactors for AuNP synthesis.

Firstly, we prepared a series of photodegradable and size-tunable SCNPs based on photo-responsive main-chain coumarin-containing polyesters. The size of the SCNPs is tunable by adjusting the degree of intra-chain photo-dimerization of coumarin units which can be easily controlled by the UV irradiation time (or light intensity). The photo-degradation of SCNPs occurs under 254 nm UV irradiation due to the photo-cleavage reaction of coumarin. Owing to the biocompatible and biodegradable nature of the polyesters, they have the potential to be exploited for biomedical applications.

Secondly, we presented the first liquid crystalline SCNPs based on photo-responsive azobenzene based polymers. The liquid crystalline order and photo-isomerization of azobenzene were observed in the SCNP system despite the confinement within a tiny nanoparticle and crosslinked nature. Moreover, the liquid crystalline SCNPs have a number of interesting properties including solvent-selective photoluminescence, excitation

wavelength-dependent photo-induced deformation and mechanically stretching-induced orientation which may provide new possible applications in the field of bio-imaging and LC materials.

Finally, we reported a class of CO_2-responsive SCNPs based on a multi-stimuli-responsive (pH, CO_2, thermal) polymer, PDMAEMA. The CO_2-responsiveness of SCNPs led to gas-controlled solubility or aggregation state in aqueous solution through shifting LCST and reversibly tunable nanoparticle size by bubbling CO_2 and N_2. We also prepared gas-sensitive micelles self-assembled from amphiphilic tadpole-like single-chain 'Janus' nanoparticles which exhibit reversible volume change under alternating CO_2/N_2 stimulation. Furthermore, both CO_2-responsive SCNPs and micelles from SCJNPs can be used as gas-sensitive, rate- and size-tunable nano-reactors for the synthesis of gold nanoparticles (AuNPs).

In addition, the research works accomplished in this thesis have allowed the establishment of a universal approach to preparing stimuli-responsive multi-functional SCNPs based on a class of modular polymer structure as polymer precursors, that is, random copolymers comprising stimuli-responsive units and crosslinkable units. The modular polymer can be suitable for variety of stimuli-responsive polymers and provide more possibilities to develop multi-functional SCNPs for various applications. This achievement represents a significant contribution to the advancement of fundamental knowledge in the exciting field of polymer nanoparticles.

BIBLIOGRAPHY

(1) Elsabahy, M.; Wooley, K. L.; *Chem. Soc. Rev.* **2012**, *41* (7), 2545–2561.

(2) Ong, B. S.; Wu, Y.; Liu, P.; Gardner, S.; *Adv. Mater.* **2005**, *17* (9), 1141–1144.

(3) Hamilton, S. K.; Harth, E.; *ACS Nano* **2009**, *3* (2), 402–410.

(4) Aiertza, M. K.; Odriozola, I.; Cabañero, G.; Grande, H.-J.; Loinaz, I.; *Cell. Mol. Life Sci.* **2011**, *69* (3), 337–346.

(5) Gutekunst, W. R.; Hawker, C. J.; *J. Am. Chem. Soc.* **2015**, *137* (25), 8038–8041.

(6) Trinh, T. T.; Laure, C.; Lutz, J.-F.; *Macromol. Chem. Phys.* **2015**, *216* (14), 1498–1506.

(7) Gao, H.; *Macromol. Rapid Commun.* **2012**, *33* (9), 722–734.

(8) Bosman, A. W.; Janssen, H. M.; Meijer, E. W.; *Chem. Rev.* **1999**, *99* (7), 1665–1688.

(9) Bachler, P. R.; Wagener, K. B.; *Monatshefte Für Chem. - Chem. Mon.* **2015**, *146* (7), 1053–1061.

(10) Dobson, C. M.; *Nature* **2003**, *426* (6968), 884–890.

(11) Dill, K. A.; MacCallum, J. L.; *Science* **2012**, *338* (6110), 1042–1046.

(12) Ouchi, M.; Badi, N.; Lutz, J.-F.; Sawamoto, M.; *Nat. Chem.* **2011**, *3* (12), 917–924.

(13) Lyon, C. K.; Prasher, A.; Hanlon, A. M.; Tuten, B. T.; Tooley, C. A.; Frank, P. G.; Berda, E. B.; *Polym. Chem.* **2014**, *6* (2), 181–197.

(14) Frank, P.; Prasher, A.; Tuten, B.; Chao, D.; Berda, E.; *Appl. Petrochem. Res.* **2015**, *5* (1), 9–17.

(15) Mecerreyes, D.; Lee, V.; Hawker, C. J.; Hedrick, J. L.; Wursch, A.; Volksen, W.; Magbitang, T.; Huang, E.; Miller, R. D.; *Adv. Mater.* **2001**, *13* (3), 204–208.

(16) Hanlon, A. M.; Lyon, C. K.; Berda, E. B.; *Macromolecules* **2016**, *49* (1), 2–14.

(17) Smart Polymer. *Wikipedia*; 2016.

(18) Altintas, O.; Barner-Kowollik, C.; *Macromol. Rapid Commun.* **2016**, *37* (1), 29–46.

(19) Altintas, O.; Barner-Kowollik, C.; *Macromol. Rapid Commun.* **2012**, *33* (11), 958–971.

(20) Gonzalez-Burgos, M.; Latorre-Sanchez, A.; Pomposo, J. A.; *Chem. Soc. Rev.* **2015**, *44* (17), 6122–6142.

(21) Mavila, S.; Eivgi, O.; Berkovich, I.; Lemcoff, N. G.; *Chem. Rev.* **2016**, *116* (3), 878–961.

(22) Antonietti, M.; Sillescu, H.; Schmidt, M.; Schuch, H.; *Macromolecules* **1988**, *21* (3), 736–742.

(23) Davankov, V. A.; Ilyin, M. M.; Tsyurupa, M. P.; Timofeeva, G. I.; Dubrovina, L. V.; *Macromolecules* **1996**, *29* (26), 8398–8403.

(24) Jiang, J.; Thayumanavan, S.; *Macromolecules* **2005**, *38* (14), 5886–5891.

(25) Harth, E.; Horn, B. V.; Lee, V. Y.; Germack, D. S.; Gonzales, C. P.; Miller, R. D.; Hawker, C. J.; *J. Am. Chem. Soc.* **2002**, *124* (29), 8653–8660.

(26) Dobish, J. N.; Hamilton, S. K.; Harth, E.; *Polym. Chem.* **2012**, *3* (4), 857–860.

(27) Tuteja, A.; Mackay, M. E.; Hawker, C. J.; Van Horn, B.; Ho, D. L.; *J. Polym. Sci. Part B Polym. Phys.* **2006**, *44* (14), 1930–1947.

(28) Dukette, T. E.; Mackay, M. E.; Van Horn, B.; Wooley, K. L.; Drockenmuller, E.; Malkoch, M.; Hawker, C. J.; *Nano Lett.* **2005**, *5* (9), 1704–1709.

(29) Kim, Y.; Pyun, J.; Fréchet, J. M. J.; Hawker, C. J.; Frank, C. W.; *Langmuir* **2005**, *21* (23), 10444–10458.

(30) Croce, T. A.; Hamilton, S. K.; Chen, M. L.; Muchalski, H.; Harth, E.; *Macromolecules* **2007**, *40* (17), 6028–6031.

(31) Adkins, C. T.; Muchalski, H.; Harth, E.; *Macromolecules* **2009**, *42* (15), 5786–5792.

(32) Jiang, X.; Pu, H.; Wang, P.; *Polymer* **2011**, *52* (16), 3597–3602.

(33) de Luzuriaga, A. R.; Ormategui, N.; Grande, H. J.; Odriozola, I.; Pomposo, J. A.; Loinaz, I.; *Macromol. Rapid Commun.* **2008**, *29* (12–13), 1156–1160.

(34) Sanchez-Sanchez, A.; Asenjo-Sanz, I.; Buruaga, L.; Pomposo, J. A.; *Macromol. Rapid Commun.* **2012**, *33* (15), 1262–1267.

(35) Perez-Baena, I.; Loinaz, I.; Padro, D.; García, I.; Grande, H. J.; Odriozola, I.; *J. Mater. Chem.* **2010**, *20* (33), 6916–6922.

(36) Sanchez-Sanchez, A.; Pérez-Baena, I.; Pomposo, J. A.; *Molecules* **2013**, *18* (3), 3339–3355.

(37) de Luzuriaga, A. R.; Perez-Baena, I.; Montes, S.; Loinaz, I.; Odriozola, I.; García, I.; Pomposo, J. A.; *Macromol. Symp.* **2010**, *296* (1), 303–310.

(38) Stevens, D. M.; Tempelaar, S.; Dove, A. P.; Harth, E.; *ACS Macro Lett.* **2012**, *1* (7), 915–918.

(39) Dirlam, P. T.; Kim, H. J.; Arrington, K. J.; Chung, W. J.; Sahoo, R.; Hill, L. J.; Costanzo, P. J.; Theato, P.; Char, K.; Pyun, J.; *Polym. Chem.* **2013**, *4* (13), 3765–3773.

(40) Perez-Baena, I.; Barroso-Bujans, F.; Gasser, U.; Arbe, A.; Moreno, A. J.; Colmenero, J.; Pomposo, J. A.; *ACS Macro Lett.* **2013**, *2* (9), 775–779.

(41) Wong, E. H. H.; Lam, S. J.; Nam, E.; Qiao, G. G.; *ACS Macro Lett.* **2014**, *3* (6), 524–528.

(42) Wang, P.; Pu, H.; Jin, M.; *J. Polym. Sci. Part Polym. Chem.* **2011**, *49* (24), 5133–5141.

(43) Altintas, O.; Willenbacher, J.; Wuest, K. N. R.; Oehlenschlaeger, K. K.; Krolla-Sidenstein, P.; Gliemann, H.; Barner-Kowollik, C.; *Macromolecules* **2013**, *46* (20), 8092–8101.

(44) Willenbacher, J.; Wuest, K. N. R.; Mueller, J. O.; Kaupp, M.; Wagenknecht, H.-A.; Barner-Kowollik, C.; *ACS Macro Lett.* **2014**, *3* (6), 574–579.

(45) Frank, P. G.; Tuten, B. T.; Prasher, A.; Chao, D.; Berda, E. B.; *Macromol. Rapid Commun.* **2014**, *35* (2), 249–253.

(46) Njikang, G.; Liu, G.; Curda, S. A.; *Macromolecules* **2008**, *41* (15), 5697–5702.

(47) Xie, M. X.; Jiang, L.; Xu, Z. P.; Chen, D. Y.; *Chem. Commun.* **2015**, *51* (10), 1842–1845.

(48) Cherian, A. E.; Sun, F. C.; Sheiko, S. S.; Coates, G. W.; *J. Am. Chem. Soc.* **2007**, *129* (37), 11350–11351.

(49) Beck, J. B.; Killops, K. L.; Kang, T.; Sivanandan, K.; Bayles, A.; Mackay, M. E.; Wooley, K. L.; Hawker, C. J.; *Macromolecules* **2009**, *42* (15), 5629–5635.

(50) Zhu, B.; Qian, G.; Xiao, Y.; Deng, S.; Wang, M.; Hu, A.; *J. Polym. Sci. Part Polym. Chem.* **2011**, *49* (24), 5330–5338.

(51) Zhu, B.; Ma, J.; Li, Z.; Hou, J.; Cheng, X.; Qian, G.; Liu, P.; Hu, A.; *J. Mater. Chem.* **2011**, *21* (8), 2679–2683.

(52) Wen, J.; Yuan, L.; Yang, Y.; Liu, L.; Zhao, H.; *ACS Macro Lett.* **2013**, *2* (2), 100–106.

(53) Lehn, J.-M. Dynamers; *Prog. Polym. Sci.* **2005**, *30* (8–9), 814–831.

(54) Otto, S.; *Acc. Chem. Res.* **2012**, *45* (12), 2200–2210.

(55) Maeda, T.; Otsuka, H.; Takahara, A.; *Prog. Polym. Sci.* **2009**, *34* (7), 581–604.

(56) Aliyar, H. A.; Hamilton, P. D.; Remsen, E. E.; Ravi, N.; *J. Bioact. Compat. Polym.* **2005**, *20* (2), 169–181.

(57) Tuten, B. T.; Chao, D.; Lyon, C. K.; Berda, E. B.; *Polym. Chem.* **2012**, *3* (11), 3068–3071.

(58) Buruaga, L.; Pomposo, J. A.; *Polymers* **2011**, *3* (4), 1673–1683.

(59) Sanchez-Sanchez, A.; Fulton, D. A.; Pomposo, J. A.; *Chem. Commun.* **2014**, *50* (15), 1871–1874.

(60) Murray, B. S.; Fulton, D. A.; *Macromolecules* **2011**, *44* (18), 7242–7252.

(61) Whitaker, D. E.; Mahon, C. S.; Fulton, D. A.; *Angew. Chem. Int. Ed.* **2013**, *52* (3), 956–959.

(62) He, J.; Tremblay, L.; Lacelle, S.; Zhao, Y.; *Soft Matter* **2011**, *7* (6), 2380–2386.

(63) Zhao, Y.; Tremblay, L.; Zhao, Y.; *Macromolecules* **2011**, *44* (10), 4007–4011.

(64) Seo, M.; Beck, B. J.; Paulusse, J. M. J.; Hawker, C. J.; Kim, S. Y.; *Macromolecules* **2008**, *41* (17), 6413–6418.

(65) Foster, E. J.; Berda, E. B.; Meijer, E. W.; *J. Am. Chem. Soc.* **2009**, *131* (20), 6964–6966.

(66) Berda, E. B.; Foster, E. J.; Meijer, E. W.; *Macromolecules* **2010**, *43* (3), 1430–1437.

(67) Hosono, N.; Gillissen, M. A. J.; Li, Y.; Sheiko, S. S.; Palmans, A. R. A.; Meijer, E. W.; *J. Am. Chem. Soc.* **2013**, *135* (1), 501–510.

(68) Altintas, O.; Gerstel, P.; Dingenouts, N.; Barner-Kowollik, C.; *Chem. Commun.* **2010**, *46* (34), 6291–6293.

(69) Altintas, O.; Lejeune, E.; Gerstel, P.; Barner-Kowollik, C.; *Polym. Chem.* **2012**, *3* (3), 640–651.

(70) Altintas, O.; Rudolph, T.; Barner-Kowollik, C.; *J. Polym. Sci. Part Polym. Chem.* **2011**, *49* (12), 2566–2576.

(71) Willenbacher, J.; Altintas, O.; Roesky, P. W.; Barner-Kowollik, C.; *Macromol. Rapid Commun.* **2014**, *35* (1), 45–51.

(72) Willenbacher, J.; Altintas, O.; Trouillet, V.; Knöfel, N.; Monteiro, M. J.; Roesky, P. W.; Barner-Kowollik, C.; *Polym. Chem.* **2015**, *6* (24), 4358–4365.

(73) Mavila, S.; Rozenberg, I.; Lemcoff, N. G.; *Chem. Sci.* **2014**, *5* (11), 4196–4203.

(74) Mavila, S.; Diesendruck, C. E.; Linde, S.; Amir, L.; Shikler, R.; Lemcoff, N. G.; *Angew. Chem. Int. Ed.* **2013**, *52* (22), 5767–5770.

(75) Berkovich, I.; Mavila, S.; Iliashevsky, O.; Kozuch, S.; Lemcoff, N. G.; *Chem. Sci.* **2016**, *7* (3), 1773–1778.

(76) Jeong, J.; Lee, Y.-J.; Kim, B.; Kim, B.; Jung, K.-S.; Paik, H.; *Polym. Chem.* **2015**, *6* (18), 3392–3397.

(77) Appel, E. A.; Dyson, J.; del Barrio, J.; Walsh, Z.; Scherman, O. A.; *Angew. Chem. Int. Ed.* **2012**, *51* (17), 4185–4189.

(78) Riddles, C. J.; Zhao, W.; Hu, H.-J.; Chen, M.; Van De Mark, M. R.; *Polymer* **2014**, *55* (1), 48–57.

(79) Gillissen, M. A. J.; Voets, I. K.; Meijer, E. W.; Palmans, A. R. A.; *Polym. Chem.* **2012**, *3* (11), 3166–3174.

(80) Sun, T.; Chance, R. R.; Graessley, W. W.; Lohse, D. J.; *Macromolecules* **2004**, *37* (11), 4304–4312.

(81) Grubisic, Z.; Rempp, P.; Benoit, H. A.; *J. Polym. Sci. [B]* **1967**, *5* (9), 753–759.

(82) Moore, J. C.; *J. Polym. Sci. A* **1964**, *2* (2), 835–843.

(83) Wyatt, P. J.; *Anal. Chim. Acta* **1993**, *272* (1), 1–40.

(84) Ormategui, N.; García, I.; Padro, D.; Cabañero, G.; Grande, H. J.; Loinaz, I.; *Soft Matter* **2011**, *8* (3), 734–740.

(85) Foster, E. J.; Berda, E. B.; Meijer, E. W.; *J. Polym. Sci. Part Polym. Chem.* **2011**, *49* (1), 118–126.

(86) Altintas, O.; Willenbacher, J.; Wuest, K. N. R.; Oehlenschlaeger, K. K.; Krolla-Sidenstein, P.; Gliemann, H.; Barner-Kowollik, C.; *Macromolecules* **2013**, *46* (20), 8092–8101.

(87) Appel, E. A.; Barrio, J. del; Dyson, J.; Isaacs, L.; Scherman, O. A.; *Chem. Sci.* **2012**, *3* (7), 2278–2281.

(88) Steinkoenig, J.; Rothfuss, H.; Lauer, A.; Tuten, B. T.; Barner-Kowollik, C.; *J. Am. Chem. Soc.* **2017**, *139* (1), 51–54.

(89) Heiler, C.; Offenloch, J. T.; Blasco, E.; Barner-Kowollik, C.; *ACS Macro Lett.* **2017**, *6* (1), 56–61.

(90) Gracia, R.; Marradi, M.; Cossío, U.; Benito, A.; Vicente, A. P.-S.; Gómez-Vallejo, V.; Grande, H.-J.; Llop, J.; Loinaz, I.; *J. Mater. Chem. B* **2017**, *5* (6), 1143–1147.

(91) Wen, J.; Zhang, J.; Zhang, Y.; Yang, Y.; Zhao, H.; *Polym. Chem.* **2014**, *5* (13), 4032–4038.

(92) Inoue, Y.; Kuad, P.; Okumura, Y.; Takashima, Y.; Yamaguchi, H.; Harada, A.; *J. Am. Chem. Soc.* **2007**, *129* (20), 6396–6397.

(93) Willenbacher, J.; Schmidt, B. V. K. J.; Schulze-Suenninghausen, D.; Altintas, O.; Luy, B.; Delaittre, G.; Barner-Kowollik, C.; *Chem. Commun.* **2014**, *50* (53), 7056–7059.

(94) Zhou, F.; Xie, M.; Chen, D.; *Macromolecules* **2014**, *47* (1), 365–372.

(95) Song, C.; Li, L.; Dai, L.; Thayumanavan, S.; *Polym. Chem.* **2015**, *6* (26), 4828–4834.

(96) Wang, F.; Pu, H.; Che, X.; *Chem. Commun.* **2016**, *52* (17), 3516–3519.

(97) Ding, L.; Wang, C.; Jiang, R.; Wang, L.; Song, W.; *React. Funct. Polym.* **2016,** DOI: 10.1016/j.reactfunctpolym.2016.10.004.

(98) Sanchez-Sanchez, A.; Arbe, A.; Colmenero, J.; Pomposo, J. A.; *ACS Macro Lett.* **2014**, *3* (5), 439–443.

(99) Bai, Y.; Feng, X.; Xing, H.; Xu, Y.; Kim, B. K.; Baig, N.; Zhou, T.; Gewirth, A. A.; Lu, Y.; Oldfield, E.; Zimmerman, S. C.; *J. Am. Chem. Soc.* **2016**, *138* (35), 11077–11080.

(100) Benito, A. B.; Aiertza, M. K.; Marradi, M.; Gil-Iceta, L.; Shekhter Zahavi, T.; Szczupak, B.; Jiménez-González, M.; Reese, T.; Scanziani, E.; Passoni, L.; Matteoli, M.; De Maglie, M.; Orenstein, A.; Oron-Herman, M.; Kostenich, G.; Buzhansky, L.; Gazit, E.; Grande, H.-J.; Gómez-Vallejo, V.; Llop, J.; Loinaz, I.; *Biomacromolecules* **2016**, *17* (10), 3213–3221.

(101) Nguyen, T.-K.; Lam, S. J.; Ho, K. K. K.; Kumar, N.; Qiao, G. G.; Egan, S.; Boyer, C.; Wong, E. H. H.; *ACS Infect. Dis.* **2017**, *3* (3), 237–248.

(102) Gao, Y.; Böhmer, V. I.; Zhou, D.; Zhao, T.; Wang, W.; Paulusse, J. M. J.; *J. Controlled Release* **2016** DOI: 10.1016/j.jconrel.2016.07.046.

(103) Anfinsen, C. B.; *Science* **1973**, *181* (4096), 223–230.

(104) Fischer, T. S.; Schulze-Sünninghausen, D.; Luy, B.; Altintas, O.; Barner-Kowollik, C; *Angew. Chem. Int. Ed.* **2016**, DOI: 10.1002/anie.201602894.

(105) Mes, T.; van der Weegen, R.; Palmans, A. R. A.; Meijer, E. W.; *Angew. Chem. Int. Ed.* **2011**, *50* (22), 5085–5089.

(106) Roy, R. K.; Lutz, J.-F.; *J. Am. Chem. Soc.* **2014**, *136* (37), 12888–1289.

(107) Hosono, N.; Palmans, A. R. A.; Meijer, E. W.; *Chem. Commun.* **2014**, *50* (59), 7990–7993.

(108) Ganesh, V. A.; Baji, A.; Ramakrishna, S.; *RSC Adv.* **2014**, *4* (95), 53352–53364.

(109) Wei, M.; Gao, Y.; Li, X.; Serpe, M. J.; *Polym. Chem.* **2016**, *8* (1), 127–143.

(110) Roy, D.; Brooks, W. L. A.; Sumerlin, B. S.; *Chem. Soc. Rev.* **2013**, *42* (17), 7214–7243.

(111) Gandhi, A.; Paul, A.; Sen, S. O.; Sen, K. K.; *Asian J. Pharm. Sci.* **2015**, *10* (2), 99–107.

(112) Dai, S.; Ravi, P.; Tam, K. C.; *Soft Matter* **2008**, *4* (3), 435–449.

(113) Zhang, W. L.; Choi, H. J.; *Polymers* **2014**, *6* (11), 2803–2818.

(114) Thévenot, J.; Oliveira, H.; Sandre, O.; Lecommandoux, S.; *Chem. Soc. Rev.* **2013**, *42* (17), 7099–7116.

(115) Bertrand, O.; Gohy, J.-F.; *Polym. Chem.* **2016**, *8* (1), 52–73.

(116) Gohy, J.-F.; Zhao, Y.; *Chem. Soc. Rev.* **2013**, *42* (17), 7117–7129.

(117) Nicoletta, F. P.; Cupelli, D.; Formoso, P.; De Filpo, G.; Colella, V.; Gugliuzza, A.; *Membranes* **2012**, *2* (1), 134–197.

(118) Darabi, A.; Jessop, P. G.; Cunningham, M. F.; *Chem. Soc. Rev.* **2016**, *45* (15), 4391–4436.

(119) Liu, H.; Lin, S.; Feng, Y.; Theato, P.; *Polym. Chem.* **2016**, *8* (1), 12–23.

(120) Lin, S.; Theato, P.; *Macromol. Rapid Commun.* **2013**, *34* (14), 1118–1133.

(121) Lei, L.; Zhang, Q.; Shi, S.; Zhu, S.; *Polym. Chem.* **2016**, *7* (34), 5456–5462.

(122) Yan, Q.; Zhao, Y.; *Chem. Commun.* **2014**, *50* (79), 11631–11641.

(123) Xia, H.; Zhao, Y.; Tong, R.; Escoffre, J.-M., Bouakaz, A., Eds.; Advances in Experimental Medicine and Biology; Springer International Publishing, 2016; pp 365–384.

(124) Zardad, A.-Z.; Choonara, Y. E.; du Toit, L. C.; Kumar, P.; Mabrouk, M.; Kondiah, P. P. D.; Pillay, V.; *Polymers* **2016**, *8* (10), 359.

(125) Mahimwalla, Z.; Yager, K. G.; Mamiya, J.; Shishido, A.; Priimagi, A.; Barrett, C. J.; *Polym. Bull.* **2012**, *69* (8), 967–1006.

(126) Hirakura, T.; Nomura, Y.; Aoyama, Y.; Akiyoshi, K.; *Biomacromolecules* **2004**, *5* (5), 1804–1809.

(127) Huang, Y.; Liang, W.; Poon, J. K. S.; Xu, Y.; Lee, R. K.; Yariv, A.; *Appl. Phys. Lett.* **2006**, *88* (18), 181102.

(128) Maddipatla, M. V. S. N.; Wehrung, D.; Tang, C.; Fan, W.; Oyewumi, M. O.; Miyoshi, T.; Joy, A.; *Macromolecules* **2013**, *46* (13), 5133–5140.

(129) Ohya, S.; Sonoda, H.; Nakayama, Y.; Matsuda, T.; *Biomaterials* **2005**, *26* (6), 655–659.

(130) Suwa, K.; Morishita, K.; Kishida, A.; Akashi, M.; *J. Polym. Sci. Part Polym. Chem.* **1997**, *35* (15), 3087–3094.

(131) Zhang, H.; Guo, S.; Fan, W.; Zhao, Y.; *Macromolecules* **2016**, *49* (4), 1424–1433.

(132) Schattling, P.; Jochum, F. D.; Theato, P.; *Polym. Chem.* **2013**, *5* (1), 25–36.

(133) Li, G.; Song, S.; Guo, L.; Ma, S.; *J. Polym. Sci. Part Polym. Chem.* **2008**, *46* (15), 5028–5035.

(134) Liu, F.; Urban, M. W.; *Macromolecules* **2008**, *41* (17), 6531–6539.

(135) Cohen, B.; Huppert, D.; *J. Phys. Chem. A* **2001**, *105* (30), 7157–7164.

(136) Trenor, S. R.; Shultz, A. R.; Love, B. J.; Long, T. E.; *Chem. Rev.* **2004**, *104* (6), 3059–3078.

(137) Schade, B.; Hagen, V.; Schmidt, R.; Herbrich, R.; Krause, E.; Eckardt, T.; Bendig, J.; *J. Org. Chem.* **1999**, *64* (25), 9109–9117.

(138) Bandara, H. M. D.; Burdette, S. C.; *Chem. Soc. Rev.* **2012**, *41* (5), 1809–1825.

(139) Chang, C.-W.; Lu, Y.-C.; Wang, T.-T.; Diau, E. W.-G.; *J. Am. Chem. Soc.* **2004**, *126* (32), 10109–10118.

(140) Yu, H.; *J. Mater. Chem. C* **2014**, *2* (17), 3047–3054.

(141) Fu, S.; Zhang, H.; Zhao, Y.; *J. Mater. Chem. C* **2016**, *4* (22), 4946–4953.

(142) Bütün, V.; Armes, S. P.; Billingham, N. C.; *Polymer* **2001**, *42* (14), 5993–6008.

(143) Han, D.; Boissiere, O.; Kumar, S.; Tong, X.; Tremblay, L.; Zhao, Y.; *Macromolecules* **2012**, *45* (18), 7440–7445.

(144) Liu, B.; Zhou, H.; Zhou, S.; Zhang, H.; Feng, A.-C.; Jian, C.; Hu, J.; Gao, W.; Yuan, J.; *Macromolecules* **2014**, *47* (9), 2938–2946.

(145) Han, D.; Tong, X.; Boissière, O.; Zhao, Y.; *ACS Macro Lett.* **2012**, *1* (1), 57–61.

(146) Pomposo, J. A.; *Polym. Int.* **2014**, *63* (4), 589–592.

(147) Xu, F.; Fang, Z.; Yang, D.; Gao, Y.; Li, H.; Chen, D.; *ACS Appl. Mater. Interfaces* **2014**, *6* (9), 6717–6723.

(148) Terashima, T.; Sugita, T.; Fukae, K.; Sawamoto, M.; *Macromolecules* **2014**, *47* (2), 589–600.

(149) Chao, D.; Jia, X.; Tuten, B.; Wang, C.; Berda, E. B.; *Chem. Commun.* **2013**, *49* (39), 4178–4180.

(150) Stals, P. J. M.; Li, Y.; Burdyńska, J.; Nicolaÿ R.; Nese, A.; Palmans, A. R. A.; Meijer, E. W.; Matyjaszewski, K.; Sheiko, S. S.; *J. Am. Chem. Soc.* **2013**, *135* (31), 11421–11424.

(151) Moore, J. S.; Stupp, S. I.; *Macromolecules* **1990**, *23* (1), 65–70.

(152) Lee, J.; Maddipatla, M. V. S. N.; Joy, A.; Vogt, B. D.; *Macromolecules* **2014**, *47* (9), 2891–2898.

(153) Li, G.; Li, P.; Qiu, H.; Li, D.; Su, M.; Xu, K.; *J. Biomed. Mater. Res. A* **2011**, *98A* (1), 88–99.

(154) Zhao, Y.; *Macromolecules* **2012**, *45* (9), 3647–3657.

(155) Jiang, J.; Tong, X.; Morris, D.; Zhao, Y.; *Macromolecules* **2006**, *39* (13), 4633–4640.

(156) Babin, J.; Pelletier, M.; Lepage, M.; Allard, J.-F.; Morris, D.; Zhao, Y.; *Angew. Chem. Int. Ed.* **2009**, *48* (18), 3329–3332.

(157) Shishkan, O.; Zamfir, M.; Gauthier, M. A.; Börner, H. G.; Lutz, J.-F.; *Chem. Commun.* **2014**, *50* (13), 1570–1572.

(158) Huo, M.; Wang, N.; Fang, T.; Sun, M.; Wei, Y.; Yuan, J.; *Polymer* **2015**, *66*, A11–A21.

(159) Wang, P.; Pu, H.; Ge, J.; Jin, M.; Pan, H.; Chang, Z.; Wan, D.; *Mater. Lett.* **2014**, *132*, 102–105.

(160) Fan, W.; Tong, X.; Yan, Q.; Fu, S.; Zhao, Y.; *Chem. Commun.* **2014**, *50* (88), 13492–13494.

(161) Wong, E. H. H.; Qiao, G. G.; *Macromolecules* **2015**, *48* (5), 1371–1379.

(162) Stals, P. J. M.; Gillissen, M. A. J.; Paffen, T. F. E.; de Greef, T. F. A.; Lindner, P.; Meijer, E. W.; Palmans, A. R. A.; Voets, I. K.; *Macromolecules* **2014**, *47* (9), 2947–2954.

(163) Pomposo, J. A.; Perez-Baena, I.; Lo Verso, F.; Moreno, A. J.; Arbe, A.; Colmenero, J.; *ACS Macro Lett.* **2014**, *3* (8), 767–772.

(164) Hegmann, T.; Qi, H.; Marx, V. M.; *J. Inorg. Organomet. Polym. Mater.* **2007**, *17* (3), 483–508.

(165) Jiang, J.; Qi, B.; Lepage, M.; Zhao, Y.; *Macromolecules* **2007**, *40* (4), 790–792.

(166) Tao, X.; Gao, Z.; Satoh, T.; Cui, Y.; Kakuchi, T.; Duan, Q.; *Polym. Chem.* **2011**, *2* (9), 2068–2073.

(167) Bo, Q.; Zhao, Y.; *Langmuir* **2007**, *23* (10), 5746–5751.

(168) Ikeda, T.; Nakano, M.; Yu, Y.; Tsutsumi, O.; Kanazawa, A.; *Adv. Mater.* **2003**, *15* (3), 201–205.

(169) Yu, H.; *Prog. Polym. Sci.* **2014**, *39* (4), 781–815.

(170) Kondo, M.; Yu, Y.; Ikeda, T.; *Angew. Chem. Int. Ed.* **2006**, *45* (9), 1378–1382.

(171) Yang, Z.; Herd, G. A.; Clarke, S. M.; Tajbakhsh, A. R.; Terentjev, E. M.; Huck, W. T. S.; *J. Am. Chem. Soc.* **2006**, *128* (4), 1074–1075.

(172) Wang, D.; Wang, X.; *Prog. Polym. Sci.* **2013**, *38* (2), 271–301.

(173) Wang, D.; Liu, J.; Ye, G.; Wang, X.; *Polymer* **2009**, *50* (2), 418–427.

(174) Yager, K. G.; Barrett, C. J.; *J. Photochem. Photobiol. Chem.* **2006**, *182* (3), 250–261.

(175) Li, Y.; He, Y.; Tong, X.; Wang, X.; *J. Am. Chem. Soc.* **2005**, *127* (8), 2402–2403.

(176) Li, J.; Chen, L.; Xu, J.; Wang, K.; Wang, X.; He, X.; Dong, H.; Lin, S.; Zhu, J.; *Langmuir* **2015**, *31* (48), 13094–13100.

(177) Terashima, T.; Mes, T.; De Greef, T. F. A.; Gillissen, M. A. J.; Besenius, P.; Palmans, A. R. A.; Meijer, E. W.; *J. Am. Chem. Soc.* **2011**, *133* (13), 4742–4745.

(178) Huerta, E.; Stals, P. J. M.; Meijer, E. W.; Palmans, A. R. A.; *Angew. Chem. Int. Ed.* **2013**, *125* (10), 2978–2982.

(179) Watanabe, K.; Tanaka, R.; Takada, K.; Kim, M.-J.; Lee, J.-S.; Tajima, K.; Isono, T.; Satoh, T.; *Polym. Chem.* **2016**, *7* (29), 4782–4792.

(180) Sanchez-Sanchez, A.; Pomposo, J. A.; *Part. Part. Syst. Charact.* **2014**, *31* (1), 11–23.

(181) Wang, F.; Pu, H.; Jin, M.; Pan, H.; Chang, Z.; Wan, D.; Du, J.; *J. Polym. Sci. Part Polym. Chem.* **2015**, *53* (15), 1832–1840.

(182) Wang, F.; Pu, H.; Jin, M.; Wan, D.; *Macromol. Rapid Commun.* **2016**, *37* (4), 330–336.

(183) Offenloch, J. T.; Willenbacher, J.; Tzvetkova, P.; Heiler, C.; Mutlu, H.; Barner-Kowollik, C.; *Chem. Commun.* **2017**, *53* (4), 775–778.

(184) Danilov, D.; Barner-Kowollik, C.; Wenzel, W.; *Chem. Commun.* **2015**, *51* (27), 6002–6005.

(185) Zhang, Y.; Zhao, H.; *Polymer* **2015**, *64*, 277–284.

(186) Zhang, Y.; Chu, Z.; Dreiss, C. A.; Wang, Y.; Fei, C.; Feng, Y.; *Soft Matter* **2013**, *9* (27), 6217–6221.

(187) Ochiai, B.; Yokota, K.; Fujii, A.; Nagai, D.; Endo, T.; *Macromolecules* **2008**, *41* (4), 1229–1236.

(188) Che, H.; Huo, M.; Peng, L.; Fang, T.; Liu, N.; Feng, L.; Wei, Y.; Yuan, J.; *Angew. Chem. Int. Ed.* **2015**, *54* (31), 8934–8938.

(189) Guo, Z.; Feng, Y.; Wang, Y.; Wang, J.; Wu, Y.; Zhang, Y.; *Chem. Commun.* **2011**, *47* (33), 9348–9350.

(190) Boniface, K. J.; Dykeman, R. R.; Cormier, A.; Wang, H.-B.; Mercer, S. M.; Liu, G.; Cunningham, M. F.; Jessop, P. G.; *Green Chem.* **2015**, *18* (1), 208–213.

(191) Thang, S. H.; Chong, (Bill)Y. K.; Mayadunne, R. T. A.; Moad, G.; Rizzardo, E.; *Tetrahedron Lett.* **1999**, *40* (12), 2435–2438.

(192) Li, Y.; Smith, A. E.; Lokitz, B. S.; McCormick, C. L.; *Macromolecules* **2007**, *40* (24), 8524–8526.

(193) Li, L.-Y.; He, W.-D.; Li, W.-T.; Zhang, K.-R.; Pan, T.-T.; Ding, Z.-L.; Zhang, B.-Y.; *J. Polym. Sci. Part Polym. Chem.* **2010**, *48* (22), 5018–5029.